Late Quaternary variations of the Labrador Current in Flemish Pass

by

Nicole R. Marshall

Submitted in partial fulfillment of the requirements for the
degree of Combined Honours Bachelor of Science in Earth Sciences and Oceanography,
Department of Earth Sciences, Department of Oceanography

at

Dalhousie University
Halifax, Nova Scotia
April, 2013

Distribution License

DalSpace requires agreement to this non-exclusive distribution license before your item can appear on DalSpace.

NON-EXCLUSIVE DISTRIBUTION LICENSE

You (the author(s) or copyright owner) grant to Dalhousie University the non-exclusive right to reproduce and distribute your submission worldwide in any medium.

You agree that Dalhousie University may, without changing the content, reformat the submission for the purpose of preservation.

You also agree that Dalhousie University may keep more than one copy of this submission for purposes of security, back-up and preservation.

You agree that the submission is your original work, and that you have the right to grant the rights contained in this license. You also agree that your submission does not, to the best of your knowledge, infringe upon anyone's copyright.

If the submission contains material for which you do not hold copyright, you agree that you have obtained the unrestricted permission of the copyright owner to grant Dalhousie University the rights required by this license, and that such third-party owned material is clearly identified and acknowledged within the text or content of the submission.

If the submission is based upon work that has been sponsored or supported by an agency or organization other than Dalhousie University, you assert that you have fulfilled any right of review or other obligations required by such contract or agreement.

Dalhousie University will clearly identify your name(s) as the author(s) or owner(s) of the submission, and will not make any alteration to the content of the files that you have submitted.

If you have questions regarding this license please contact the repository manager at dalspace@dal.ca.

Grant the distribution license by signing and dating below.

_____ _____

Name of signatory Date

DATE _____

AUTHOR _____

TITLE
_____

_____

_____

Degree _____ Convocation _____ Year _____

Permission is herewith granted to Dalhousie University to circulate and to have copied for non-commercial purposes, at its discretion, the above title upon the request of individuals or institutions.

_____

Signature of Author

ABSTRACT

Sediment drifts of alternating sand and mud, shaped by the Labrador Current in 1000 to 1200 m water depth, formed during the Late Quaternary in Flemish Pass, seaward of the Grand Banks of Newfoundland. These drifts, or contourite deposits, preserve Labrador Current flow variations throughout the last glacial cycle. Previous work in northern Flemish Pass shows that significant grain-size variations with time are influenced by the Labrador Current. During a CCGS Hudson cruise, 2011031, high-resolution seismic profiles and numerous sediment cores were obtained throughout Flemish Pass. A seismic profile and four sediment cores from southern Flemish Pass, an area not previously well studied, form the basis of this research. A transect of four cores was collected across the pass, including one core on the top of a prominent drift, the Beothuk Drift, located on the eastern side of southeast Flemish Pass. Core descriptions, X-radiography, and down-core measurements of colour, grain size, X-ray fluorescence, P-wave velocity and bulk density measurements were used to correlate the cores and to provide an age model based on previous Heinrich layer identifications.

The grain-size variations, down-core and laterally, and changes in sedimentation rates provide evidence for flow variations of the Labrador Current in the Late Quaternary. Drift sedimentation between H2 (24 ka) and H1 (16 ka) had an approximate sedimentation rate of 170 mm/ka with a minimum of 61 ka/mm on the west of Flemish Pass. In the past 16 ka, there has been strong sediment partitioning across Flemish Pass with an approximate drift sedimentation rate of 260 mm/ka, decreasing to 16 mm/ka on the west.

Sortable silt percent (SS %) is used as a proxy for current strength. SS % prior to H1, and excluding H2, ranged from 32-41 %, averaging 36 %. After H1, SS % ranged from 43-57 % with an average of 48 %. This increase in SS % suggests that the Labrador Current has strengthened after deposition of H1. The highest SS % is 57 %, at the top of the drift, suggesting that the Labrador Current is stronger today than it has been in at least the past 24 ka.

A 0.12 m thick interval of alkaline basaltic lapilli tuff is found 4 m beneath the seafloor in piston core 0022, between H3 (30 ka) and H2 (24 ka). No similar bed has been previously found in Flemish Pass, an area where hundreds of cores have been collected. A comparison of trace element geochemistry suggests that the basalt source is the Snaefellsnes Volcanic Zone in Iceland. However, the major element geochemistry suggests that the two are not related and that the core 0022 tuff does not originate from Iceland or Jan Mayen. The method of transport of the basaltic lapilli tuff found in core 0022 was likely ice-rafting by an iceberg or sea ice. A probable method of deposition was a rolling iceberg dumping the basaltic lapilli tuff onto the core 0022 location during a time of intermittent erosion of the seafloor.

Keywords: Flemish Pass, Labrador Current, Beothuk Drift, Heinrich Layer, Late Quaternary sedimentation, contourite deposits, ocean circulation

ACKNOWLEDGEMENTS

I would like to take a moment to express how much I appreciate all the support and guidance I have received from my honours supervisor, David Piper, at the Geological Survey of Canada (GSC), Bedford Institute of Oceanography, throughout this past year. I have learned so much from him and I owe him many thanks for his help with everything. Francky Saint-Ange and Calvin Campbell were also mentors to me. I am very grateful to Jenna Higgins and Kate Jarrett for their help in the GSC Core Processing Laboratory. I owe Owen Brown a tremendous thank you for teaching me to use the Coulter laser and other instruments in the GSC Sediment Lab. There are numerous GSC co-op students that I need to thank, including Danika Wong, Michael Wang, Naveed Anis and Joyce Roswell who each helped me with numerous tasks throughout my thesis in the fall 2012. I also must thank the CCGS Hudson crew who helped make the 2011 cruise to Flemish Pass a success. Finally, Martin Gibling deserves a standing ovation for being the Earth Sciences honours coordinator and for always being available when I needed feedback and advice.

TABLE OF CONTENTS

LIST OF FIGURES

LIST OF TABLES

LIST OF ABBREVIATIONS

a*: Red-green colour ratio
AMOC: Atlantic Meridional Overturning Circulation
b*: Blue-yellow colour ratio
CCGS: Canadian Coast Guard Ship
DTS: Deep Tow System
EFZ: Eastern Volcanic Zone
GSC: Geological Survey of Canada
H1: Heinrich layer/event 1 (1 identifies layer/event)
HREE: Heavy rare earth elements
ICP-MS*:* Inductively coupled plasma mass spectrometry
IRD: Ice-rafted detritus
IUGS: International Union of Geological Sciences
JM: Jan Mayen
ka: Thousands of years
L*: White-black colour ratio
LGM: Last Glacial Maximum
LREE: Light rare earth elements
Ma: Millions of years
mm: millimetres
MST: Multi-Sensor Track
MTD: Mass-transport deposit
NASG: North Atlantic Subpolar Gyre
pc: Piston core
REE: Rare earth element
SFZ: Southern Volcanic Zone
SNFZ: Snaefellsnes Volcanic Zone
SS %: Sortable silt percent
TAS: Total alkalis vs. SiO_2
twc: Trigger weight core
µm: Micron or micrometres
WBU: Western boundary undercurrent

CHAPTER 1: INTRODUCTION

1.1 Opening Statement

Flemish Pass is a narrow and perched sedimentary basin in approximately 1000 to 1200 m water depth seaward of the Grand Banks of Newfoundland and west of Flemish Cap (Fig. 1.1). Sand and mud are transported by the Labrador Current, deposited predominantly on the eastern side of Flemish Pass, creating sedimentary architecture known as a sediment drift or a contourite deposit. Contourite deposits have significant paleoceanographic importance because they record fine variations in current strength through time and are an important source of ocean/climate proxies (McCave & Hall, 2006).

Labrador Current strength variability is important because it provides clues for variations of ocean circulation in the North Atlantic. The circulation in these subpolar waters is important because even small instabilities in this circulation can weaken or inhibit deepwater formation critical for Atlantic Meridional Overturning Circulation (AMOC) and associated heat transport across the North Atlantic (Hillaire-Marcel et al., 2001).

Four piston cores (pc), four trigger weight cores (twc) and a seismic profile from across a drift in southern Flemish Pass were used for this study to determine variations in Labrador Current strength. Core descriptions, Multi-Sensor Track (MST) physical properties, X-ray fluorescence and X-ray images were used to characterize cores, supporting a Late Quaternary chronological model for this part of the drift. The sediment architecture, sedimentation rates and grain size allow interpretations of

Labrador Current flow in the Late Quaternary. Grain size is used to determine relative current strength (McCave & Hall, 2006), particularly the sortable silt (10-63 μm) fraction.

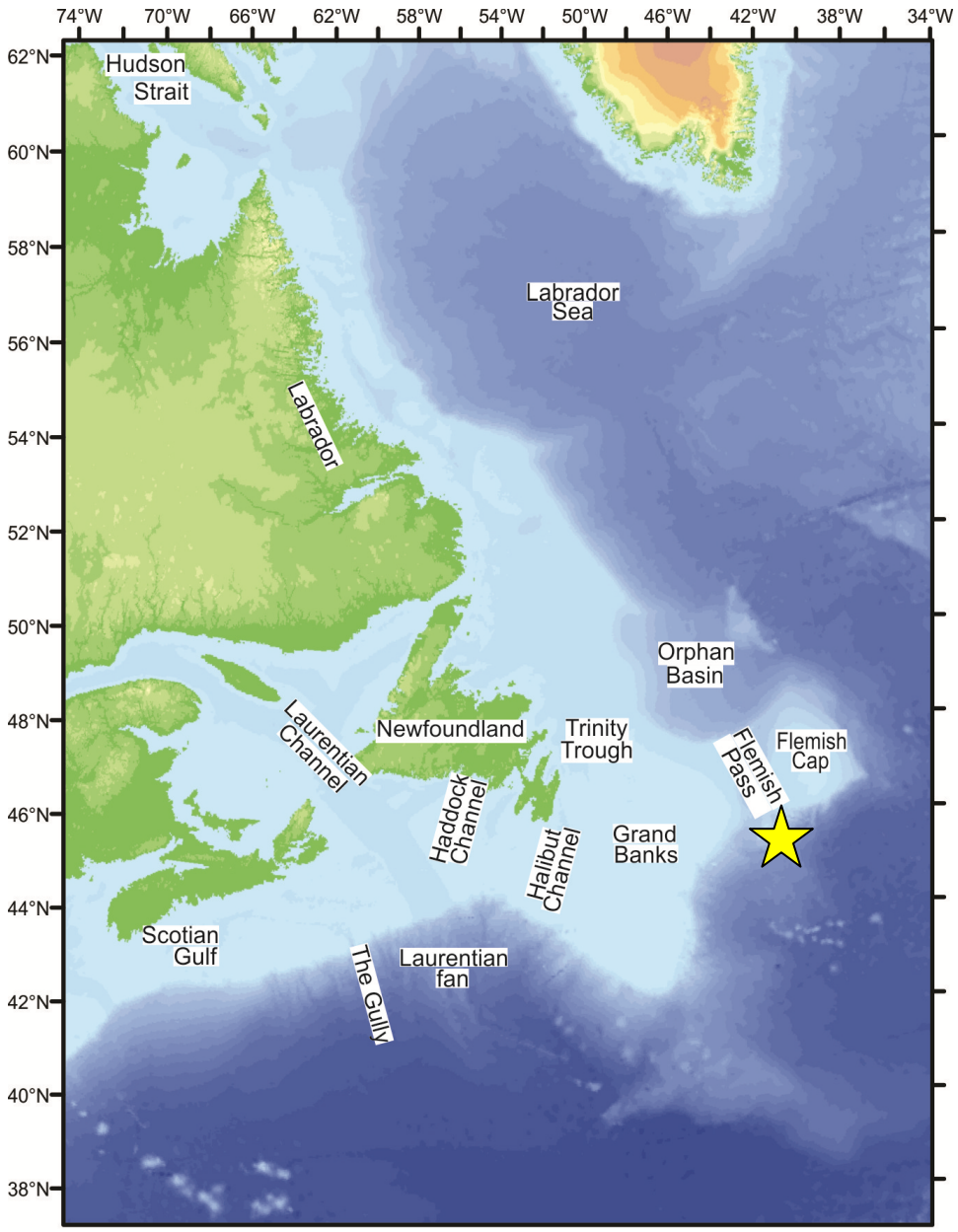

Figure 1.1. Map of Eastern Canada identifying Flemish Pass. (Modified from an original figure provided by D.J.W. Piper).

1.2 Thesis Objective

The aim of this thesis is to provide a history of the relative strength of the Labrador Current throughout the Late Quaternary in Flemish Pass. This thesis will provide a paleocurrent record for nearly the past 30 ka from cores using grain-size variations and sedimentation rates from across the Beothuk Drift in southeast Flemish Pass. This objective contributes to improving our understanding and interpretation of the North Atlantic Subpolar Gyre circulation and climate change.

The approach involves correlating cores from across the Beothuk Drift in Flemish Pass. Analysis of Heinrich layers and a basaltic lapilli unit provide a means to interpret pathways of flow, which can give us a better understanding of ocean circulation at the time of deposition. Lithological studies provide a chronology based on correlations with previously dated cores that have accelerator mass spectrometry ^{14}C dates.

CHAPTER 2: GEOLOGIC AND OCEANOGRAPHIC SETTING

2.1 Bathymetry

Monahan and MacNab (1974) produced the first detailed bathymetric map of Flemish Pass, based on widely spaced seismic survey lines. A modified version of this map (Fig. 2.1) includes numerous seismic lines from Armstrong et al. (1988). Multibeam bathymetry of Flemish Pass (Fig. 2.2) was collected by the Nereida Program in 2009 and 2010.

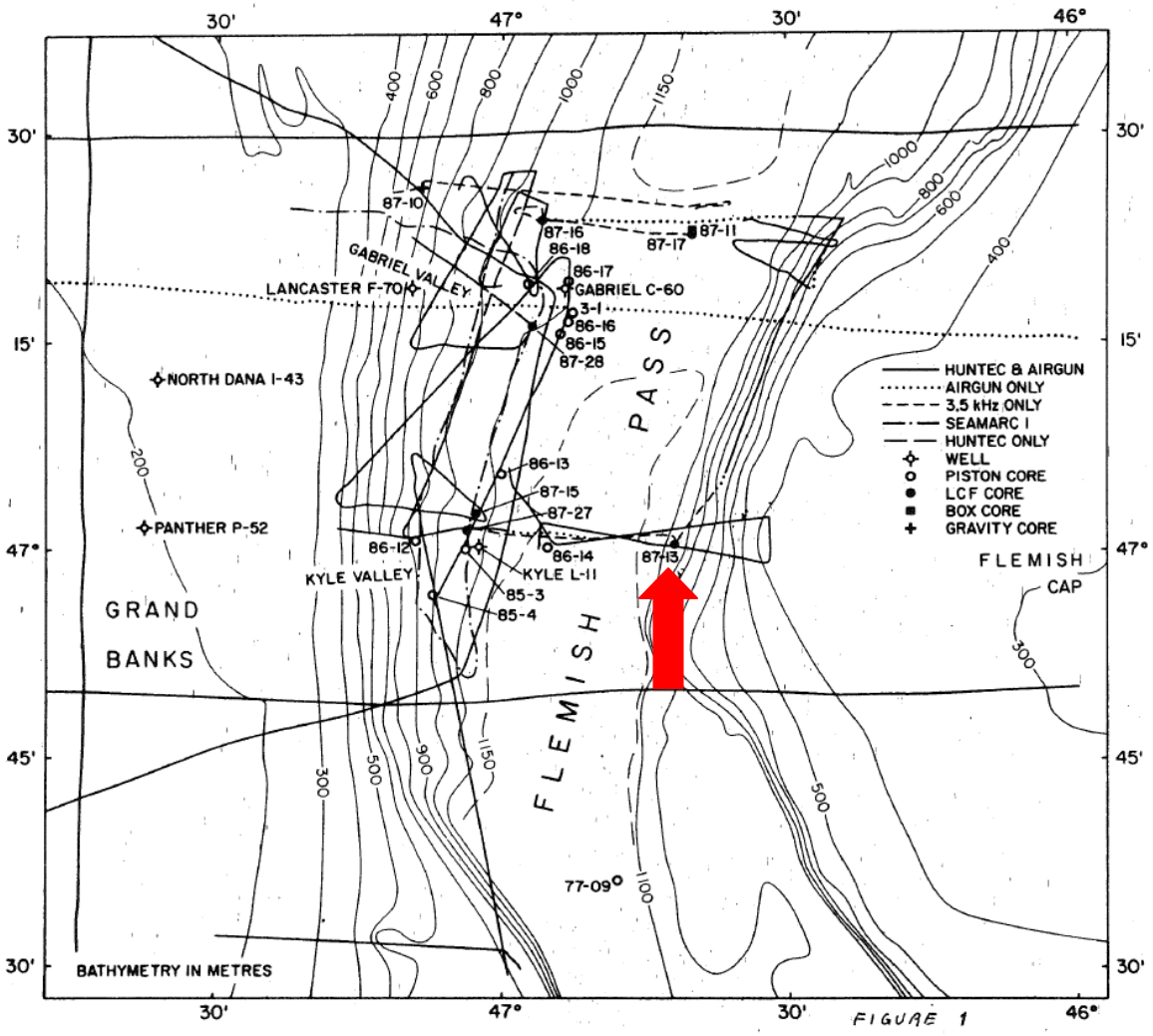

Figure 2.1. The first detailed bathymetric map of Flemish Pass (Monahan & MacNab, 1974) modified by Armstrong et al. (1988). Core 87-13 in the red box is used for core correlations in Chapter 5.

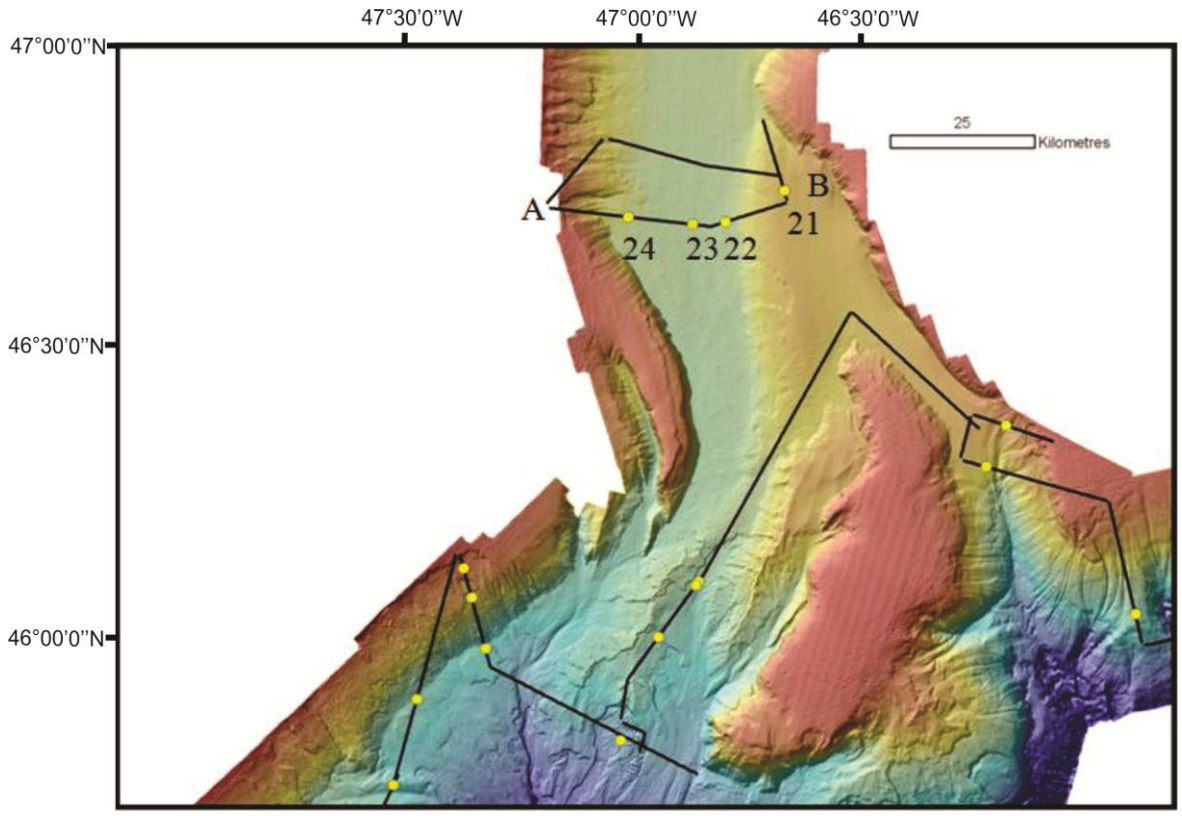

Figure 2.2. Multibeam bathymetry of the study area within southern Flemish Pass (Courtesy of the Nereida Program). The location of the seismic profile used for this thesis is indicated by A-B and four long cores (abbreviated here as 21-24) were collected from the locations (yellow dots) on the A-B transect. Towards B the profile runs into Beothuk Drift. Modified from Campbell (2011).

2.2 Geologic Setting

Flemish Pass is a narrow and perched sedimentary basin that overlies a graben formed during rifting of the northern Atlantic Ocean (Grant, 1972), separating Flemish Cap from the Grand Banks of Newfoundland. Precambrian basement rocks are exposed on Flemish Cap, a roughly circular submarine knoll that has an approximately 150 km base diameter and is the most easterly extension of North American continental crust (King et al., 1985). The Grand Banks, an area with a maximum water depth of 300 m, contains numerous banks separated by transverse troughs (Piper et al., 1990). Flemish Pass is bounded to the north by Sackville Spur (a contourite deposit) and Orphan Basin, which is a deep-water basin that forms part of the continental margin offshore Eastern

Canada (Campbell, 2005). The continental slope is to the south of Flemish Pass. The slope gradients off the Grand Banks of Newfoundland range from 5° to 3°, and the Flemish Pass seafloor has a nearly flat slope of <0.3° (Huppertz & Piper, 2009).

2.2.1 Seismic Studies in Flemish Pass

Seismic refraction studies (Keen & Barrett, 1981) along Flemish Pass indicate an anomalously thin continental crust, with a total depth to the Mohorovicic discontinuity of 23 km, as a result of crustal extension. One crustal layer is overlain by several sedimentary strata (Keen & Barrett, 1981).

Piper and Pereira (1992) investigated the Late Quaternary history of Flemish Pass using side-scan sonar, high-resolution seismic profiles and ^{14}C dated cores. Detailed logs of selected cores (Piper & Pereira, 1992) highlight lithology, radiocarbon dates, and correlations of rock units as shown in Figure 2.3 representing numerous locations in Flemish Pass. Updated interpretations of the cores will be discussed in Chapter 5.

Huppertz and Piper (2009) investigated the effect of ice extent on slope sedimentation processes using piston cores and a regional high-resolution seismic stratigraphy with different dating methods. They determined that the sedimentation rate (greatly controlled by shelf-crossing ice sheets) was an order of magnitude lower in Flemish Pass compared to the Scotian Slope during the Last Glacial Maximum (LGM).

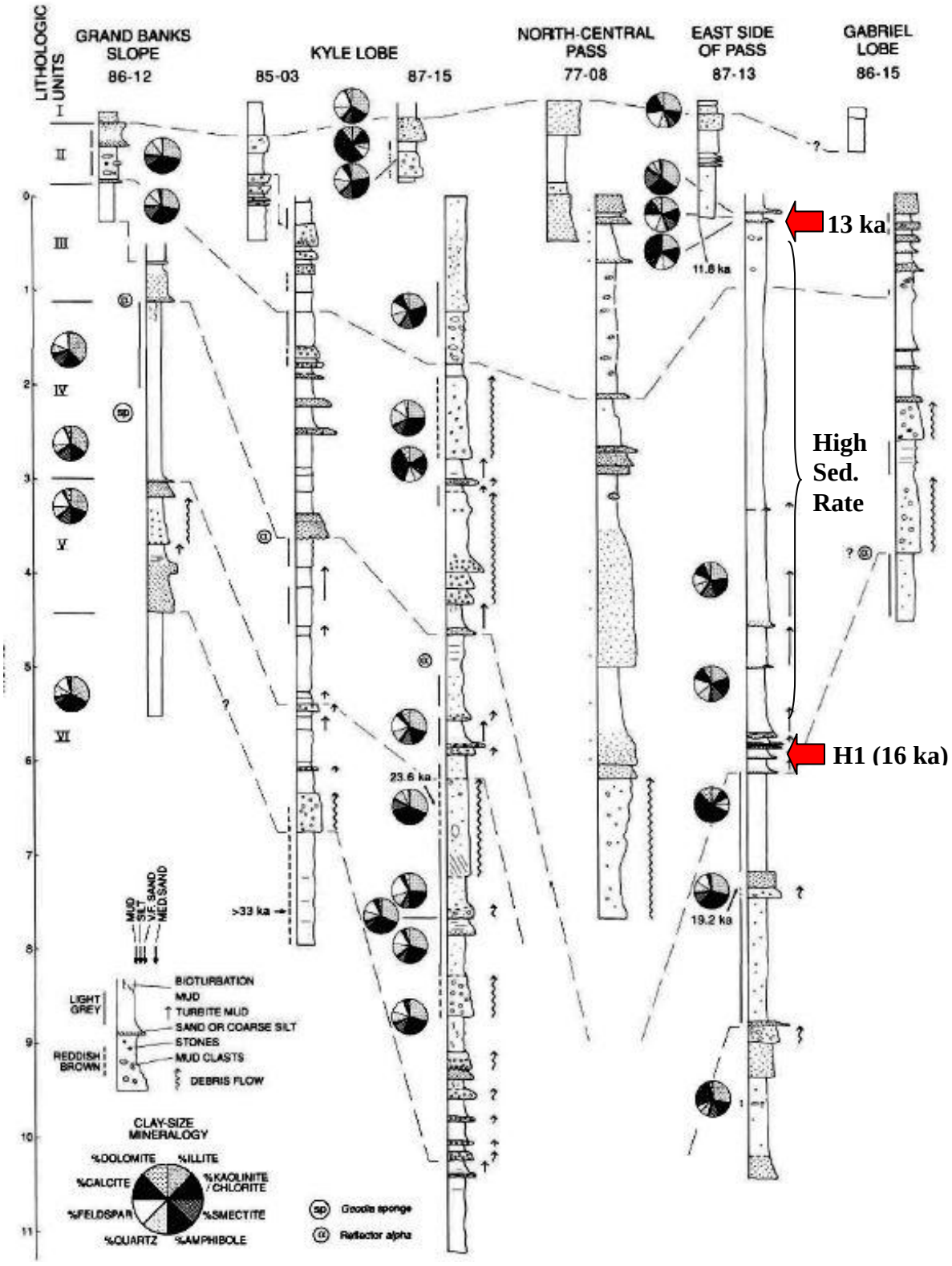

Figure 2.3. Detailed logs of selected cores from Flemish Pass (Modified from Piper & Pereira, 1992). These cores will be discussed in Chapter 5 in relation to the thesis cores. H1= Heinrich layer 1.

2.2.2 Cenozoic and Quaternary History of Flemish Pass

Flemish Pass has been continuously infilled by prograding sequences of Cenozoic (and some Late Cretaceous) sediments originating from the Grand Banks of Newfoundland (Piper & Normark, 1989). The Quaternary sediments consist predominantly of mud with thin interbedded turbidites from the Grand Banks slope (Piper & Pereira, 1992). Piper and Campbell (2005) interpreted some thick-bedded sand and mud along the base of the Flemish Cap slope as contourite deposits, including the sediment drift in this thesis, the Beothuk Drift.

Glacial ice completely crossed most of the eastern Canadian continental shelf during major glacial stages (Shaw, 2006) although maximum ice extent during the LGM only reached the middle shelf on the Grand Banks (Sonnichsen & King, 2005).

2.3 Oceanographic Setting

The oceanographic setting provides context for the importance of current flow and ocean circulation in relation to geological features in the study area.

2.3.1. The Labrador Current

The Labrador Current is a southwestward-flowing surface current close to the continental shelf break along Labrador and Newfoundland (Lazier & Wright, 1993) that originates in the northern Labrador Sea adjacent to Greenland and is centered at 1000 m water depth (Cuny et al., 2002). The flow of the Labrador Current is well known from temperature-salinity (T-S) measurements (Lazier, 1988). This flow of cold water reaches Orphan Basin, where it splits into two branches as it approaches Flemish Pass. The main (inner) branch of the Labrador Current flows through Flemish Pass and the smaller (outer) branch flows northwards around Flemish Cap (Fig. 2.4). Reference to the

Labrador Current throughout this thesis refers to the main branch, flowing through Flemish Pass.

The Labrador Current transports icebergs from Greenland and the Canadian Arctic to the Flemish Pass area, creating large iceberg pits and smaller scours on the shelf and upper slope (Piper & Pereira, 1992). Interestingly, there are relict Pleistocene scours that are below 600 m water depth, are 2-3 m deep and locally greater than 50 m wide (Piper & Pereira, 1992).

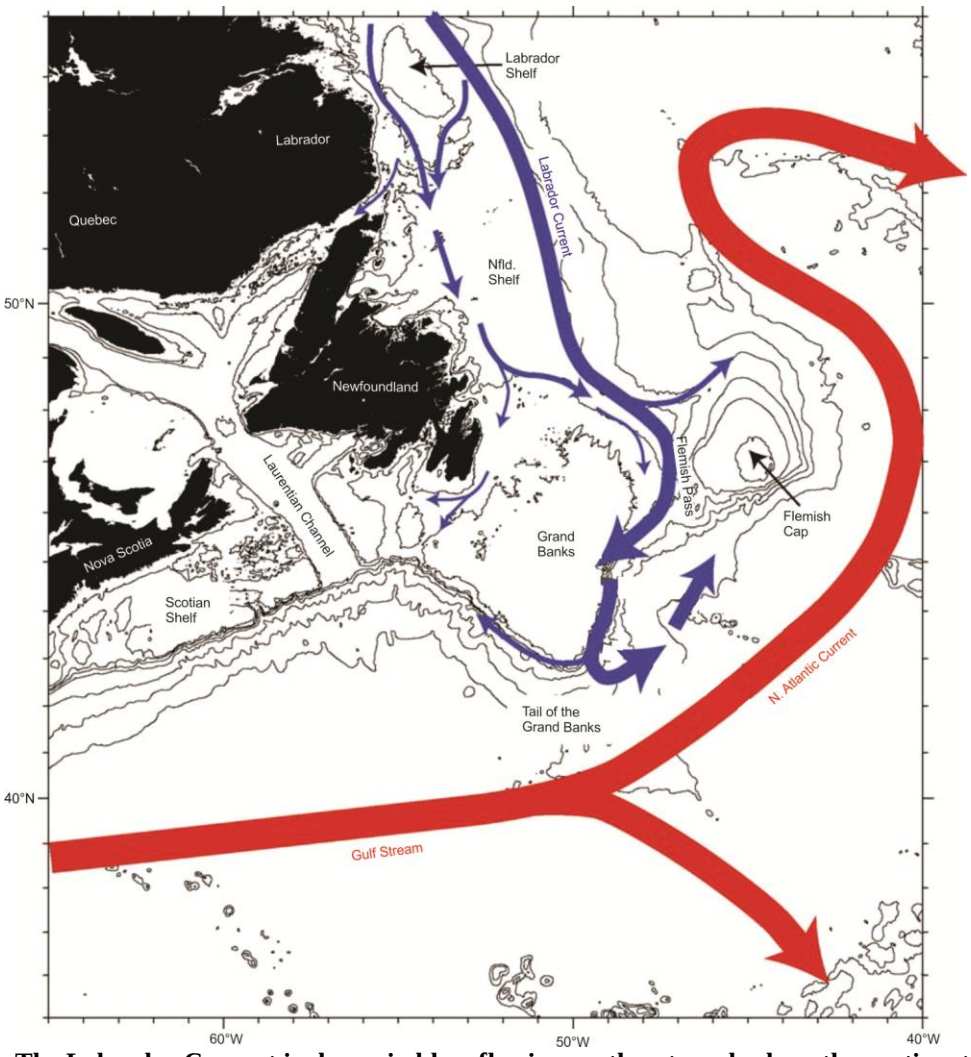

Figure 2.4. The Labrador Current is shown in blue, flowing southeastwards along the continental shelves and slopes of Labrador and Newfoundland. The Gulf Stream, transitioning to the North Atlantic Current as it splits, is shown in red. (Modified from Fratantoni & McCartney, 2010).

2.3.2 The North Atlantic Subpolar Gyre

A gyre is a rotational body of water that spans an ocean basin, such as the anticlockwise circulation shown in Figures 2.5-2.7. The North Atlantic Subpolar Gyre (NASG) is composed of numerous currents that complexly interact together. Currents change their behaviour based on the circulation around them. The NASG is composed of numerous currents including the Labrador Current, the North Atlantic Current (smaller northward continuation of the Gulf Stream), the Irminger Current, the East Greenland Current and the West Greenland Current (Fig. 2.6). The Norwegian Atlantic Current draws water from this gyre near Iceland and the United Kingdom (Langehaug et al., 2012). The western side of the North Atlantic includes currents that add to the North Atlantic Subpolar Gyre such as the Gulf Stream (which turns into the North Atlantic Current after it meets the Labrador Current), and water coming from Baffin Bay and Hudson Strait, denoted as the Canadian Archipelago Throughflow (Fig. 2.7).

Eastward- and northward-flowing sections of the NASG are dominated mostly by the warm and salty waters of the North Atlantic Current and the southward-flowing current in the western basin of the North Atlantic is dominated by the East Greenland Current (Irvali et al., 2012) and the Labrador Current along the eastern Canadian margin.

The modified NASG that existed in glacial periods was semi-isolated from the sub-tropical gyre, and this isolation would have helped maintain the presence of colder and fresher waters (the Labrador Current) along the continental margin off Labrador (Vilks, 1981).

During a Heinrich event, the Labrador Current strength is first increased by a cold, freshwater flux (Nye, 2010), followed by a strength decrease. The latter is caused by a

resultant weakening in the NASG (Fig. 2.5) due to the semi-isolation of the NASG from the sub-tropical gyre (Vilks, 1981).

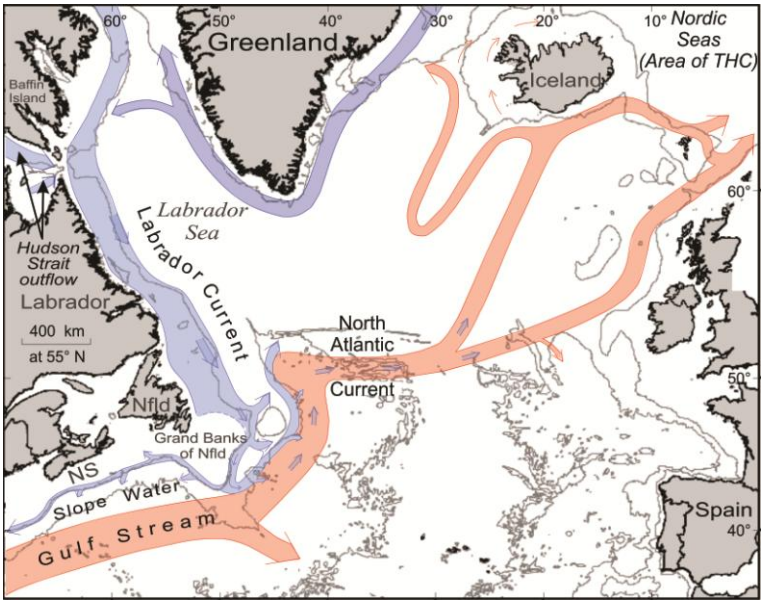

Figure 2.5. A simplified view of the present NASG. (Modified from an original figure provided by C.F.M. Lewis).

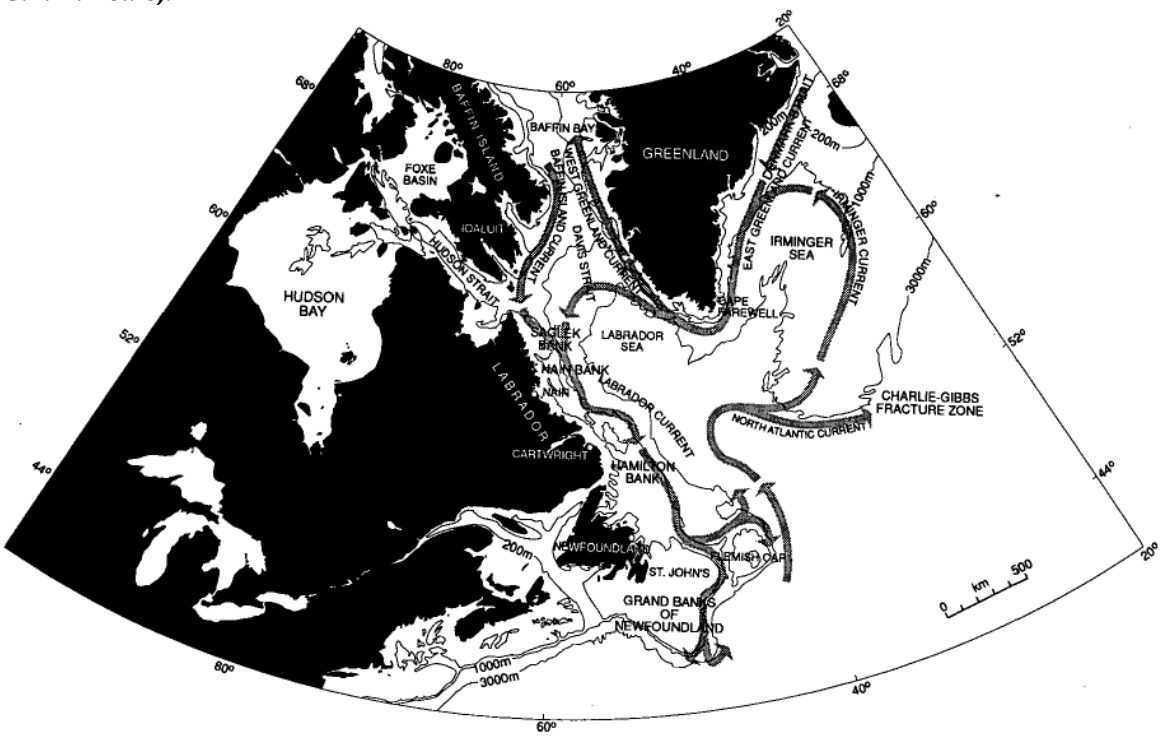

Figure 2.6. The NASG highlighting the surface currents involved in this circulation. (Lazier & Wright, 1993).

Analysis of variability in Labrador Current strength provides one piece of evidence for an interpretation of changes in flow variations of the North Atlantic Subpolar Gyre. An increase in freshwater flux causes the North Atlantic Subpolar Gyre circulation to slow down, which substantially weakens deepwater formation (Hillaire-Marcel et al., 2001; Thornalley et al., 2009) and inhibits warmer and saltier Gulf Stream waters from moving northwards (Vilks, 1981), which cools northwestern Europe because of a reduction in northward heat transport (Johnson & McClure, 1976). Freshwater fluxes, such as those released during Heinrich events, exit through the Canadian Archipelago Throughflow and enter the subpolar gyre via the Labrador Current.

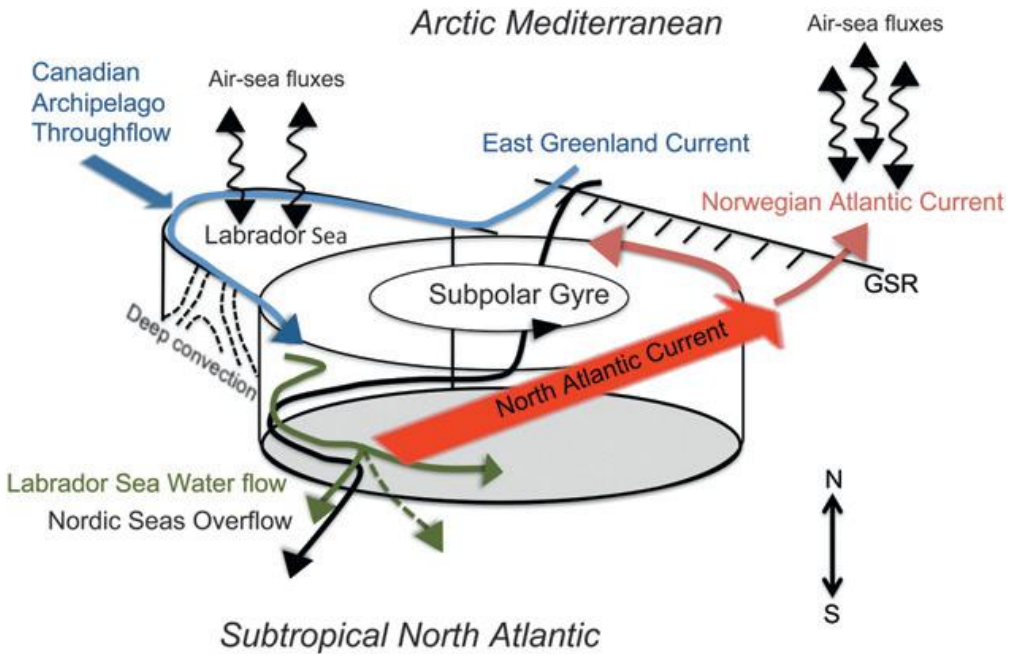

Figure 2.7. Model of the North Atlantic Subpolar Gyre circulation, including areas of deep convection near the East Greenland Current and in the Labrador Sea. GSR is the Greenland-Scotland Ridge. (Langehaug et al., 2012).

Deepwater formation takes place offshore Greenland and in the Labrador Sea where cold, dense water forms due to thick ice formation. The surface waters become

sufficiently cold and dense when ice forms that the surface waters sink vertically to a depth at which neutral buoyancy is obtained deeper in the water column. This is the main initiation of the AMOC, a density-driven process essential for advection of ocean currents worldwide. AMOC helps maintain a warm northwestern European climate, and is a critical component of the Earth's climate system (Thornalley et al., 2009).

2.3.3. Western Boundary Undercurrent

The Western Boundary Undercurrent (WBU) is a southward-flowing "contour current" that moves at lower slope to upper rise depths (Carter & Schafer, 1983). Deepwater circulation forms the WBU, which is swifter during times of more deepwater formation, for example during interglacials (Piper, 2005). However, the WBU does not affect sedimentation in the study area because Flemish Pass has a maximum depth of approximately 1300 m and feels only the effects of the Labrador Current. The WBU influences the seabed only at depths greater than 2500 m (Carter & Schafer, 1983; Lazier & Wright, 1993), as shown in Figure 2.8.

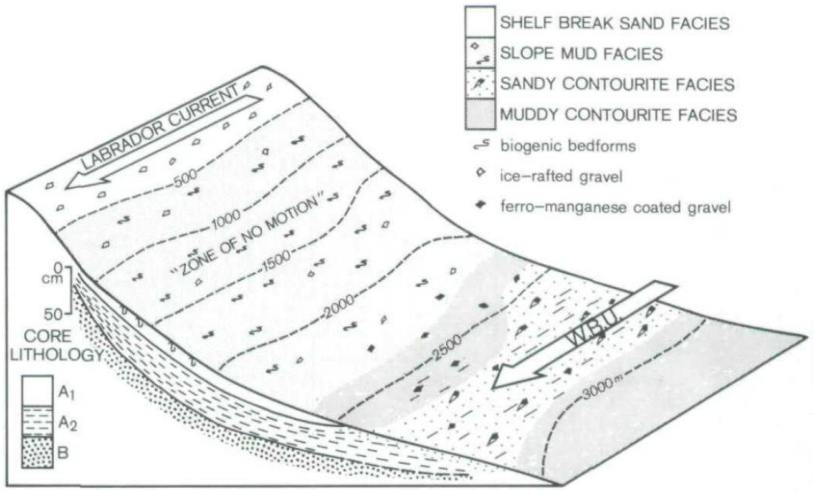

Figure 2.8. The WBU and the Labrador Current offshore Newfoundland (Carter & Schafer, 1983). Only the Labrador Current flows through Flemish Pass, which has a maximum depth of approximately 1300 m.

2.4 Oceanographic and Climatic Significance

The Labrador Current has varied in intensity and temperature through time, on a variety of timescales. Recent time-series measurements show that there are small, annual velocity variations in the Labrador Current (Lazier & Wright, 1993). According to Keigwin et al. (2003), within the past 1600 years, the Labrador Current in Emerald Basin, offshore Nova Scotia was relatively cold and strong until 150 years ago, based on numerous proxies and age dating of cores from the study area. Their conclusions state that prior to ~AD 1850, the Labrador Current, after flowing southwards through Flemish Pass, flowed over the Scotian Shelf. After ~AD 1850, the Labrador Current shifted further offshore and weakened in strength within Emerald Basin (Keigwin et al., 2003).

Scott et al. (1984) similarly recognized cooling and associated strengthening off Newfoundland based on foraminifera, dinoflagellates and pollen evidence, showing that the two branches (inner branch is along the shelf and outer branch is further offshore and flows around Flemish Cap) of the Labrador Current provide indications of glacial stages. A cold event (inner Labrador Current) followed by the earlier outer Labrador Current cold event preceded the latest glacial interval, suggesting strong ocean cooling before the LGM (Scott et al., 1984).

Data about the Labrador Current in the more distant geological past, referring to variations spanning larger than inter-annual, annual, decadal and centennial variability was non-existent. Using a core and seismic study across a transect from Flemish Pass, this thesis documents the Late Quaternary long-timescale relative strength variations of the Labrador Current, predominantly from 24 ka and through to the present.

Understanding Labrador Current variations provides clues not only to North Atlantic Subpolar Gyre circulation and deepwater formation but also to climatic conditions because gyre behaviour affects heat transport to northern latitudes. Therefore, this thesis is important because it advances our understanding of ocean circulation and climate during the Late Quaternary.

2.5 Sediment Drifts

Numerous sediment drifts that lie along the eastern Canadian margin are believed to have been deposited and shaped under the influence of deep thermohaline flows such as the WBU, although the Sackville Spur sediment drift just north of Flemish Pass (Fig. 2.9) and other sediment drifts within Flemish Pass owe their growth to the Labrador Current (Kennard et al., 1990). Sackville Spur is a well-studied and prominent sediment drift that lies north of Flemish Pass extending northeastwards for approximately 140 km (Kennard et al., 1990). The sediment drifts south of Flemish Pass and within southern Flemish Pass are not well known.

Figure 2.10 shows Flemish Pass with the locations of the seismic profiles (black lines) and cores (yellow dots) collected during the Canadian Coast Guard Ship (CCGS) Hudson 2011031 cruise. The cores and seismic profile, forming a transect across Flemish Pass within the red box, are of interest to this thesis.

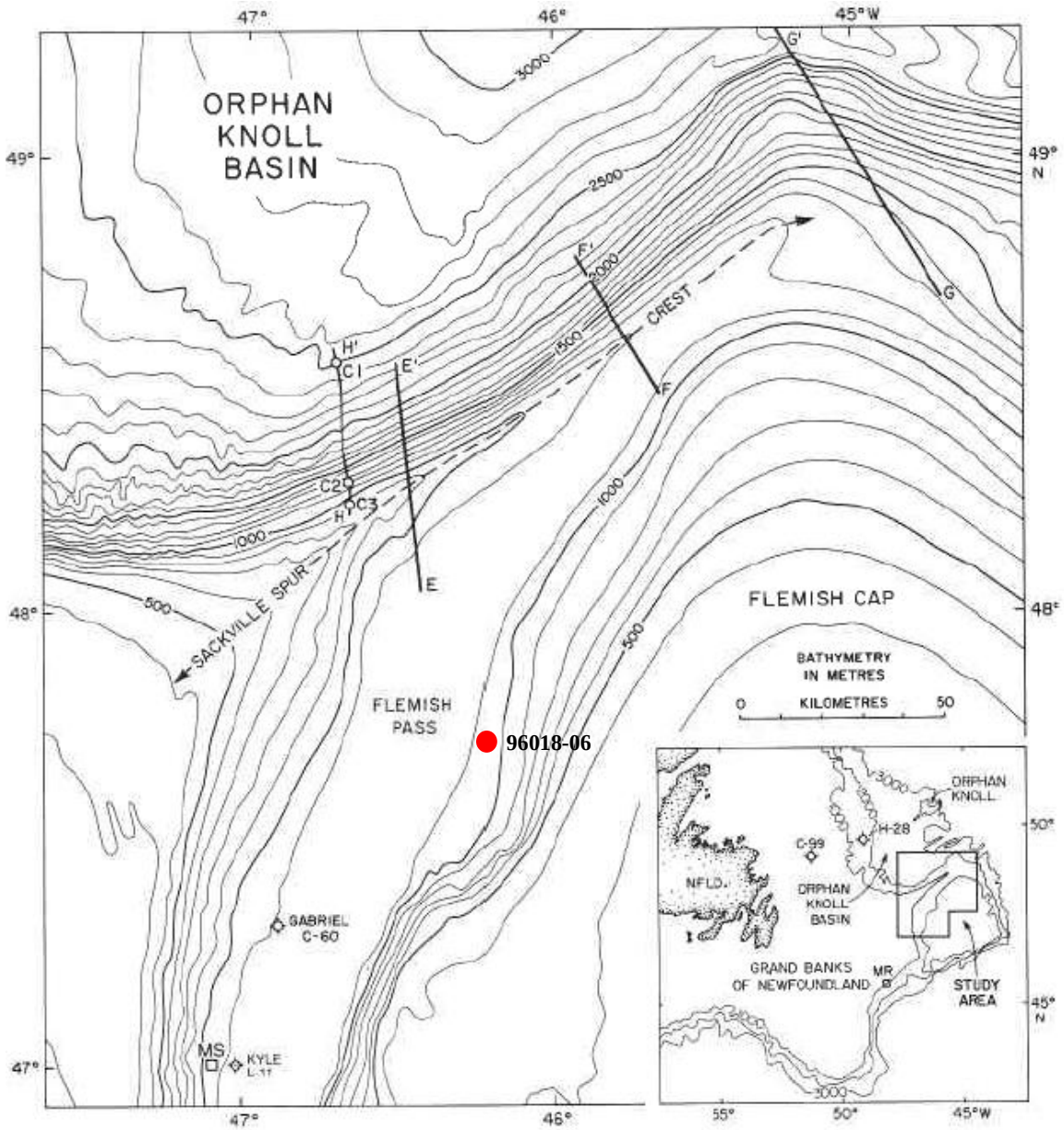

Figure 2.9. Sackville Spur along the northern end of Flemish Pass. (Kennard et al., 1990). Thesis area is further south than the southern boundary of this map. Core 96018-06 (red dot) is used for core correlations in Chapter 5.

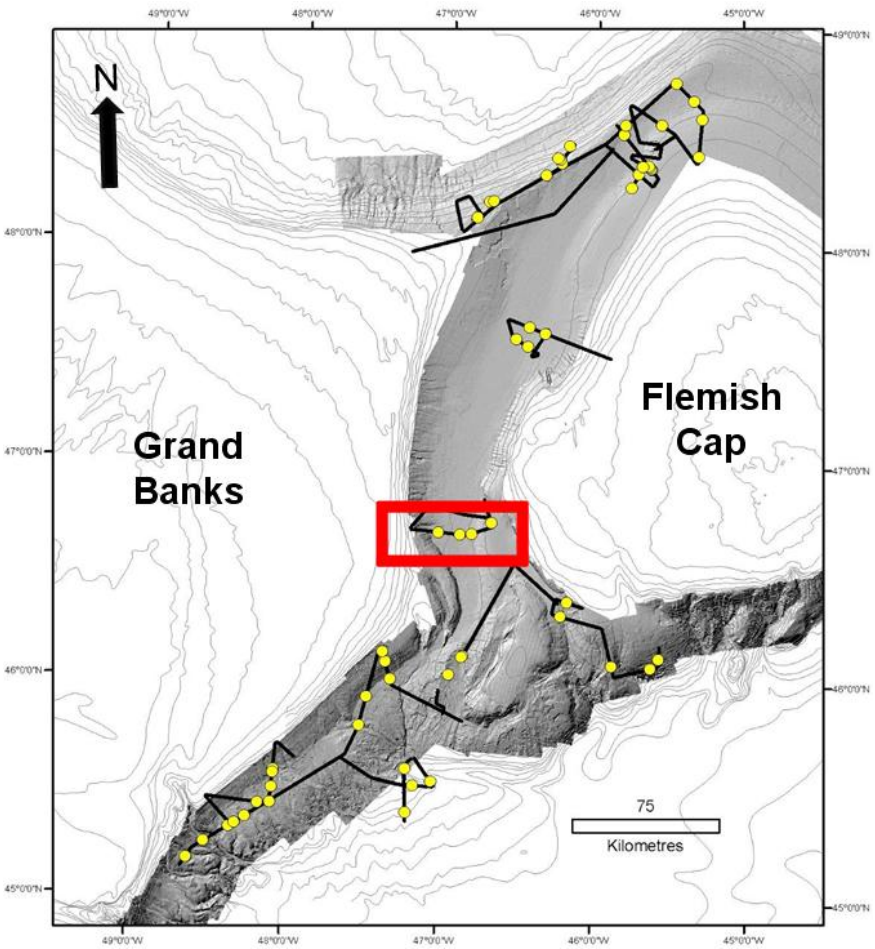

Figure 2.10. Map of Flemish Pass showing the locations where seismic profiles (black lines) and cores (yellow dots) were collected during the HUD2011031 cruise. The red box highlights the seismic profile and the four cores used for this thesis. Multibeam bathymetry is courtesy of the Nereida Program. Modified from Campbell (2011).

A multibeam bathymetry map of the study area was previously presented in Figure 2.2 where Beothuk Drift is clearly shown on the east side of Flemish Pass, intersected by the A-B seismic track line used for this thesis. The Labrador Current flow is swifter on the western side of Flemish Pass, as interpreted from more reflectivity (sand) in the backscatter imagery (Fig. 2.11). There is an obstruction from Flemish Cap basement rock upstream from the Beothuk Drift (Fig. 2.10). This obstructed flow causes drift sedimentation on the eastern side of Flemish Pass, where there is a slower flow and a higher sedimentation rate compared to the central and western side of the pass.

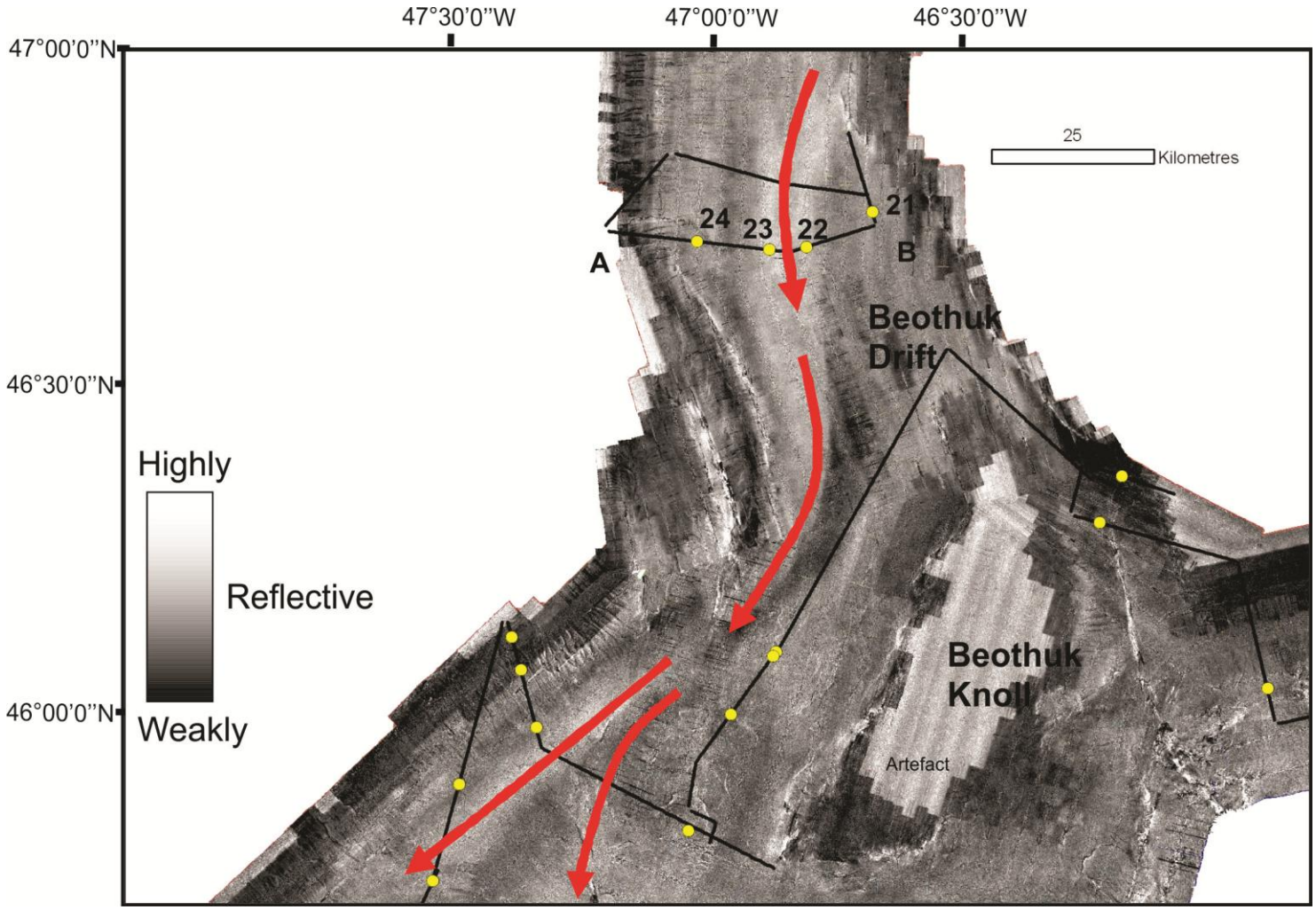

Figure 2.11. Backscatter data of southern Flemish Pass. Backscatter data delineate bottom current pathway. The lighter (highly reflective) seafloor represents a sandier bottom, and where current flow is faster. The darker (weakly reflective) seafloor, such as the Beothuk Drift, is a mud-dominated substrate and is therefore not as reflective.

2.6 Heinrich Layers

There are several Heinrich (H) layers within each core examined for this thesis. H layers are rich in carbonate and ice-rafted-detritus (IRD), as first described by Heinrich (1988) and named after him by Broecker et al. (1992). These H layers were deposited throughout the North Atlantic, and resulted from periodic, intensified iceberg discharges through Hudson Strait (Broecker et al., 1992). The detrital carbonates originate due to glacial erosion of the Paleozoic limestone in the Ungava Bay and in Hudson Bay itself (Andrews et al., 1995). H layers throughout Flemish Pass and the Labrador Sea are dated in the literature (Rashid et al., 2003a; Rashid et al., 2003b; Huppertz & Piper, 2010; Stanford et al., 2011; and others) and are used for paleoclimatic reconstructions because their timing is well constrained. See Table 2.1 for the approximate ages of Heinrich layers identified in this thesis.

A recent study by DeGelleke et al. (2013) concluded that H1 deposition was dominated by plume transport within 1000 km of the Hudson Strait outlet and distal H1 sediment transport was dominated by ice-rafting. Flemish Pass is approximately 2000 km from the Hudson Strait outlet, within the zone of ice-rafting as a dominant method of H1 sediment transport.

Heinrich layer	Age (ka cal)
H1	16
H2	24
H3	30
H4	39
H5	46

Table 2.1. Approximate ages (Rashid et al., 2003a, b; Huppertz & Piper, 2010; Stanford et al., 2011) of Heinrich layers that have been identified in this thesis.

CHAPTER 3: METHODOLOGY

3.1 Shipboard Seismic Collection and Sediment Sampling

The seismic data for this thesis came from the 2011031 cruise on the CCGS Hudson. Using a high-resolution shallow penetration Huntec Deep Tow System (DTS) and lower-resolution deeper penetration airgun, seismic profiles were collected along with numerous long sediment cores. Sediment sampling was conducted using a piston corer (Fig. 3.1). Core (Table 3.1) and profile locations (Fig. 2.10) are based on the multibeam bathymetry collected during the 2009 and 2010 Nereida Program.

Figure 3.1. The piston corer on the CCGS Hudson. Photographed by Calvin Campbell, 2011.

Core (pc and twc)	Latitude (°N)	Longitude (°W)	Water Depth (m)
20110310021	46°45.05990	46°41.04080	991
20110310022	46°42.00540	46°48.90540	1230
20110310023	46°41.71890	46°53.39340	1251
20110310024	46°42.25070	47°02.13700	1184

Table 3.1. Core locations and water depths.

3.2 Core Processing

Detailed standard laboratory procedures are found in Tripsanas et al. (2007). The four long cores were split in halves using a splitter (Fig. 3.2) at the GSC Atlantic Core Processing Laboratory. The splitter cut the plastic liner of each core longitudinally. The sediment in the core was then split along the cuts in the plastic liner by pulling a piece of fine wire through the sediment. The core halves were designated as archive and working halves. They were covered in plastic wrap and each half was labelled with an up arrow, cruise number, sample number and section, and metre tape was placed along the side of each half, indicating down-core depth. The archival half was photographed and described visually. The colour of the core was estimated using the Munsell colour system chart. The working half was immediately measured for physical properties (shear strength (see Fig. 3.3 for a photograph of the shear vane used), P-wave velocity, and additional discrete samples were extracted to calculate bulk density and water content). These physical properties change as the core dries.

Figure 3.2. The core splitter in the GSC Core Processing Laboratory.

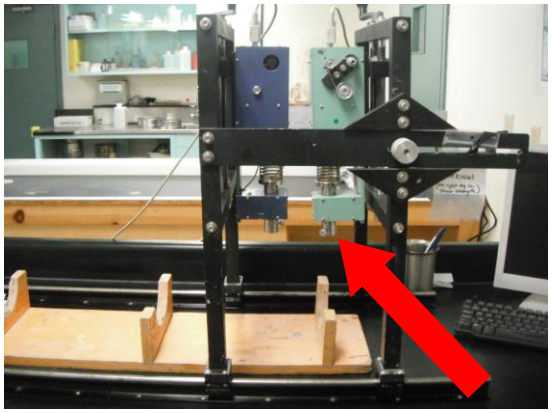

Figure 3.3. Shear vane (arrow) used to measure shear strength of the sediment in the cores.

Core X-ray and Multi-Sensor Track (MST) data were used to study the cores after splitting. X-ray imaging allows for core evaluation and assessment of sediment structure and composition, not necessarily visible at the split core surface. The X-ray machine in the GSC Atlantic Core Processing Laboratory yielded images that were displayed using the software program ImagePilot by Konica Minolta. Following X-ray imaging, the archive halves of the core sections were run through the MST for measurements of p-wave velocity, bulk density by gamma ray attenuation, and magnetic susceptibility at a 1 cm down-core resolution using the Geotek MST Core Logger (Fig. 3.4). P-wave velocity was determined using a velocimeter, which measures longitudinal and transverse velocity of sound waves passing through the sediment. Magnetic susceptibility measures sediment response to an induced magnetic field. A spectrophotometer on the MST was used to measure sediment colour numerically. The L* (lightness) value is a ratio of white-black, a* (chroma) value is a ratio of red-green, and b* (hue) value is a ratio of blue-yellow. These ratios give colour profiles that help with the identification of Heinrich layers and red beds. Lastly, both core halves were rewrapped in plastic, sealed

in plastic core sleeving, labelled in plastic D-tubes and stored in the GSC Atlantic Core Repository.

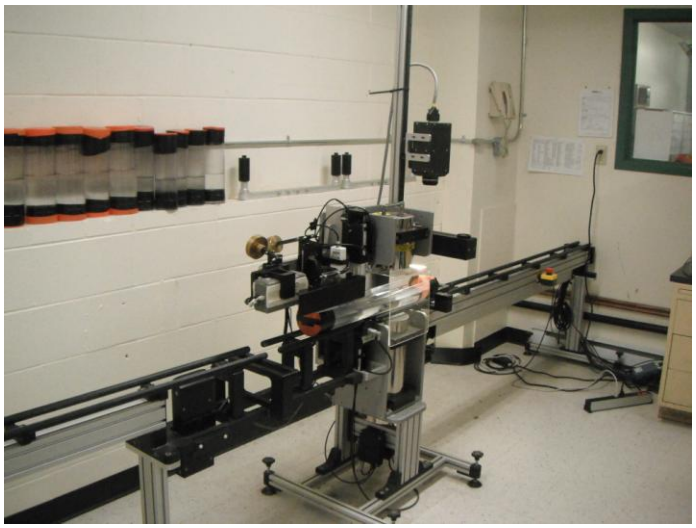

Figure 3.4. The Geotek Multi-Sensor Track (MST) Core Logger. This machine was used for spectrophotometer measurements, bulk density, p-wave velocity, magnetic susceptibility, high resolution photography and XRF measurements.

3.3 Coulter Laser Grain-Size Studies

Grain-size data for this study were acquired with the Beckman Coulter LS230 Laser Diffraction Particle Size Analyzer (0.04-2000 µm) (Fig. 3.5) in the Sediment Laboratory at the GSC Atlantic. The 750 nanometer wavelength laser light becomes diffracted by particles in the water column within the device and when the sample was added it scattered the incident light through the water in a characteristic pattern (a diffraction pattern) dependent on size (Beckman Coulter, 2011). Using a Fourier lens to focus the light, the moving diffraction patterns of the particles changed into a stationary composite pattern using time-averaging, which is then used to measure the particle size distribution (Beckman Coulter, 2011).

Working halves of core 0021 (Figs. 3.6 & 3.7) were subsampled every 40 cm, and 20 cm within carbonate-rich (Heinrich) layers, and the samples were mixed with water and put into the Coulter laser for grain-size analysis. The processed data obtained from this analysis are plotted in terms of sortable silt percent (SS %) down-core, where SS % is the volume percent of sediment in a sample with a 10-63 µm diameter.

Figure 3.5. The Coulter laser in the GSC Sediment Laboratory. The sample, once mixed with water in a beaker, goes into the laser by pouring it into the column identified by the red arrow. Photographed by Owen Brown, 2012.

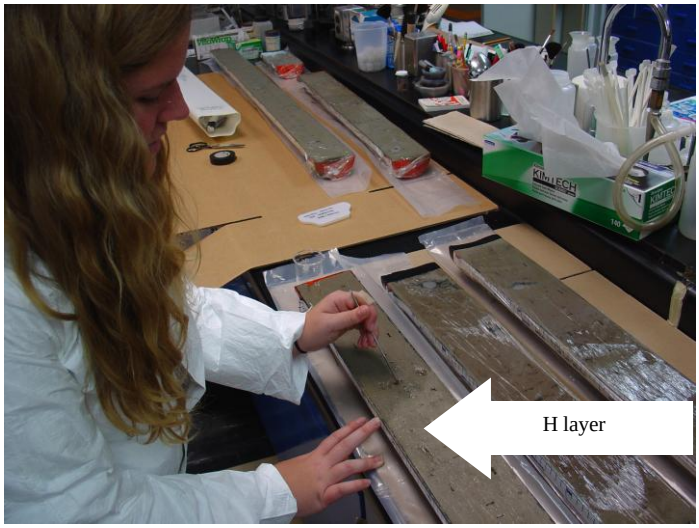

Figure 3.6. Taking a grain-size subsample in 0021pc, directly above a Heinrich layer. Photographed by Owen Brown, 2012.

Figure 3.7. Close-up of the subsample being taken above a Heinrich layer shown in Figure 3.5. Photographed by Owen Brown, 2012.

The dynamics of sediment erosion, deposition and aggregate breakup suggest that fine sediment is cohesive below diameters of 10 µm, and noncohesive above (McCave et al., 1995). Silt sizes greater than 10 µm display size sorting in response to flow processes and these silts and their properties can be used to infer relative current strength (McCave et al., 1995). The basis for designating the 10-63 µm fraction as sortable silt is because it is sorted by its primary particle size, whereas finer silt is not since it occurs in aggregates (McCave, 2008). Since short-term flow events last hours to days, they cannot usually be resolved and the information gained from the sortable silt fraction represents information on average current speed (Hass, 2002).

McCave and Hall (2006) demonstrated that, while both the Coulter laser and the Sedigraph provide grain-size analysis, the major benefit to using the Coulter laser is the speed at which this procedure can be completed. The Sedigraph is the instrument of choice for the study of deep-sea sediments when obtaining proxies for current intensity because it is more accurate within the 1-70 µm range (McCave & Hall, 2006). However, the Coulter laser gives more timely results and is the only instrument capable of a wide

spectrum analysis and provides accurate results where SS % is generally >40 % (McCave & Hall, 2006). The weakness of the Coulter laser is that it fails to accurately measure the SS <30 μm fraction because it is influenced by the platy shape of clay and fine silt particles. This results in these particles being assessed as the same size as coarser equant grains, which affects the size distribution up to 30 μm (McCave & Hall, 2006). For this thesis, the Coulter laser weakness is not a concern because of the high SS %.

3.4 X-ray Fluorescence

X-ray fluorescence (XRF) is a diagnostic technique that can be used to detect and measure elemental abundances (Geotek, 2011). Fluorescence is the phenomenon of absorbing incoming X-rays, causing individual elements to fluoresce or re-radiate lower-energy X-rays (Murphy et al., 2010). XRF is caused by incoming X-rays that eject high-energy electrons from the innermost-electron shells of atoms (Murphy et al., 2010). The atom is now unstable, causing an electron from an outermost shell to fill in the place of the ejected electron. This 'dropping in' releases a specific amount of energy in the form of a characteristic X-ray (Murphy et al., 2010). Thus, by analyzing the energies of the spectrum of fluorescent X-rays emitted, the elements present and their concentrations in the substance (e.g. core) can be determined (Murphy et al., 2010).

XRF was completed for 0021pc, using the Geotek MST Core Logger (Fig. 3.4). XRF was completed in soil mode using Beam 2 and Beam 3 (Table 3.2). Each beam was used for 30 seconds at every 1 cm depth interval.

Soil			
Beam 2		**Beam 3**	
Primary	Secondary	Primary	Secondary
Fe	Ti	P	V
Co	V	S	Fe
Ni	Cr	Cl	
Cu	Mn	K	
Zn	W	Ca	
Hg	U	Ti	
As	Sr	Cr	
Se	Zr	Mn	
Pb	Th		
Bi	Mo		
Rb	Ag		
	Cd		
	Sn		
	Sb		

Table 3.2. The elements analyzed in 0021pc using XRF.

3.5 Detrital Volcanic Geochemistry

A 10 g subsample from piston core 0022 between 4.11 and 3.99 m, where there is a moderately sorted unit of volcanic lapilli tuff, was taken in order to geochemically analyze it for major and trace elements. The subsample was first washed to remove the <63 µm fraction. The rest of the sample was wet sieved through a 500 µm sieve so that the <500 µm fraction was removed. The coarse fraction (>500 µm) was sieved through the 1 mm sieve to obtain only the coarse fraction (>1 mm). The sample was examined with the binocular microscope. Any fragments that were not basalt (e.g. quartz) were excluded from the sample. The sample was crushed to finer than 150 µm. Once 4 g of crushed sample was obtained, it was put in a vial and sent for analysis of major and trace elements using inductively coupled plasma mass spectrometry (ICP-MS), following methods 4B, 4B1 and 4B2 of Activation Laboratories (2011). The returned geochemical data were plotted using the software program MinPet to make a total alkalis vs. SiO_2

(TAS) diagram, a rare earth element (REE) plot and a spidergram. These data were compared with other volcanic rocks in the North Atlantic, to help yield a possible source of the volcanic lapilli tuff found in Flemish Pass, providing another piece of evidence for ocean circulation in glacial times.

Another cleaned volcanic sample was obtained from the same depth interval and this sample was grain-mounted onto a thin section with epoxy, giving a polished thin section. The petrographic characteristics were described using a petrographic microscope, in the Department of Earth Sciences, Dalhousie University.

CHAPTER 4: RESULTS

4.1 Seismic Profiles

The airgun profile (Fig. 4.1) provides context for the Flemish Pass area by displaying a low-resolution, deep penetration view of the seafloor, extending well below the piston core depths. DTS Huntec profiles (Fig. 4.2) have a high-resolution, shallow penetration view of the seafloor. The airgun profile shows a buried mass-transport deposit (MTD) on the Grand Banks side and an apparent draping of sediment across the pass to the Beothuk Drift. This drift is nearly 200 m in height and several kilometers (>15 km) across. All four cores penetrate broadly blanketing sediments across Flemish Pass.

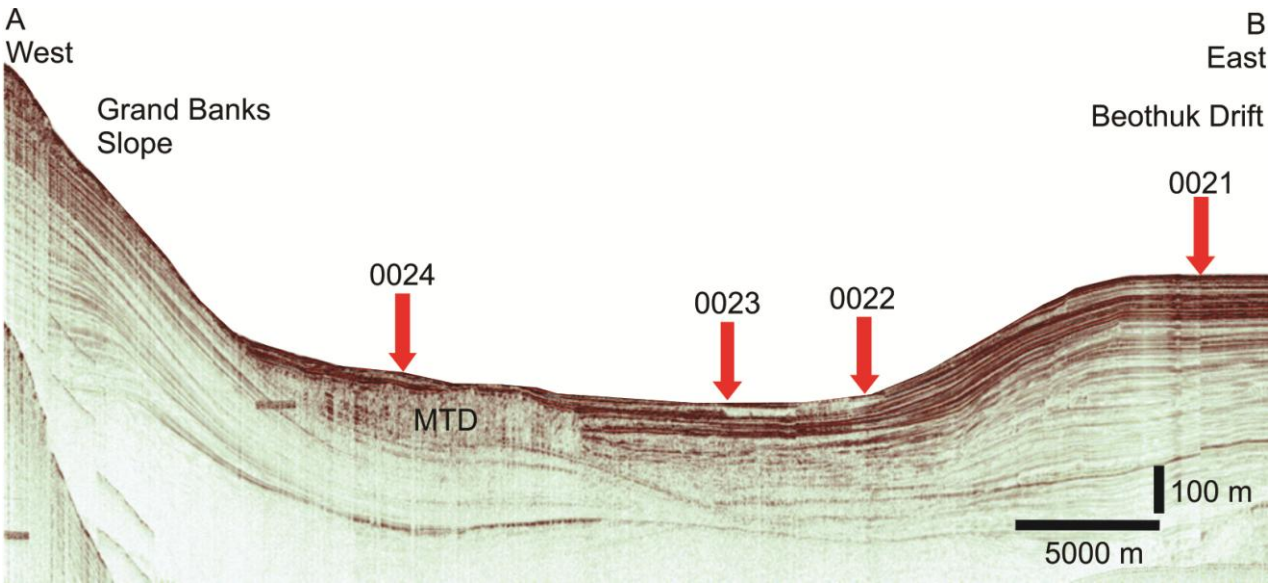

Figure 4.1. The airgun seismic profile showing the core locations (red arrows). The airgun allows a view of the seafloor geometry that is deeper than the piston cores penetrate.

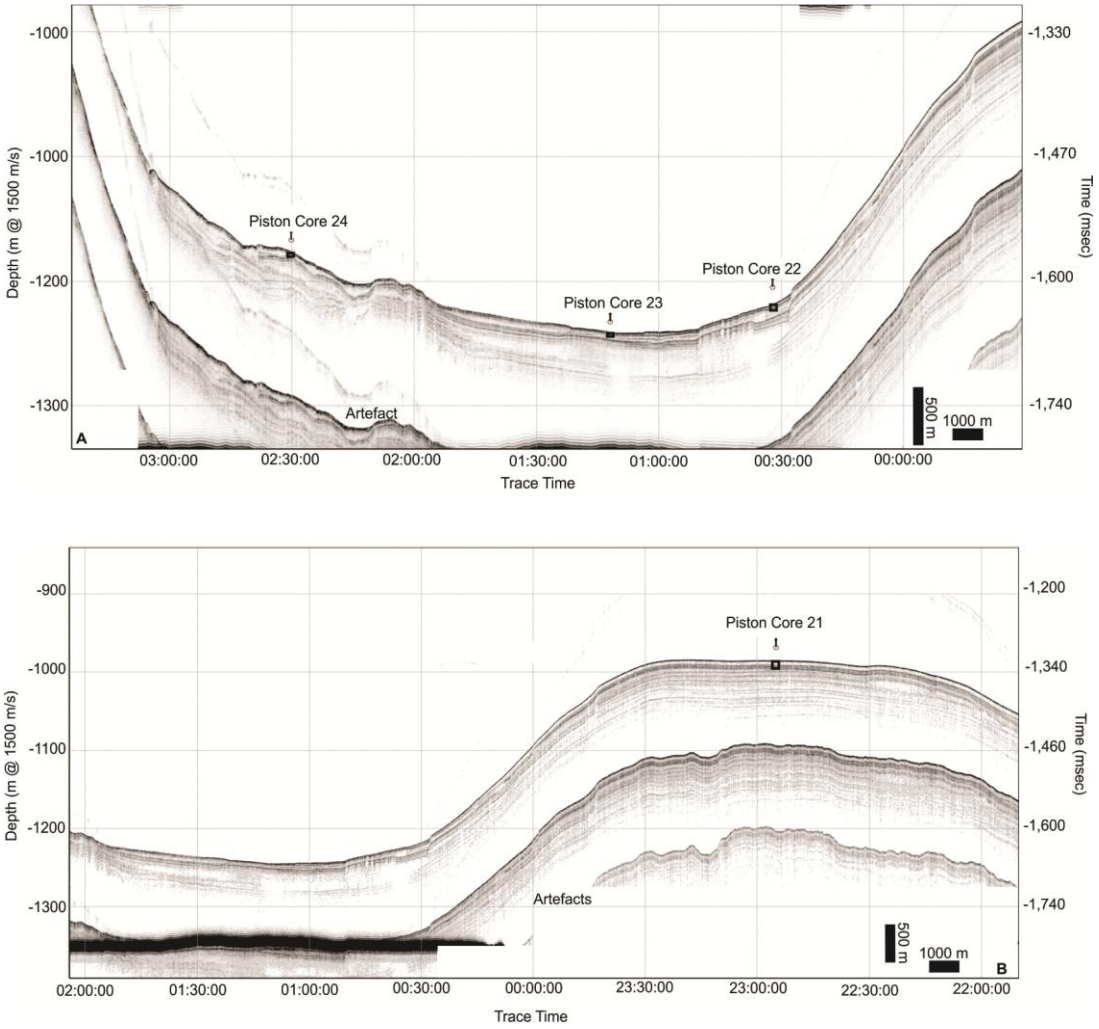

Figure 4.2. The DTS Huntec seismic profiles showing the approximate core locations with the boxes indicating the approximate depth of core into the subsurface.

Core 0021 penetrates the top of the drift. Core 0022 is at the foot of the drift, where there was a small slope failure and buried MTD at depth. Core 0023 penetrates into an area of highly reflective horizons, where erosion is prominent. Core 0024 is at the foot of the Grand Banks slope and penetrates a horizon dominated by mass-transport deposits. From A to B (Figs. 4.1 and 4.2), across the transect of cores, the seafloor changes to more draping sediments with progressively thicker accumulation moving

into the Beothuk Drift on eastern Flemish Pass. The cores consist predominantly of sand on the floor of Flemish Pass and mud on the drift.

4.2 Down-Core Properties

Appendix A provides compiled images of high-resolution core photographs and Appendix B shows compiled X-ray images. Down-core physical properties and spectrophotometry plots for all piston and trigger weight cores are located in Appendix C. MST split core measurements, spectrophotometer colour, core 0021 XRF and grain-size measurements are provided in Appendices D-G, respectively. The other cores do not have grain size and XRF measurements due to time constraints.

Piston core 0021 is shown in Figure 4.3 with spectrophotometry L* and a* colour values. The XRF Ca and Fe data (in ppm) are also plotted down core (Fig. 4.3). There are significant variations in L*, a*, Ca and Fe throughout 0021pc. The increases in L*, a* and Ca with the decreases in Fe correspond to tan-coloured sections in the core. The a* colour in places correlates with the L* colour and in places also shows independent peaks. These a* peaks where L* does not peak, are at locations of red beds, where a* peaks correspond to increased Fe. These data can be further compared with physical property measurements that are plotted with spectrophotometry plots as provided for all cores in Appendix C.

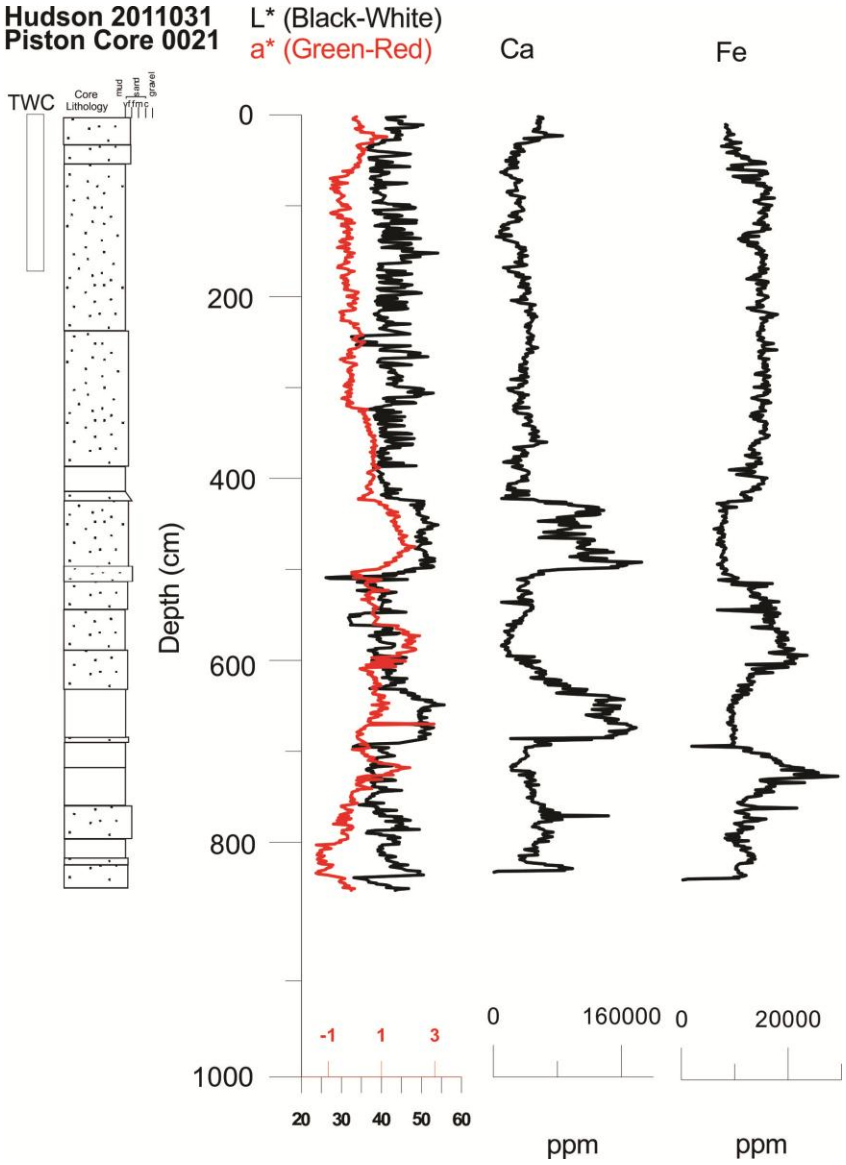

Figure 4.3. Core 0021pc is shown with the spectrophotometry colour data and XRF (Fe and Ca) measurements. Note: Core lithology legend: sand/silty sand/sandy silt is represented by dots, and no symbols represent silt/silty clay. This legend holds true for all core lithology columns in this thesis.

Figure 4.4 highlights the spectrophotometry values for piston cores 0021-0024. The L* and a* simultaneous peaks allow for the identification of Heinrich layers (Chapter 5) within the cores, which were noted during initial core descriptions.

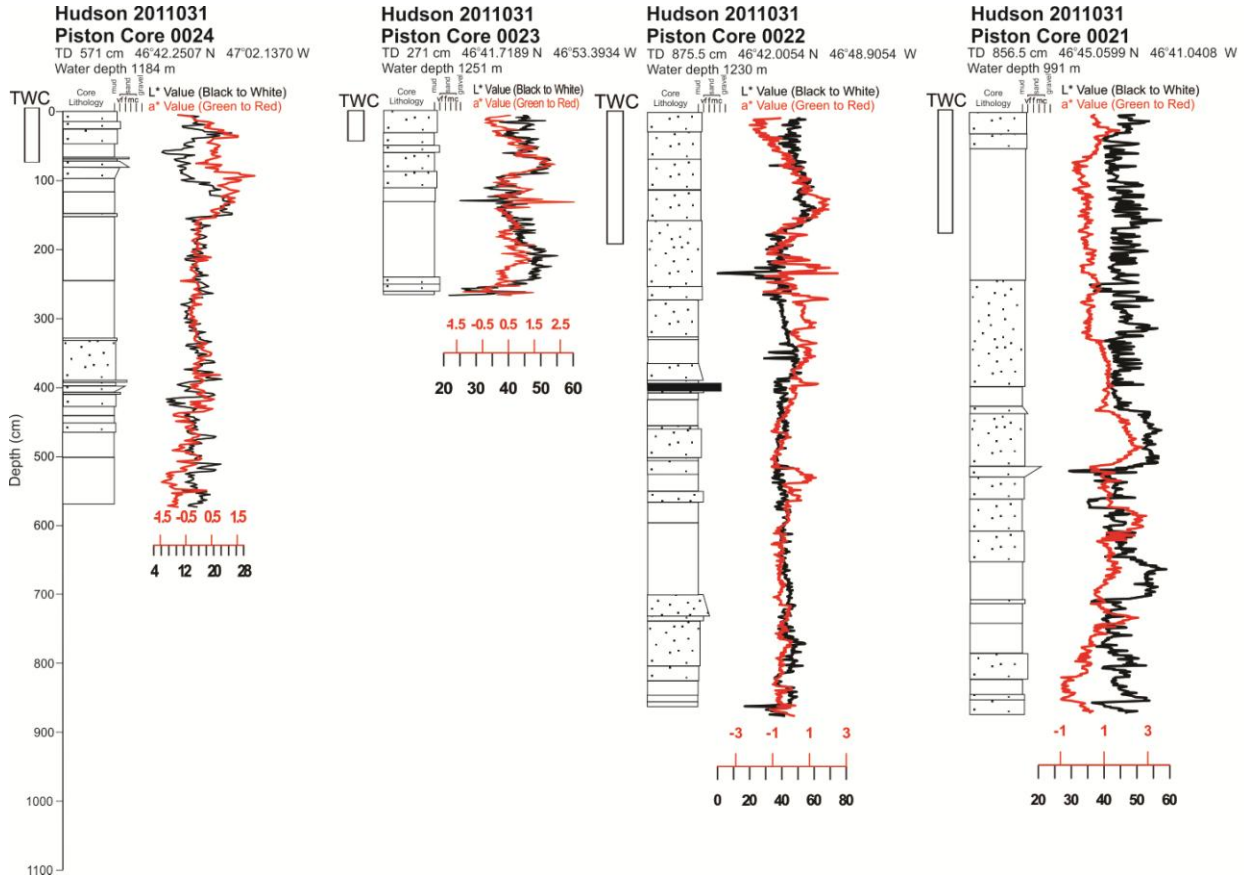

Figure 4.4. Cores 0021pc-0024pc with spectrophotometer L* and a* values.

4.3 Grain Size

Sortable silt percentage (SS %) data for piston core 0021 are found in Appendix G and are plotted in Figure 4.5. SS % in 0021pc in the bottom 3.56 m, excluding the carbonate-rich interval from 6.92-6.34 m, ranged from 32-41 %, averaging 36 %. In the top 4.00 m of 0021pc, SS % ranged from 43-57 % with an average of 48 %.

The highest SS % throughout 0021pc is at the seafloor (0 cm) with 57 SS %. Within the 0021pc carbonate-rich intervals (6.92-6.34 m and 5.00-4.20 m) there are significant variations in SS %, particularly prevalent are the SS % decreases at 5.00 m and 4.20 m.

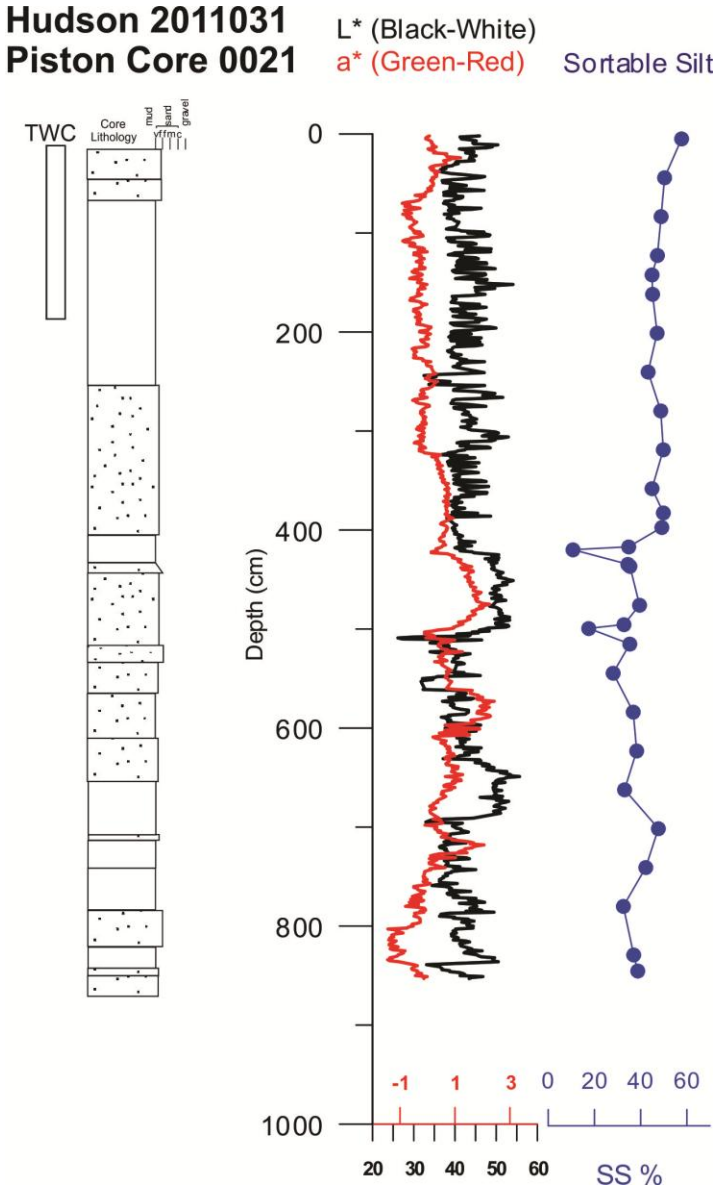

Figure 4.5. Core 0021pc plotted with spectrophotometry colour data and sortable silt (volume) %.

It appears that the L* and SS % curves have similar trends down-core, with the exception of a carbonate-rich interval from 6.92-6.34 m. The SS % trend generally follows L*, suggesting that the SS % is influenced by IRD, particularly at 4.20 m and 5.00 m. Hass (2002) highlights that misinterpretations in current strength may occur when IRD is present, whether or not it forms part of the silt or clay fractions, which is discussed in Chapter 5.

4.4 Volcanic Lapilli Tuff Layer

At a depth of 4.11-3.99 m below the seafloor in core 0022pc, at the foot of the Beothuk Drift, there is a layer of volcanic lapilli tuff. This interval is highlighted in Figure 4.6 and is directly below the second carbonate-rich layer beneath the seafloor and above the third. These carbonate- and IRD-rich layers have been identified as Heinrich layers (Chapter 5). The volcanic unit has an erosive base (Fig. 4.7), is a graded bed and moderately sorted throughout.

Using the binocular microscope at the GSC Core Processing Laboratory, initial assessments indicate that this sample is volcanic based on the abundance of vesicles. Glassy fragments are also visible. Looking at the thin section (Fig. 4.8) under the petrographic microscope it is clear that the sample is rich in glass, with individual fragments and textures visible at a high magnification. There are brown glassy areas that have elongated and stretched gas bubbles (Fig.4.8). There is a uniaxial fragment (not pictured) of what appears to be calcite, likely from the layer either above or below this volcanic unit.

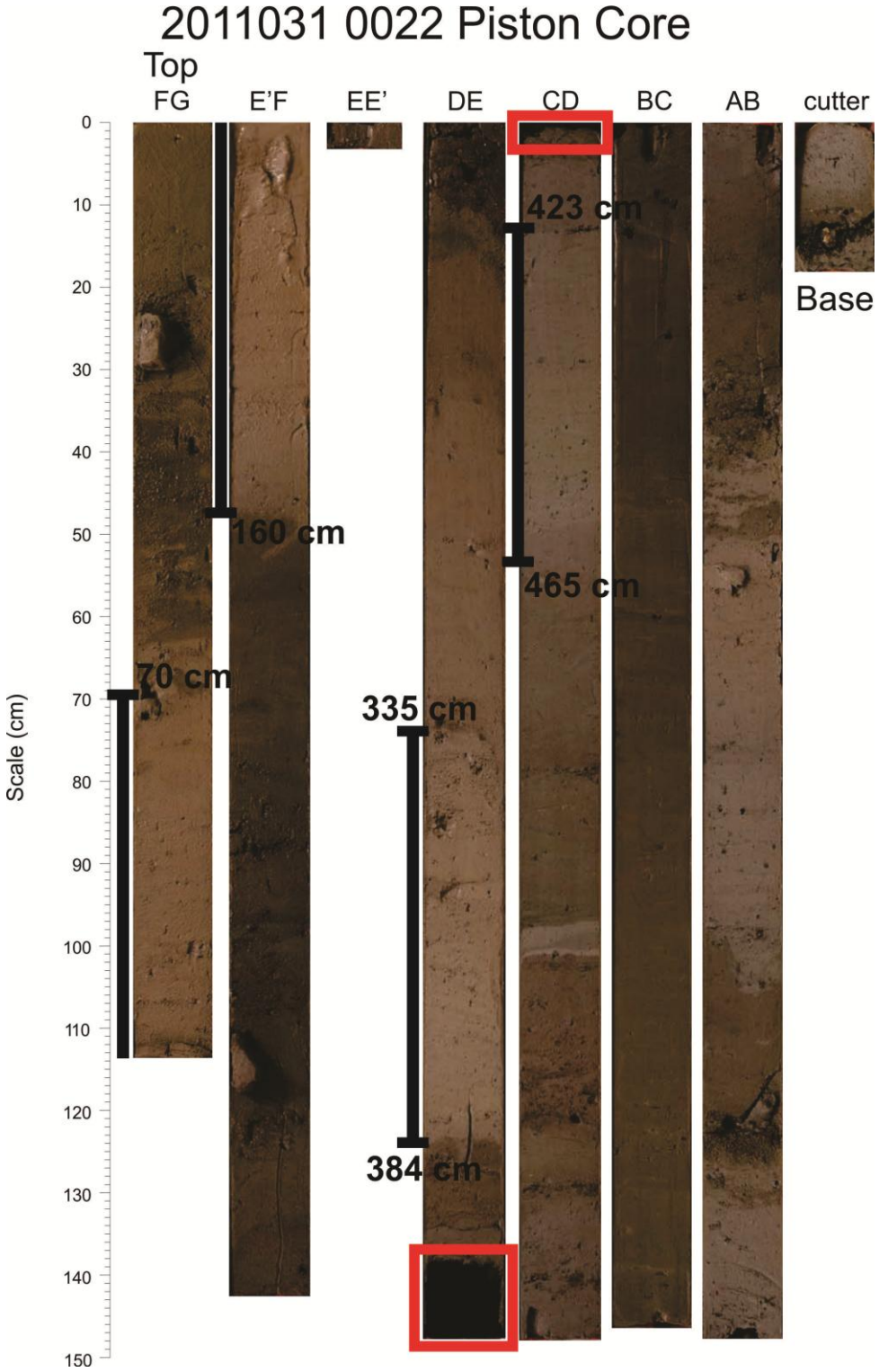

Figure 4.6. Compiled image of all 0022pc sections. The youngest three carbonate-rich intervals are noted by the black bars and the volcanic lapilli tuff unit is highlighted by the red boxes. The volcanic base is at the very top few centimeters of section CD whereas most of the lapilli tuff is at the base of section DE.

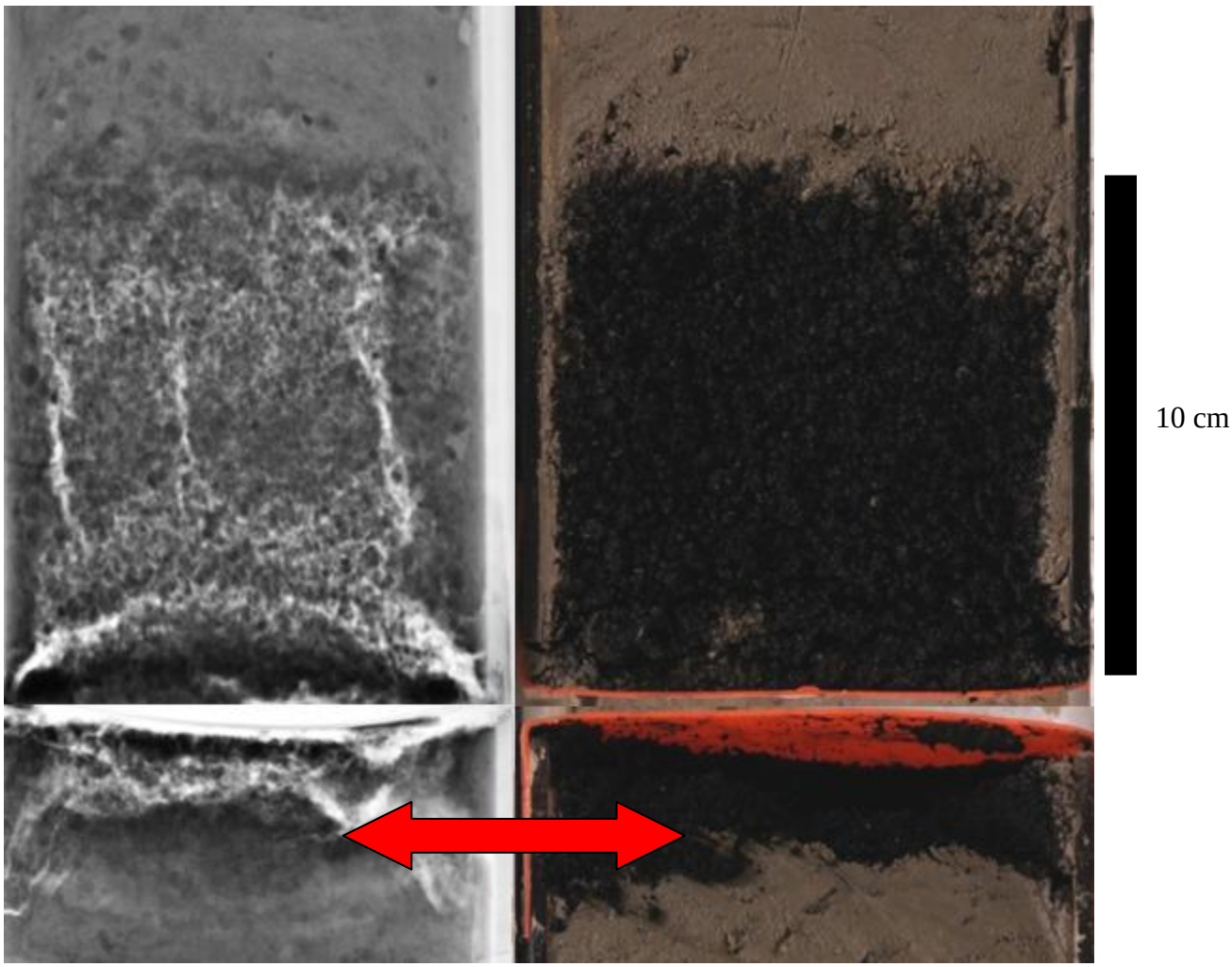

Figure 4.7. Left: X-ray image of the volcanic lapilli tuff. Right: High-resolution image of the volcanic lapilli tuff. Note the erosive base, as indicated by the double-ended arrow.

A sample of this volcanic unit was prepared and sent to Activation Laboratories for geochemical analysis. The geochemical data (Appendix H) are illustrated in three figures, a TAS diagram (Fig. 4.9), an REE plot (Fig. 4.10) and a spidergram (Fig. 4.11). The TAS diagram (Fig. 4.9) confirms that this sample is basalt, and the spidergram (Fig. 4.11) shows it is highly alkaline.

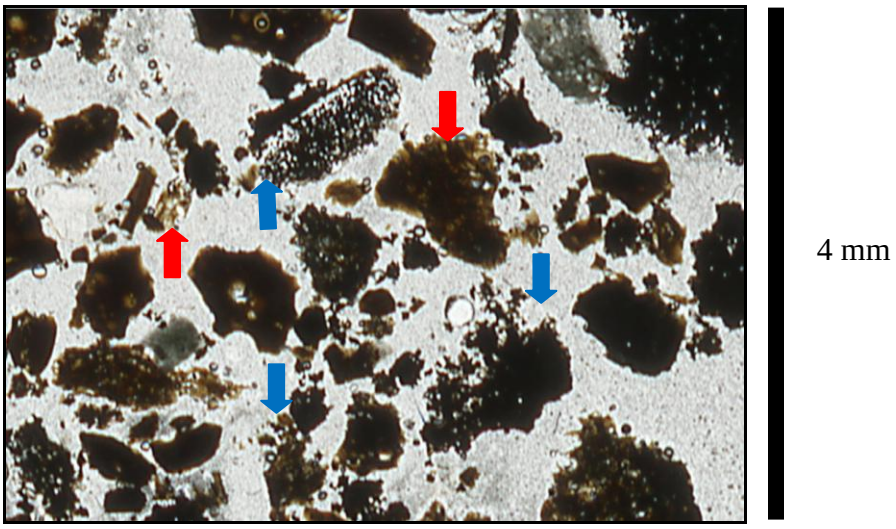

Figure 4.8. The grain-mounted thin section of the volcanic lapilli tuff highlighting elongated bubbles (red arrows) and bubble escape features (blue arrows).

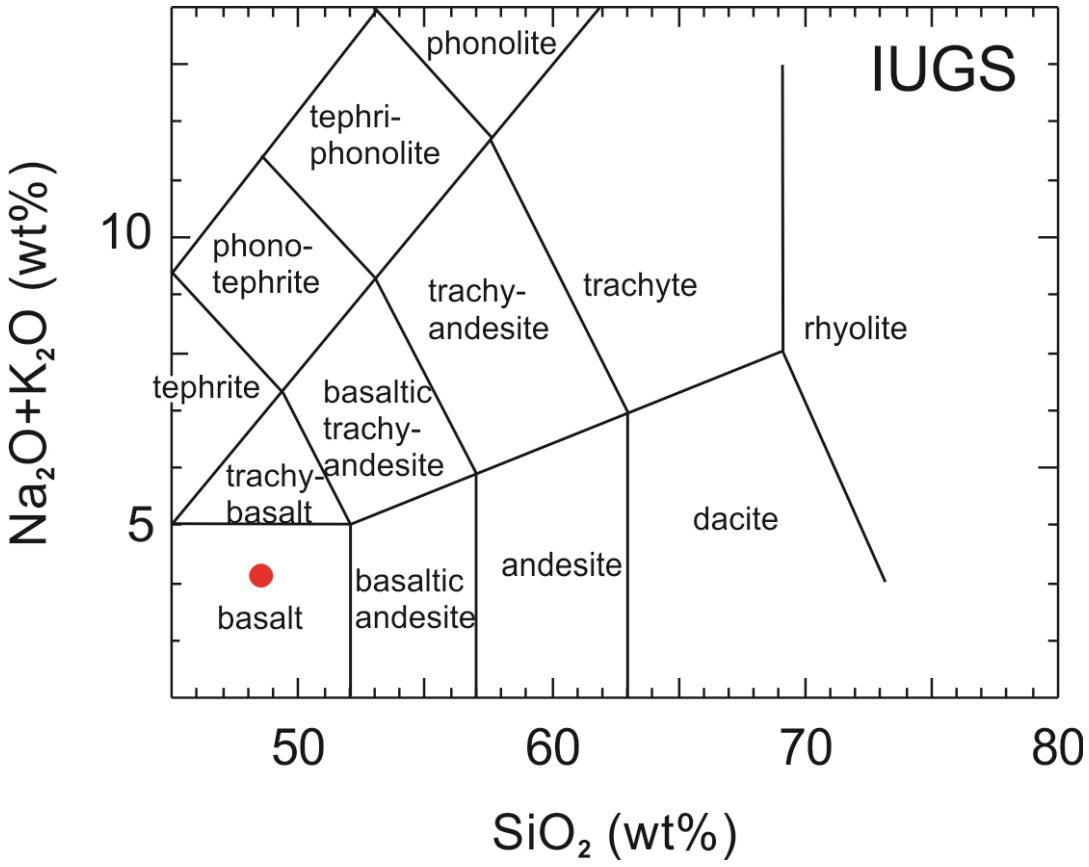

Figure 4.9. A total alkalis vs. SiO_2 (TAS) diagram (Le Bas et al., 1986) from the International Union of Geological Sciences (IUGS) classification scheme showing that the volcanic sample in 0022pc (red dot) is a basalt.

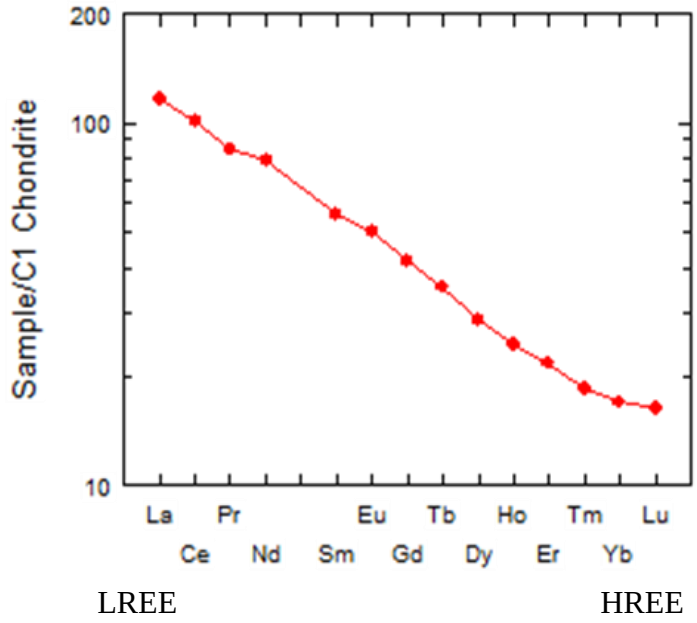

Figure 4.10. REE plot of the geochemical results of the basalt sample from 0022pc. The left section of the x-axis is the relatively light rare earth elements (LREE) and the right section of the x-axis is the relatively heavy rare earth elements (HREE). C1 Chondrite concentrations are from Sun and McDonough (1989).

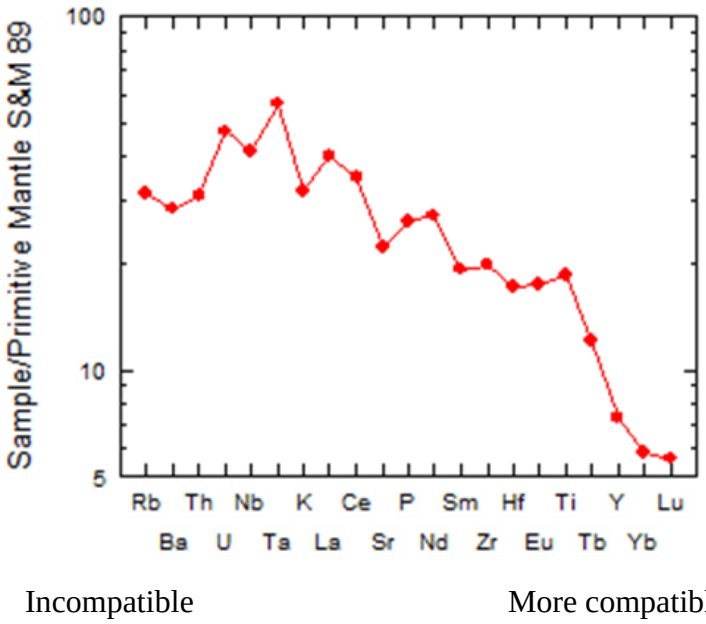

Figure 4.11. Spidergram of the geochemical results of the basalt sample from 0022pc. The left part of the x-axis is the relatively incompatible elements and the right section of the x-axis is the relatively compatible elements. Primitive mantle concentrations are from Sun and McDonough (1989).

CHAPTER 5: DISCUSSION

5.1 Identification of Heinrich Layers

Heinrich layer identifications are most readily achieved using the L* and a* peaks (Fig. 5.1), and can be further confirmed with down-core physical properties, XRF, core descriptions and core photography. A red mud (between H2 and H1) aided in correlation (Fig. 5.2) and represents deposition during the LGM (Tripsanas & Piper, 2008). Heinrich layer identifications for H3-H1 are reliable and H4 and H5 Heinrich layer identifications are speculative (Fig. 5.1) and require further work beyond the scope of this thesis.

The H layer identifications do have a margin of error based on human error picking the top and base of each H layer when it is limited by the resolution of the spectrophotometer peaks. It was occasionally unclear when the peaks started and ended in order to assign a top and base for each Heinrich layer, so the core photography (Appendix A), X-ray photography (Appendix B) and core descriptions (not provided, but accessible at the GSC Core Processing Laboratory) provided additional constraints regarding the top and base of each H layer in all four cores.

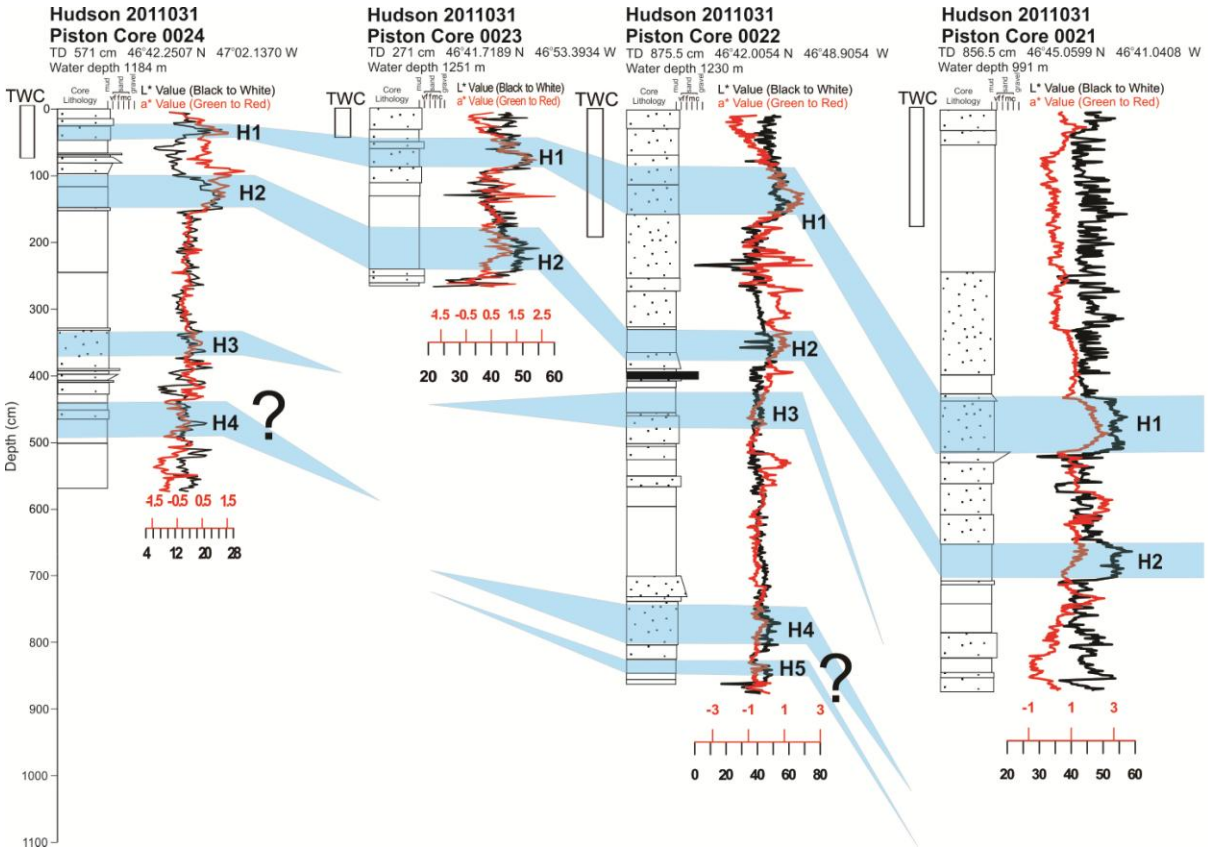

Figure 5.1. The four piston cores correlated together based on Heinrich layer identifications.

5.2 Core Correlations

Core correlations in the transect across Beothuk Drift, with each other and with previously correlated and dated cores in Flemish Pass, are important to establish an age model. In particular, correlation assists in identifying specific Heinrich layers in cores 0021-0024. Core 96018-06 (47°44.73000 N, 46°12.18780 W) (Fig. 2.9), which has been dated previously (Huppertz, 2008; Huppertz & Piper 2010), has radiocarbon dates that were recalibrated (Table 5.1) and used this core was used as a dated reference core to establish which H events correspond to peaks in core 0021 (Fig. 5.2). This correlation (Fig. 5.2) matches the 0021pc XRF calcium peaks and peaks in L* and a* spectrophotometry with 96018-06 $CaCO_3$ peaks and L* and a* spectrophotometry. Core

87008-013 (47°00.70020 N, 46°42.07020 W) (Fig. 2.1) adds additional spectrophotometry correlation as a dated reference core using updated calibrated radiocarbon dates (Table 5.1) by providing further evidence that H1 and H2 have confidently been identified in 0021pc. Core 96018-06 is not from a contourite deposit and does not exhibit high sedimentation seen in the other cores in Figure 5.2, which are closer in proximity. The first prominent peak of Ca, L* and a* has the age of H1 (16 ka). Refer back to Table 2.1 for the approximate Heinrich layer ages. Assumptions with these correlations to dated reference cores include that the H layers are represented in each core and are found in every core in the region, which is logical given the large sediment supply to the study area during Heinrich events. Within the shallow seismic interval that the cores penetrate, there is no evidence of erosion throughout Flemish Pass on a scale commensurate to the typical Heinrich layer thicknesses, so there is no evidence of enough erosion to completely erode H layers. Additionally, DeGelleke et al. (2013) showed the distribution of H1 everywhere along the Grand Banks deep-water margin. Published core summaries (e.g. Piper & Skene, 1998) suggest that the H2 distribution map would be similar.

Selected radiocarbon dates in Flemish Pass					
core	^{14}C age (BP)	calibrated age (2σ)		depths [cm]	lab no.
87008-013	11900 ± 110	13228	249	75	UCIAMS 94006
87008-013	13120 ± 100	14746	492	597	UCIAMS 98025, TO-7924
87008-013	23130 ± 190	27294	642	920	UCIAMS 98026, TO-7925
96018-06	17860 ± 60	20566	412	207	UCIAMS 121186
96018-06	24940 ± 140	29226	457	386	UCIAMS 121189
96018-06	26250 ± 170	30538	360	440	UCIAMS 121190

Table 5.1. Reservoir corrected ages from cores 87008-013 (Piper & Pereira, 1992; Huppertz, 2008) and 96018-06 (Huppertz & Piper, 2010). Calib v. 6.0 was used to calibrate ^{14}C ages and the local delta R (reservoir correction) used was 144 ± 38 (McNeely et al., 2006).

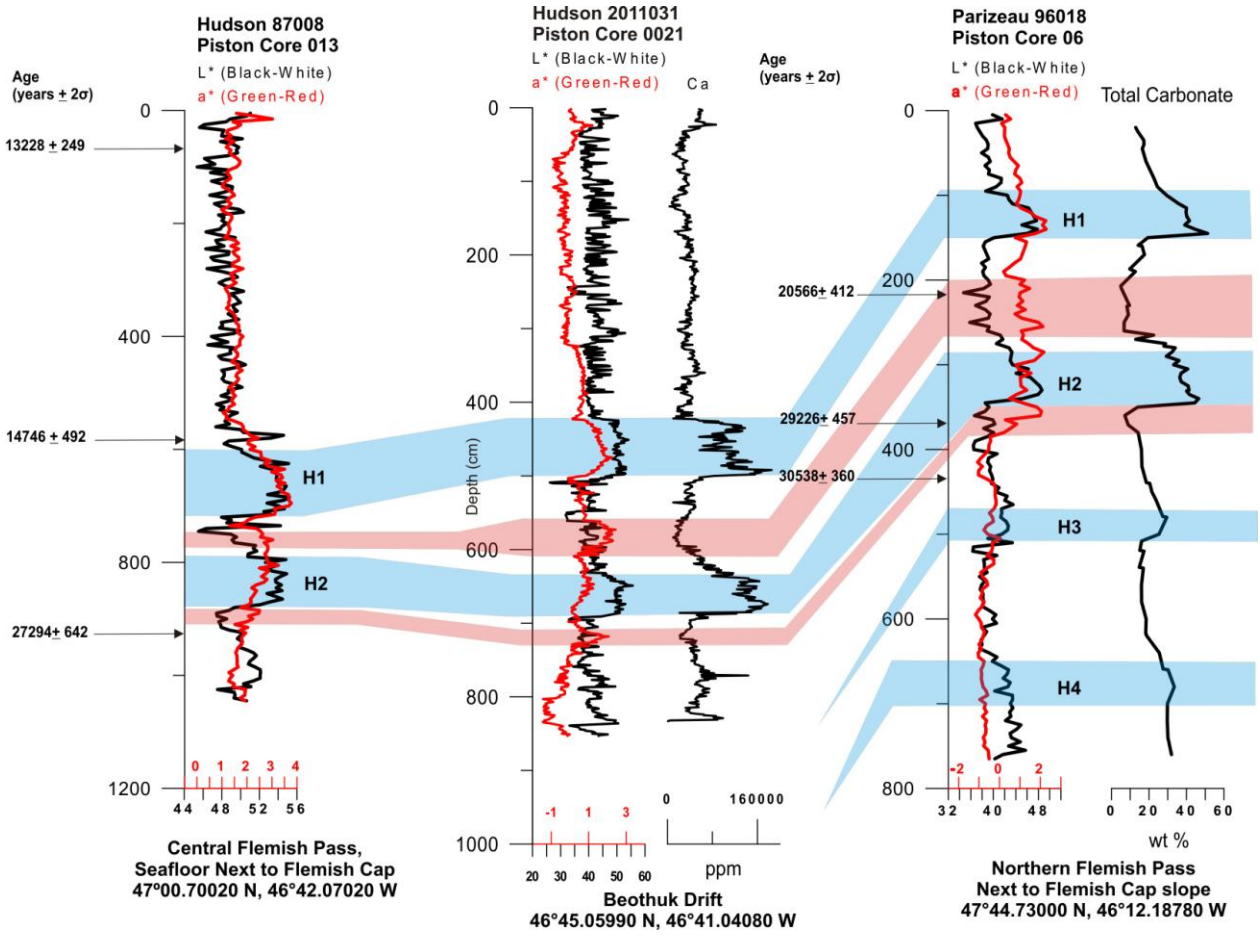

Figure 5.2. The 0021pc spectrophotometry colour plot and XRF Ca plot correlated to spectrophotometry colour and $CaCO_3$ measurements made down-core for core 96018-06, from northern Flemish Pass, and spectrophotometry from 87008-013, from Central Flemish Pass. All reported dates are calibrated (Table 5.1) and Heinrich layers have undergone reclassification from the original correlations for core 96018-06. Cores 96018-06 and 87008-013 were chosen for their proximity to 2011031-0021 and their stratigraphy is consistent with other dated cores throughout Flemish Pass. (87008-013 data is from Huppertz, 2008 and 96018-06 data is from Huppertz & Piper, 2010).

5.3 Age Model

An age model relates depth in core with time. The known ages of H layers (Table 2.1) allows an age model to be developed for core 0021pc (Fig. 5.3). This age model shows the relative change in the Labrador Current flow since nearly H3 (30 ka) based on Heinrich layer identifications and SS % in 0021pc from the Beothuk Drift. H3 is not seen in 0021pc. Future improvements to this model should include better age control, particularly for the most recent 16 ka. The samples at the base and top of H1 contained coarse IRD, skewing the results at those depths to have low percentages of sortable silt, which cannot be used to infer current strength.

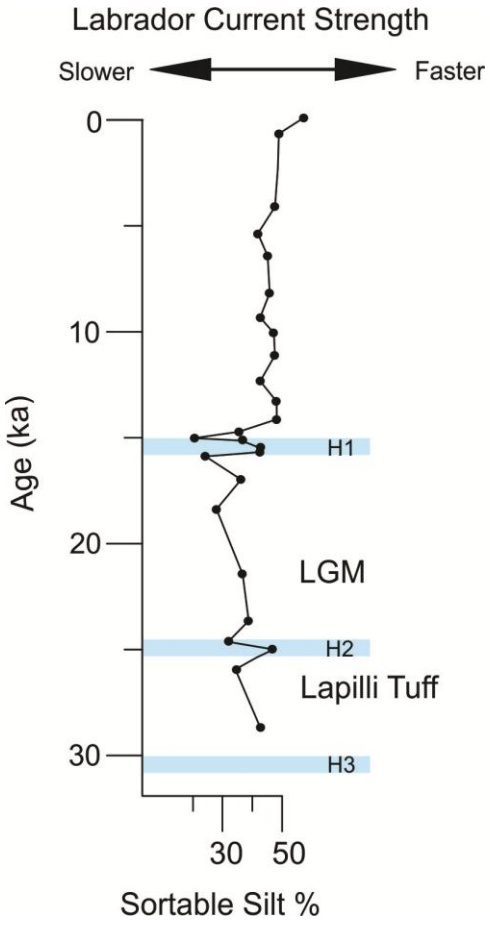

Figure 5.3. An age model for the Labrador Current using sortable silt % plotted against age. The Labrador Current strength axis is a relative change and cannot be used to infer flow velocity. This age model is based solely on H layers and all other intervals are based on extrapolation.

5.4 Sedimentation Rates

H layers can be correlated together and examination of these correlations with the age model yields approximate sedimentation rates, in mm/ka, between the identified Heinrich layers (Fig. 5.4), and within the Heinrich layers (Fig. 5.5), based on layer thicknesses. See Table 5.2 for sedimentation rate calculations.

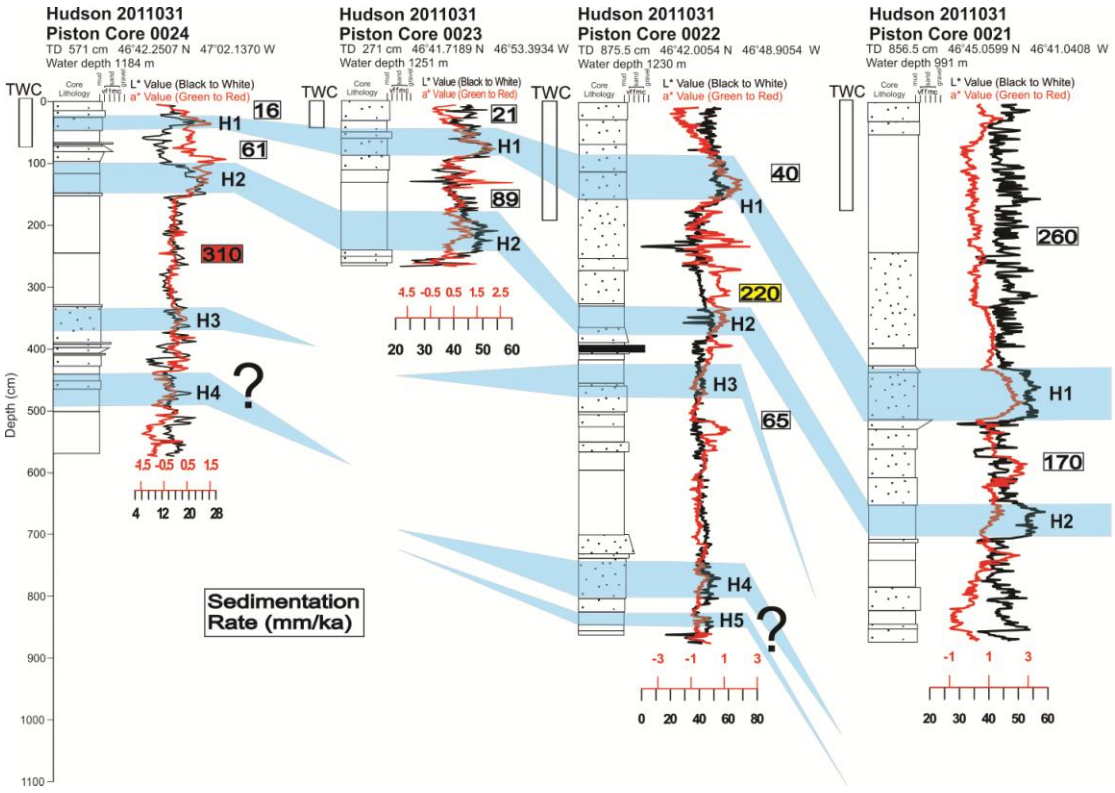

Figure 5.4. Approximate sedimentation rates in Flemish Pass, excluding Heinrich layers. The two rates highlighted in red and yellow are anomalies as explained in the text.

The uncharacteristically high sedimentation rates of some strata between H layers in 0022pc and 0024pc (red and yellow coloured boxes in Fig. 5.4) are attributed to the seafloor morphology. The high sedimentation rate between H3 and H2 in piston core 0024 (red box in Figure 5.4) is due to the presence of a MTD within that interval (Fig. 4.2). In piston core 0022, at the foot of the Beothuk Drift, the abnormally high sedimentation rate between H2 and H1 (yellow box in Figure 5.4) can be explained by a

local depression at the foot of the drift as a result of a buried submarine landslide (Fig. 4.2). The headwall scarp is beneath the seafloor at the foot of the drift. The buried MTD left a local depression where sediment preferentially accumulated, which caused an increased sedimentation rate in the lee of the depression wall.

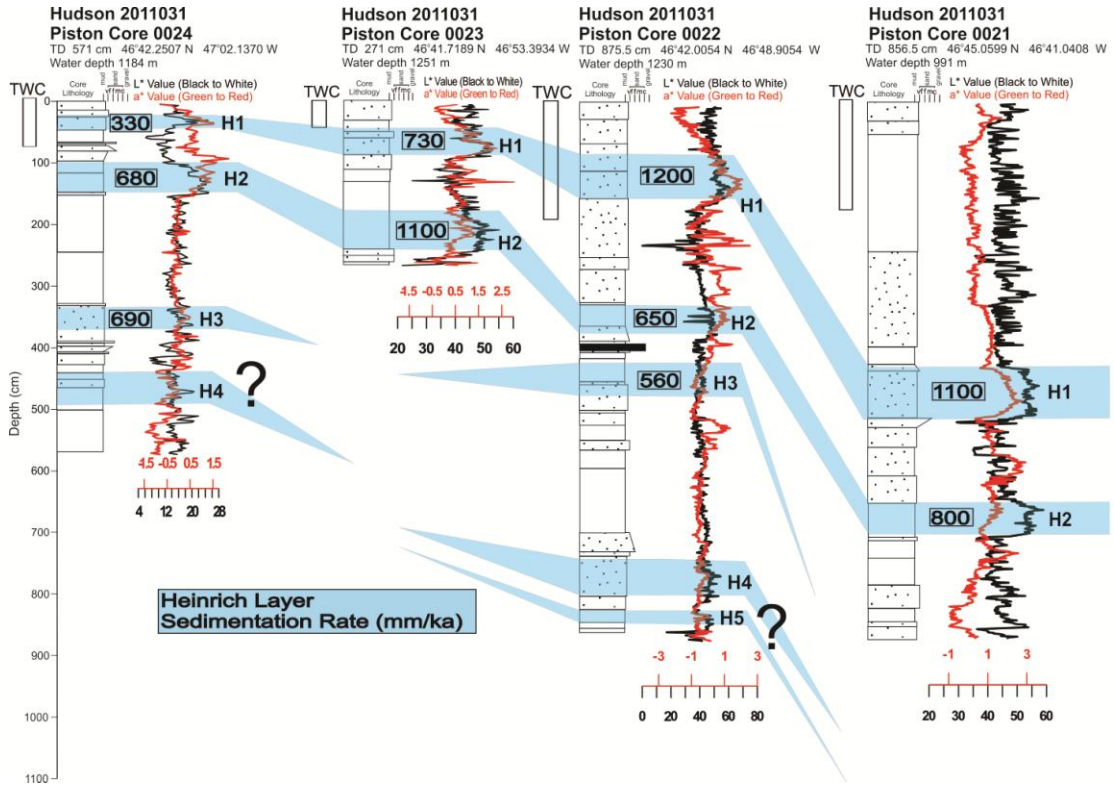

Figure 5.5. Sedimentation rates within the Heinrich layers, using an assumed deposition of 750 years (0.750 ka), based on the ice-purge model from Alley and MacAyeal (1994) and data and interpretation from Stanford et al. (2011).

Sedimentation rates in Flemish Pass are a consequence of the supply of sediment and the Labrador Current strength. During Heinrich events the sediment supply is sufficiently large to account for the high sedimentation rates seen across the pass within H layers. Current strength may hinder deposition, and even cause winnowing. Sediment deposition occurs where the current is weak enough such that the supply of sediments coming in does not exceed that of the sediments being eroded.

Core	Sediment interval	Depth of interval base (cm)	Depth of interval top (cm)	Sediment thickness (cm)	Sediment thickness (mm)	Time for deposition (ka)	Sedimentation Rate (mm/ka)	Sedimentation Rate (mm/ka) (2 sig. figs)
0021pc	Top of H1-seafloor	420	0	420	4200	16	262.5	260
0021pc	H1	500	420	80	800	0.75	1066	1100
0021pc	Top of H2-Base of H1	634	500	134	1340	8	167	170
0021pc	H2	692	634	58	580	0.75	773	800
0022pc	Top of H1-seafloor	70	0	70	700	16	43	40
0022pc	H1	160	70	90	900	0.75	1200	1200
0022pc	Top of H2-Base of H1	335	160	175	1750	8	218	220
0022pc	H2	384	335	49	490	0.75	653	650
0022pc	Top of H3-Base of H2	423	384	39	390	6	65	65
0022pc	H3	465	423	42	420	0.75	560	560
0023pc	Top of H1-seafloor	34	0	34	340	16	21	21
0023pc	H1	89	34	55	550	0.75	733	730
0023pc	Top of H2-Base of H1	160	89	71	710	8	89	89
0023pc	H2	245	160	85	850	0.75	1133	1100
0024pc	Top of H1-seafloor	25	0	25	250	16	16	16
0024pc	H1	50	25	25	250	0.75	333	330
0024pc	Top of H2-Base of H1	99	50	49	490	8	61	61
0024pc	H2	150	99	51	510	0.75	680	680
0024pc	Top of H3-Base of H2	333	150	183	1830	6	305	310
0024pc	H3	385	333	52	520	0.75	693	690

Table 5.2. Sedimentation rates for all intervals between Heinrich layers and within Heinrich layers for H3-present (where possible) in piston cores 0021-0024. Heinrich layer deposition is assumed to be 750 years (0.750 ka) based on the ice-purge model from Alley and MacAyeal (1994) and data and interpretation from Stanford et al. (2011).

There are error estimates for radiocarbon age dating and the ages at the tops and bases of each H layer have associated errors. Rigorous radiocarbon age calibrations are discussed in Fairbanks et al. (2005) and variability in Heinrich layer top and base ages can be seen in Rashid et al. (2012). For the purpose of this thesis, Heinrich layer age variability does not have a large enough effect on the sedimentation rates for the purpose of highlighting the general trend of how sedimentation has changed across Flemish Pass. Therefore, an average and approximate age is used to designate the Heinrich layers rather than calculating insignificant age differences between the top and base of Heinrich layers for the sole purpose of calculating sedimentation rates to see general sedimentation trends.

The correlation of cores by Piper and Pereira (1992) shown in Figure 2.4 requires a new interpretation, since it predates the recognition of Heinrich layers. Figure 2.4 has been modified to include Heinrich layer identification of H1 (16ka) and a 13 ka calibrated age. Table 5.1 provides updated reservoir corrected dates from core 87008-013 and for the purpose of calculating a sedimentation rate in this core, dates in Figure 2.4 are approximated. Given the recent dating of the Heinrich layers in this area (Huppertz, 2008), the sedimentation rate between H1 (16 ka) and 13 ka was extremely high at approximately 1750 mm/ka, providing another example of a thick sedimentary deposit in Flemish Pass that records Holocene sedimentation.

5.5 Sortable Silt and Labrador Current flow at Beothuk Drift

The Beothuk Drift records fine variations in grain size through time, as seen down core and laterally across Flemish Pass. Grain-size analysis was completed only for

0021pc. Prior to H1 (16 ka) and older, the average SS % was approximately 12 SS % lower than it is on average from the last 16 ka. The highest SS % (including SS % within H layers) in at least the past 24 ka is at the seafloor (57 SS %), suggesting that the Labrador Current is stronger today than it has been in at least the past 24 ka.

There are variations within Heinrich layers where SS % increased at the base of the H layer, decreased, then increased towards the top of the H layer but did not return to the same SS % as before the H event. This grain-size pattern within Heinrich layers is seen in cores elsewhere (Hall & McCave, 2000; Jonkers et al., 2012). This study does not address the Labrador Current variability within Heinrich layers because this thesis focuses on long-timescale variability and the presence of IRD within H layers violates a condition crucial for interpretations using sortable silt. When using grain size to determine current strength, conditions necessary for interpretation include a constant sediment supply, a constant direction of the current that sorts the sediments, sortable sediments and no external processes such as input of IRD, turbidity currents or any other gravitational mass movement (Hass, 2002). During H events the sediment supply is increased and IRD has a large influence on grain size, so relative current strength within H layers is not interpreted.

Using sortable silt as a proxy for current strength, it can be interpreted that in the past 24 ka there have been periods of stronger and weaker flow. The Labrador Current is inferred to have strengthened and more strongly influenced the morphology of the seafloor from H1 to present than it did prior to H1. It is also inferred from the SS % that the modern Labrador Current is stronger than it has been in at least the past 24 ka.

The increase in SS % at the top of core 21 may support the work of Scott et al. (1984), who concluded from their micropaleontological study that the inner branch of the Labrador Current (that flows through Flemish Pass) has undergone abrupt cooling associated with stronger flow in the last 2000 years. This support requires further investigation with better age control in the last few thousand years.

5.6 Origin of the Basaltic Lapilli Tuff

The 0.12 m thick section of basaltic lapilli tuff 4.00 m below the seafloor in 0022pc has been determined to be highly alkaline basalt based on silica content (Fig. 4.8), the REE diagram (Fig. 4.9) and spidergram (Fig. 4.10). An important observation is the glassy appearance of this basalt, which implies contemporary volcanism and, in the North Atlantic, suggests an origin from Iceland, Jan Mayen, the Faroe Islands or the Canary Islands. The basalt must be from contemporary volcanism because glass would not be preserved in older basaltic deposits. This basalt cannot be from the eastern Canadian margin because there is no contemporary volcanism along this margin. The basalt is not from the late Precambrian volcanics of the Avalon terrane in Newfoundland because it would not be glassy and should be widespread in the Grand Banks and Flemish Pass area, where hundreds of cores have been taken, but this basaltic lapilli tuff is known only from core 0022pc. It is highly unlikely that the basalt was deposited throughout Flemish Pass, and then was subsequently eroded everywhere except in the 0022pc location. Using the Ferguson and Church (2004) equation for settling solids, it would have taken less than five minutes for the basalt (all sizes) deposition to occur, as it settled from the sea surface. The grading seen in the deposit could be due to fallout, but

could also a result of bedload transport, from winnowing the material as it was deposited.

The age of the basalt is assumed to be close to its depositional age because the sample is uncontaminated (does not contain fragments of other rocks) and is glassy. The Fugloyarbanki Tephra, which is best known around Iceland, is the top candidate for tephra in the North Atlantic that could be related to the 0022pc basalt in because it is also located between H3 and H2.

Haflidason et al. (2000) collected numerous marine sediment cores (Fig. 5.6) in order to construct a tephrochronology of Iceland and the North Atlantic region for the past 400 ka. Core SO82-05 (Fig. 5.7) (location in the red box in Fig. 5.6) shows a record of basaltic and rhyolitic tephra and IRD. The Fugloyarbanki tephra is found throughout the North Atlantic and it has been dated at 23.56 ^{14}C ka, yielding a calibrated age of approximately 27.5 cal ka (Haflidason et al., 2000; Davies et al., 2008). This age fits comfortably between H3 (30 ka) and H2 (24 ka), suggesting a possible relation to the basaltic unit found in 0022pc in Flemish Pass, which is also found between H3 and H2.

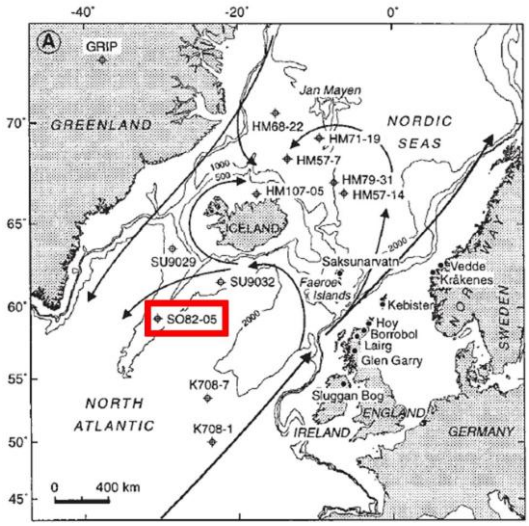

Figure 5.6. The study area for the cores collected by Haflidason et al. (2000). Data shown in Figure 5.7 are from the core highlighted by the red box. The arrows represent the surface currents in the eastern North Atlantic (Modified from Haflidason et al., 2000).

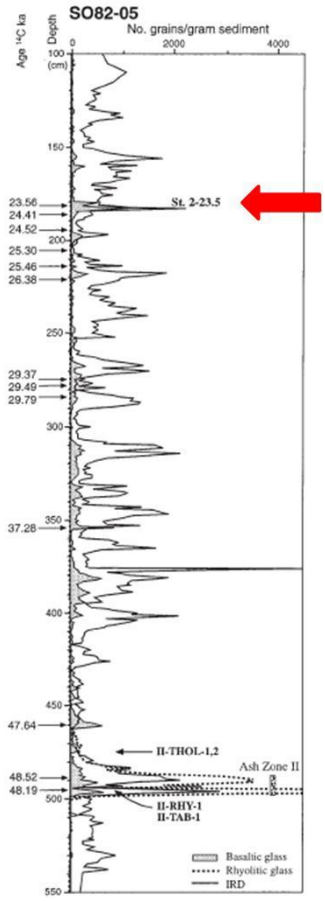

Figure 5.7. The record of basaltic, rhyolitic and ice rafted detritus in core SO82-05 from the North Atlantic. The red arrow denotes down-core location of the Fugloyarbanki tephra. (Modified from Haflidason et al., 2000).

Comparison of the spidergram (Fig. 4.10) with the spidergrams presented in Debaille et al. (2009) shows a good fit with the trace elements of the alkaline basalts in the Snaefellsnes Volcanic Zone, western Iceland (Fig. 5.8). However, major element geochemistry (Debaille et al., 2009) indicates that the 0022pc sample is too alkaline to match basalts from the volcanic zones in Iceland and Jan Mayen. For further verification, an additional comparison with the major element geochemistry of the Fugloyarbanki tephra (Davies et al., 2008), whose distinctive geochemical signature suggests that the origin of the Fugloyarbanki tephra is the Hekla-Vatnafjoll volcanic system in the Eastern Volcanic Zone (Fig. 5.9), SW Iceland (Davies et al., 2008), provides further evidence that the major element geochemistry of the basaltic lapilli tuff from Flemish Pass is too alkaline to be matched with the source of the Fugloyarbanki tephra. The Fugloyarbanki tephra may have been deposited throughout the North Atlantic when the 0022pc tuff was deposited (between H3 and H2), however, the two do not share the same source.

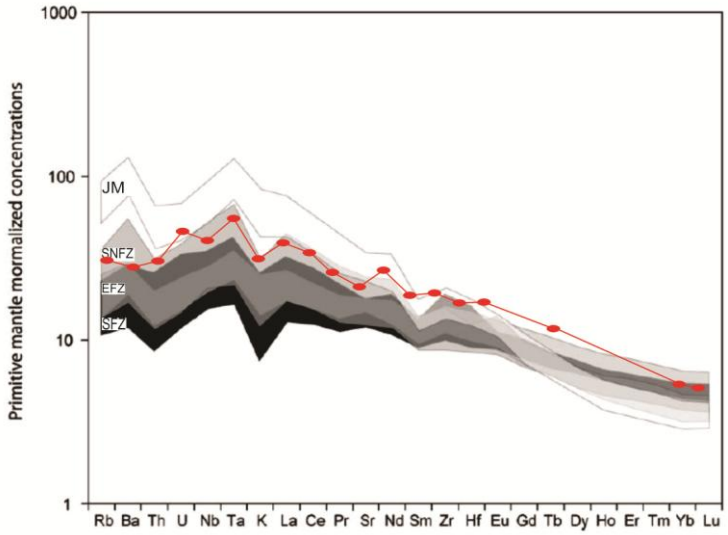

Figure 5.8. Comparison of spidergrams from numerous locations in the North Atlantic, including Jan Mayen Island (JM), the Snaefellsnes Volcanic Zone (SNFZ), the Eastern Volcanic Flank Zone (EFZ) and the Southern Volcanic Flank Zone (SFZ). Primitive mantle concentration is from McDonough and Sun, 1995. Modified from Debaille et al. (2009). The basalt spidergram from this study is plotted in red.

For Figure 5.8, note that the overlay plot with red dots from this study is plotted using primitive mantle concentrations from Sun and McDonough (1989) but the Debaille et al. (2009) spidergram plots use primitive mantle concentrations from McDonough and Sun (1995). The differences between the two plots are within an acceptable range of error compared to the precision of REE analyses, so using the two different primitive mantle concentrations are not problematic.

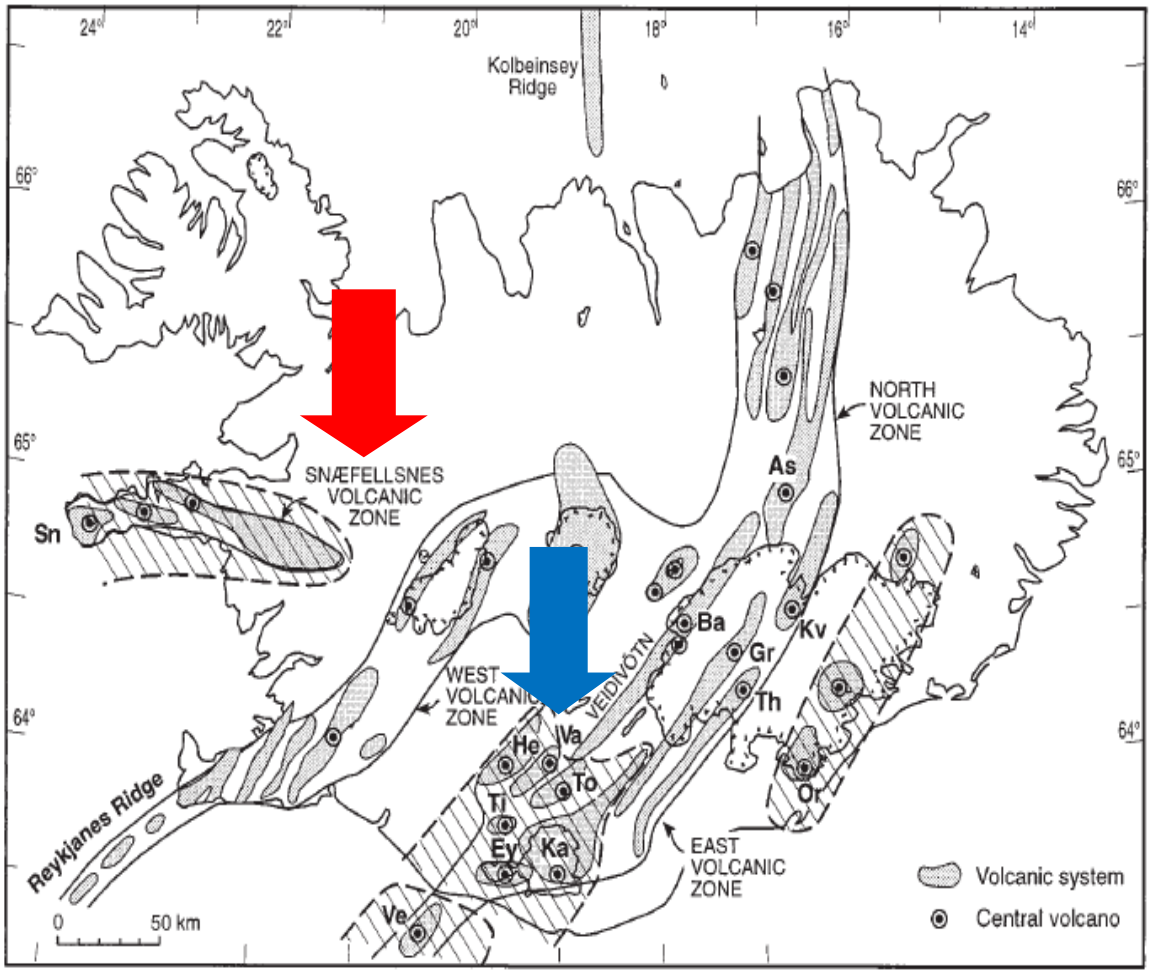

Figure 5.9. Location of the Snaefellsnes Volcanic Zone (red arrow) in western Iceland and the Hekla-Vatnafjoll volcanic system (blue arrow) in the Eastern Volcanic Zone, southwestern Iceland. (Modified from Haflidason et al., 2000). The Hekla-Vatnafjoll volcanic system in the Eastern Volcanic Zone is the source location of the Fugloyarbanki tephra (Davies et al., 2008).

The method of transport of the basaltic lapilli tuff found in 0022pc is likely ice-rafting by an iceberg or sea ice due to the presence of this lapilli being unique within Flemish Pass, implying that the basaltic lapilli tuff was dumped there after being transported to that location, explaining the lack of deposition throughout the entire study area. The grain size of the tuff implies that its method of transport of was not airborne. The method for deposition was possibly from an iceberg rolling over in Flemish Pass that was carrying the tuff and dumping the sediment on the seafloor in only this specific location during a time of intermitted erosion, which explains the erosional surface at the base of the lapilli tuff bed in 0022pc and the moderate sorting of the basaltic lapilli tuff itself.

5.7 History of the Labrador Current

The long-timescale history of the Labrador Current is provided as a synthesis in Table 5.3. The average sedimentation rates (Table 5.3) are important for the overall view of the sediment deposited in Flemish Pass between Heinrich events. The average sedimentation rates across the floor of the pass (cores 0022-0024), excluding the drift (core 0021), are listed along with a column listing the sedimentation rates from only the drift (Table 5.3). The sedimentation rates across Flemish Pass between H2 to H1 had less lateral variation compared to the variations in sedimentation rates across Flemish Pass from H1 to present. There is a larger difference in sedimentation rates between the floor of Flemish Pass and the Beothuk Drift from H1 to present (Table 5.3). Individual sedimentation rates between H layers (Fig. 5.4) at each core location are helpful for determining how sediment is being deposited across Flemish Pass over time, providing

an indication of lateral current flow variations. Drift sedimentation between H2 to H1 was 170 mm/ka and then nearly doubled between H1 to present (260 mm/ka). The floor of Flemish Pass (cores 0022-0024) shows sedimentation rates have decreased by nearly two-thirds from approximately 72 mm/ka (between H2 and H1) to 26 mm/ka (between H1 to present). These changes in sedimentation rates across Flemish Pass suggest sediment was deposited in more of a blanketing style across Flemish Pass between H2 to H1 and after H1 the drift is where most sediment accumulated, with significantly lower sedimentation rates on the floor of the pass and higher sedimentation rates on the drift, as a result of swifter current flow through Flemish Pass.

Hass (2002) illustrated that during cold climate (glacial) phases current flow through Fram Strait, an input to the NASG, is weaker than the current flow during warm climate (interglacial) phases (Fig. 5.10), such as the Holocene (12 ka to present). This situation may be analogous to the Labrador Current. However, the transition between the two main current strength variations found in this thesis appears to be earlier than 12 ka, at H1 (16 ka), which represents a large surge of ice bergs entering the North Atlantic through Hudson Strait. Melting of these icebergs caused an increase in IRD and lower salinity, triggering the current to be more buoyant and move more swiftly. Decreased sea ice cover over the ocean surface also would have allowed wind stress to be a larger factor in increasing Labrador Current strength. After H1, the Labrador Current strengthened (Fig. 5.3), as inferred from SS %. Another point to examine is how these iceberg purge events change the NASG circulation, which likely relies on more than flow

variations from the Labrador Current for circulation changes, such as flow variations in the Gulf Stream.

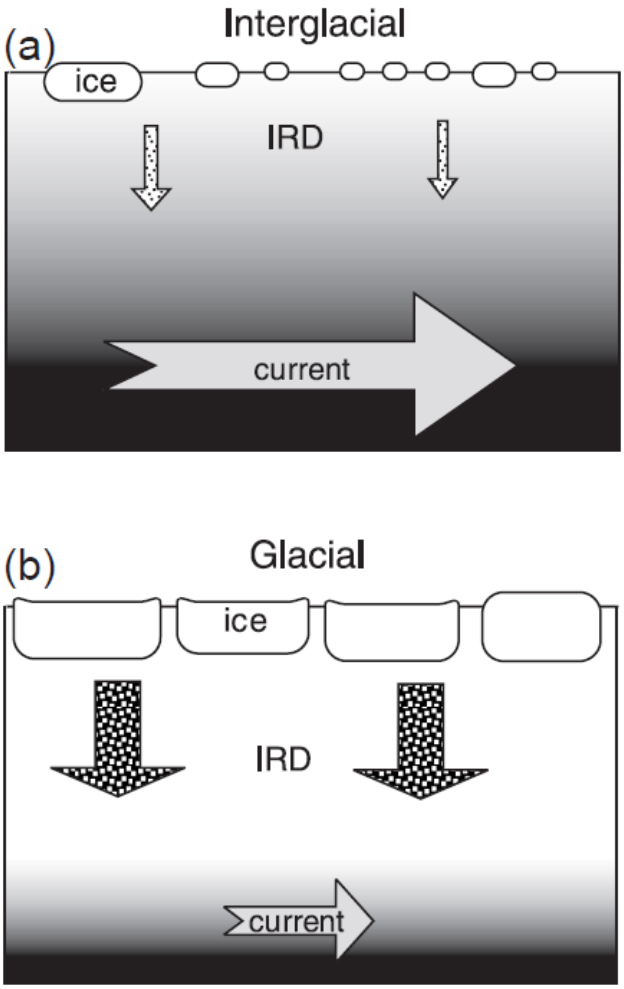

Figure 5.10. Current conditions during warm (a) and cold (b) climate phases. (Hass, 2002).

Attempts to discuss the NASG in relation to the Labrador Current strength remain preliminary and speculative as there are many unknowns. This thesis provides one proxy of evidence for the NASG circulation, but multiple proxies are required to conclude with confidence how the NASG circulation spanning an ocean basin has changed through the Late Quaternary.

Time	Average Sedimentation Rate (mm/ka) (Floor of the pass)	Drift Sedimentation Rate (mm/ka)	Sediment (SS %), grain size, processes	Relative Current Strength
16 ka - Present	26	260	Highest SS % at 0 cm (57 SS %) 48 SS % average. More sand on Pass floor, mud on drift **DRIFT GROWTH**	**Strong, and increasing in strength**
H1	750	1100	Variable, not determined	Not determined
24 ka – 16 ka	72	170	36 SS % average (below H1 to base of core, excluding H2). **DRIFT BLANKETING**	**Weak**
H2	810	800	Variable, not determined	Not determined
30 ka – 24 ka	Not determined	Not determined	Alkaline basalt deposited at foot of drift	Not determined

Table 5.3. The important evidence for the history of the Labrador Current flow in the past 30 ka in Flemish Pass. Current strength was not determined for H3 (30 ka) to H2 (24 ka) because 0021pc does not penetrate into H3 so no SS % measurements are available for this interval. Current strength was also not interpreted within Heinrich layers due to the high presence of IRD. This history of Labrador Current flow variations uses the assumption that the proportion of Labrador Current flow through Flemish Pass has remained the same through time, and that the flow around the outside of Flemish Cap has was not intensified prior to H1.

5.8 Broader Economic and Environmental Implications

This thesis has implications for drift geohazard assessments within Flemish Pass, where drifts were not previously well recognized. Drilling in Flemish Pass and other areas beyond the shelf break provides a unique set of industry challenges. It is critically important that the oceanographic conditions are carefully considered prior to operations beyond the shelf break to ensure work safety (Stow et al., 2012). Currents

are present throughout the ocean, at all water depths. The Labrador Current is a surface current that is wind and buoyancy driven (Lazier & Wright, 1993), and it affects the Flemish Pass seafloor, approximately 1000 m below the sea surface. Flemish Pass, being a restricted and perched basin, has a classic example of a morphological obstruction acting to increase current velocity. Where any water mass is restricted, its velocity increases and seafloor features (such as Flemish Cap) provide conditions for greatest increase in water velocity (Stow et al., 2012). A major concern for the offshore petroleum industry is the effect current flow has on drilling risers, which are temporary and flexible tubes that transport fluids from the sub-surface to a surface platform. A breakage in the risers due to current strength increasing beyond the threshold deemed safe for that equipment would have major negative environmental and economic consequences.

Thorough risk assessment requires detailed knowledge of existing currents, a potential mass transport and turbidity current analysis along shelf edges, contourite slopes and an understanding of potential for formation of local gas hydrates (Stow et al., 2012). Pipelines, cables, subsea installations, key connections and other seafloor infrastructure are vulnerable to damage (Stow et al., 2012). This study provides a synthesis of Labrador Current variability on a glacial-interglacial timescale and a close examination of four cores from across the Beothuk Drift, aiding in a future geohazard assessment of the Beothuk Drift and surrounding area for petroleum infrastructure development.

There are barriers to sorting out paleoclimatic issues on the eastern Canadian margin because of the general lack of Holocene sedimentary records. However, the Beothuk Drift in southern Flemish Pass is one of few areas where Holocene sedimentation is preserved, providing useful information for assessing paleoceanographic and climatic changes of the study area.

Flow variations throughout the North Atlantic and tie with climate variability are more complicated than one current strength parameter for implications of North Atlantic Subpolar Gyre circulation, deepwater formation and global climate change. Paleoclimatic reconstructions in numerous locations need to be completed to better understand these Late Quaternary variations.

CHAPTER 6: CONCLUSION

6.1 Summary

The Labrador Current has experienced two periods of long-term flow variations in at least the past 24 ka. The Labrador Current from at least 24 ka, to 16 ka was relatively weaker, when drift sedimentation was less pronounced and sedimentation was more of a blanketing style, than from 16 ka to present, when there was prominent sediment partitioning across Flemish Pass, with significant drift growth as a result of a swifter current. The Labrador Current is stronger today than it has been for more than 24 ka.

Some time between 30-24 ka, a 0.12 m thick unit of highly alkaline basaltic lapilli tuff, from an undetermined source of contemporary volcanism, was deposited at the foot of the Beothuk Drift. The basalt is too alkaline to be from Iceland or Jan Mayen and it is too young to be from the eastern Canadian margin. The probable method of transport is by sea ice or iceberg from the source to the Flemish Pass area. A rolling iceberg dumping the basaltic lapilli tuff onto the 0022pc location during a time of intermittent erosion of the seafloor is the likely method of deposition of the basaltic lapilli tuff.

6.2 Further Research

Deeper core penetration and more grain-size analyses of drifts in other areas affected by the Labrador Current, and similar studies throughout the North Atlantic can give us enough information about numerous current variations within the NASG to provide a holistic view of the gyre circulation and climatic changes from the last glacial interval, to present.

Additional research could focus on the basalt, including its source and journey to Flemish Pass. Modeling of ocean currents, global ice sheets and sea ice may lead to a history of travel. Further geochemical comparisons with other basalts in the North Atlantic are required to determine the source. Correlating 0022pc to a seismic profile will aid in determining the possible lateral extent of this basalt deposit, in addition to confirming Heinrich layer correlations.

Flemish Pass seismic correlations and interpretations should be completed in order to better understand the seafloor and sediment architecture, and to confirm Heinrich layer correlations and thickness variations throughout Flemish Pass. The age model provided in this thesis can be improved by adding additional age constraints through radiocarbon dating numerous core locations, particularly within the top 4 m of piston core 0021 in order to better constrain the timing of the recent increase in strength of the Labrador Current.

REFERENCES

Activation Labs, 2011, Lithogeochemistry. h*ttp://www.actlabs.com/page.aspx?menu=74&app=244&cat1=595&tp=2&lk=no*

Alley, R.B. & D.R. MacAyeal, 1994, Ice-rafted debris associated with binge/purge oscillations of the Laurentide Ice Sheet, *Paleoceanography*, 9, 4, 53-511.

Andrews, J.T., A.E. Jennings, M. Kerwin, M. Kirby, W. Manley, G.H. Miller, G. Bond & B. Maclean, 1995, A Heinrich-like event, H-0 (DC-0): source(s) for detrital carbonate in the North Atlantic during the Younger Dryas chronozone, *Paleoceanography*, 10, 5, 943-952.

Armstrong, R., D.J.W. Piper & C.G.P. Pereira, 1988, Pleistocene stratigraphy and sedimentation of western Flemish Pass: a seismostratigraphic interpretation. Geological Survery of Canada Open File 1741, 53p.

Beckman Coulter Inc., 2011, Coulter LS Series Product Manual, 358pp.

Broecker, W., G. Bond, M. Klas, E. Clark & J. McManus, 1992, Origin of the northern Atlantic's Heinrich events, *Climate Dynamics*, 6, 265-273.

Campbell, D.C., 2005, Major Quaternary mass-transport deposits in southern Orphan Basin, offshore Newfoundland and Labrador, Geological Survey of Canada, *Current Research 2005-D3*, 10p.

Campbell, D.C., 2011, CCGS Hudson 2011031 Cruise Report. Geological Survey of Canada, Bedford Institute of Oceanography.

Carter, L. & C.T. Schafer, 1983, Interaction of the Western Boundary Undercurrent with the continental margin off Newfoundland, *Sedimentology*, 30, 751-768.

Cuny, J., P.B. Rhines, P.P. Niiler & S. Bacon, 2002, Labrador Sea boundary currents and the fate of the Irminger Sea Water, *Journal of Physical Oceanography*, 32, 627-647.

Davies, S.M., S. Wastegard, T.L. Rasmussen, A. Svensson, S.J. Johnsen, J.P. Steffensen & K.K. Anderson, 2008, Identification of the Fugloyarbanki tephra in the NGRIP ice core: a key tie-point for marine and ice-core sequences during the last glacial period, *Journal of Quaternary Science*, 23, 5, 409-414.

Debaille, V., R.G. Tronnes, A.D. Brandon, T.E. Waight, D.W.Graham & C.-T.A. Lee, 2009, Primitive off-rift basalts from Iceland and Jan Mayen: Os-isotopic evidence for a mantle source containing enriched subcontinental lithosphere*, Geochimica et Cosmochimica Acta*, 73, 3423-3449.

DeGelleke, L., P.S. Hill, M. Kienast & D.J.W. Piper, 2013, Sediment dynamics during Heinrich event H1 inferred from grain size, *Marine Geology*, 10 pp.

Fairbanks, R.G., R.A. Mortlock, T.-C. Chiu, L. Cao, A. Kaplan, T.P. Guilderson, T.W. Fairbanks, A.R. Bloom, P.M. Grootes & M.-J. Nadeau, 2005, Radiocarbon calibration curve spanning 0 to 50,000 years BP based on paired ^{230}Th/ ^{234}U/ ^{238}U and ^{14}C dates on pristine corals, *Quaternary Science Reviews*, 24, 1781-1796.

Ferguson, R.I. & M. Church, 2004, A simple equation for grain settling velocity, *Journal of Sedimentary Research*, 74, 6, 993-937.

Fratantoni, P.S. & M.S. McCartney, 2010, Freshwater export from the Labrador Current to the North Atlantic Current at the tail of the Grand Banks of Newfoundland, *Deep-Sea Research I*, 57, 258-283.

Geotek, 2011, Multi-sensor core logger manual, 6, 215p.

Grant, A.C., 1972, The continental margin off Labrador and eastern Newfoundland-Morphology and Geology, *Canadian Journal of Earth Sciences*, 9, 1394-1429.

Haflidason, H., J. Eriksson & S. van Kreveld, 2000, The tephrochronology of Iceland and the North Atlantic region during the Middle and Late Quaternary: a review, *Journal of Quaternary Science*, 15, 1, 3-22.

Hall, I.R. & I.N. McCave, 2000, Paleocurrent reconstruction, sediment and thorium focusing on the Iberian margin over the last 140 ka, *Earth and Planetary Science Letters*, 178, 151-164.

Hass, H.C., 2002, A method to reduce the influence of ice-rafted debris on a grain size record from northern Fram Strait, Arctic Ocean, *Polar Research*, 21, 2, 299-306.

Heinrich. H., 1988, Origin and consequences of cyclic ice rafting in the Northeast Atlantic Ocean during the past 130,000 years, *Quaternary Research*, 29, 2, 142-152.

Hillaire-Marcel, C., A. de Vernal, G. Bilodeau & A.J. Weaver, 2001, Absence of deep-water formation in the Labrador Sea during the last interglacial period, *Nature*, 410, 1073-1077.

Huppertz, T.J., 2008, Data on Late Quaternary geology of Flemish Pass, Geological Survey of Canada Open File 5819, 485p.

Huppertz, T.J. & D.J.W. Piper, 2009, The influence of shelf-crossing glaciation on continental slope sedimentation, Flemish Pass, eastern Canadian continental margin, *Marine Geology*, 265, 67-85.

Huppertz, T.J. & D.J.W. Piper, 2010, Interbedded Late Quaternary turbidites and contourites in Flemish Pass, off southeast Canada: their recognition, origin and temporal variation, *Sedimentary Geology*, 228, 46-60.

Irvali, N., U.S. Ninnemann, E.V. Galaasen, Y. Rosenthal, D. Kroon, D.W. Oppo, H.F. Kleiven, K.F. Darling & C. Kissel, 2012, Rapid switches in subpolar North Atlantic hydrography and climate during the Last Interglacial (MIS 5e), *Paleoceanography*, 27, 16 pp.

Johnson, R.G. & B.T. McClure, 1976, A model for Northern Hemisphere continental ice sheet variation, *Quaternary Research*, 6, 3, 325-353.

Jonkers, L., M.A. Prins, M. Moros, G.J. Weltje, S.R. Troelstra & G.-J.A. Brummer, 2012, Temporal offsets between surface temperature, ice-rafting and bottom flow speed proxies in the glacial (MIS 3) northern North Atlantic, *Quaternary Science Reviews*, 48, 43-53.

Keen, C.E. & D.L. Barrett, 1981, Thin and subsided continental crust on the rifted margin of Eastern Canada: crustal structure, thermal evolution and subsidence history, *Geophysical Journal. Royal Astronomical Society*, 65, 443-465.

Keigwin, L.D., J.P. Sachs & Y. Rosenthal, 2003, A 1600-year history of the Labrador Current off Nova Scotia, *Climate Dynamics*, 21, 53-62.

Kennard, L., C. Schafer & L. Carter, 1990, Late Cenozoic evolution of Sackville Spur: a sediment drift on the Newfoundland continental slope, *Canadian Journal of Earth Sciences*, 27, 863-878.

King, L.H., G.B Fader, W.H. Poole & R.K. Wanless, 1985, Geological setting and age of the Flemish Cap granodiorite, east of the Grand Banks of Newfoundland, *Canadian Journal of Earth Sciences*, 22, 1286-1298.

Langehaug, H.R., I. Medhaug, T. Eldevik & O.H. Ottera, 2012, Arctic/Atlantic Exchanges via the Subpolar Gyre, *Journal of Climate*, 25, 2421-2439.

Lazier, J.R.N. & D.G. Wright, 1993, Annual velocity variations in the Labrador Current, *Journal of Physical Oceanography*, 23, 659-678.

Lazier, J.R.N., 1988, Temperature and salinity changes in the deep Labrador Sea, 1962-1986, *Deep Sea Research*, 35, 1247-1253.

Le Bas, M.J., R.W. Le Maitre, A. Streckeisen & B. Zanettin, 1986, A chemical classification of volcanic rocks based on the total alkali-silica diagram, *Journal of Petrology*, 27, 3, 745-750.

McCave, I.N., 2008, Size sorting during transport and deposition of fine sediments: sortable silt and flow speed, In: *Developments in Sedimentology*, 60, Elsevier, ISSN 0070-4571, 121-142.

McCave, I.N. & I.R. Hall, 2006, Size sorting in marine muds: Processes, pitfalls, and prospects for paleoflow-speed proxies, *Geochem. Geophys. Geosyst.*, 7, 10, 37pp.

McCave, I.N., B. Manighetti & S.G. Robinson, 1995, Sortable silt and fine sediment size/composition slicing: parameters for paleocurrent speed and paleoceanography, *Paleoceanography*, 10, 3, 593-610.

McDonough, W.F. & S.-s. Sun, 1995, The composition of the Earth, *Chemical Geology*, 120, 223-253.

McNeely, R., A.S. Dyke & J.R. Southon, 2006, Canadian marine reservoir ages, preliminary data assessment, Geological Survey of Canada Open File 5049, 3p.

Monahan, D. & R.F. MacNab, 1974, Macro- and meso-morphology of Flemish Cap, Flemish Pass, and the northeastern Grand Banks of Newfoundland. Geological Survey of Canada Paper 74-30, 207-216.

Murphy, R., H. Maharaj, J. Lachapelle & P.K. Yuen, 2010, Operator of portable X-ray fluorescence analyzers certification information and examination preparation booklet, NRCan, Government of Canada, 3, 82p.

Nye, J., 2010, Climate change and its effects on ecosystems, habitats and biota, State of the Gulf of Maine Report, Gulf of Maine Council: Marine Environment, 20 pp.

Piper, D.J.W., 2005, Late Cenozoic evolution of the continental margin of eastern Canada, *Norwegian Journal of Geology*, 85, 231-244.

Piper, D.J.W. & D.C. Campbell, 2005, Quaternary Geology of Flemish Pass and its application to geohazard evaluation for hydrocarbon development, *Petroleum Resources and Reservoirs*, Special Paper 43, 29-43.

Piper, D.J.W. & W.R. Normark, 1989, Late Cenozoic sea-level changes and the onset of glaciation - impact on continental-slope progradation off eastern Canada, Marine and Petroleum Geology, 6, 4, 336-347.

Piper, D.J.W. & C.P.G. Pereira, 1992, Late Quaternary sedimentation in central Flemish Pass, *Canadian Journal of Earth Sciences*, 29, 535-550.

Piper, D.J.W. & K.I. Skene, 1998, Latest Pleistocene ice-rafting events on the Scotian Margin (eastern Canada) and their relationship to Heinrich events, *Paleoceanography*, 13, 2, 205-214.

Piper, D.J.W., P.J. Mudie, G.B. Fader, H.W. Josenhans, B. MacLean & G. Vilks, 1990, Quaternary Geology, Chapter 10 in Geology of the Continental Margin of Eastern Canada, M.J. Keen and G.L. Williams (ed.): Geological Survey of Canada, Geology of Canada, 2, 465-607.

Rashid, H., R. Hesse & D.J.W. Piper, 2003a, Evidence for an additional Heinrich event between H5 and H6 in the Labrador Sea*, Paleoceanography*, 18, 4, 1077, 15 pp.

Rashid, H., R. Hesse & D.J.W. Piper, 2003b, Distribution, thickness and origin of Heinrich layer 3 in the Labrador Sea, *Earth and Planetary Science Letters*, 205, 281-293.

Rashid, H., F. Saint-Ange, D.C. Barber, M.E. Smith & N. Devalia, 2012, Fine scale sediment structure and geochemical signature between eastern and western North Atlantic during Heinrich events 1 and 2, *Quaternary Science Reviews*, 46, 136-150.

Rasmussen, T.L., S. Wastegard, A. Kuijpers, T.C.E. van Weering, J. Heinemeier & E. Thomsen, 2003, Stratigraphy and distribution of tephra layers in marine sediment cores from the Faeroe Islands, North Atlantic, *Marine Geology*, 199, 263-277.

Scott, D.B., P.J. Mudie, G. Vilks & D.C. Younger, 1984, Latest Pleistocene-Holocene paleoceanographic trends on the continental margin of eastern Canada: Foraminiferal, dinoflagellate and pollen evidence, *Marine Micropaleontology*, 9, 181-218.

Shaw, J., 2006, Paleogeography of the Atlantic Canadian continental shelves from the Last Glacial Maximum to the present, with an emphasis on Flemish Cap, *Journal of Northwest Atlantic Fishery Science*, 37, 119-126.

Sonnichsen, G.V. & E.L. King, 2005, Grand Bank seabed and shallow subsurface geology in relation to subsea engineering design, *Petroleum Resources and Reservoirs*, Special Paper 43, 11-27.

Stanford, J.D., E.J. Rohling, S. Bacon, A.P. Roberts, F.E. Grousset & M. Bolshaw, 2011, A new concept for the paleoceanographic evolution of Heinrich event 1 in the North Atlantic, Quaternary Science Reviews, 30, 1047-1066.

Stow, D.A.V., R. Brackenridge, U. Patel & S. Toulmin, 2012, Geohazards and ocean hazards in deepwater: overview and methods of assessment, Offshore Technology Conference, OTC Number 23697-PP, 29 pp.

Sun, S-s. & W.F. McDonough, 1989, Chemical and isotopic systematics of oceanic basalts: implications for mantle composition and processes, In: Saunders, A.D. & M.J. Norry, (eds), 1989, Magmatism in the ocean basins, Geological Society Special Publication No. 42, 313-345.

Svensson, A., K.K. Anderson, M. Bigler, H.B. Clausen, D. Dahl-Jensen, S.M. Davies, S.J. Johnsen, R. Muscheler, F. Parrenin, S.O. Rasmussen, R. Rothlisberger, I. Seierstad, J.P. Steffensen & B.M. Vinther, 2008, A 60 000 year Greenland stratigraphic ice core chronology, *Clim. Past*, 4, 47-57.

Thornalley, D.J.R., H. Elderfield & I.N. McCave, 2009, Holocene oscillations in temperature and salinity of the surface Subpolar North Atlantic, *Nature*, 457, 711-714.

Tripsanas, E.K. & D.J.W. Piper, 2008, Late Quaternary Stratigraphy and sedimentology of Orphan Basin: Implications for meltwater dispersal in the southern Labrador Sea, *Palaeogeography, Palaeoclimatology, Palaeoecology*, 260, 521-539.

Tripsanas, E.K., D.J.W. Piper & K.A. Jarrett, 2007, Logs of piston cores and interpreted ultra-high-resolution seismic profiles, Orphan Basin, Geological Survey of Canada, Open File 5299, 338p.

Vilks, G., 1981, Late glacial-postglacial foraminiferal boundary in sediments of Eastern Canada, Denmark and Norway, *Geoscience Canada*, 8, 2, 8 pp.

APPENDIX A: CORE PHOTOGRAPHY

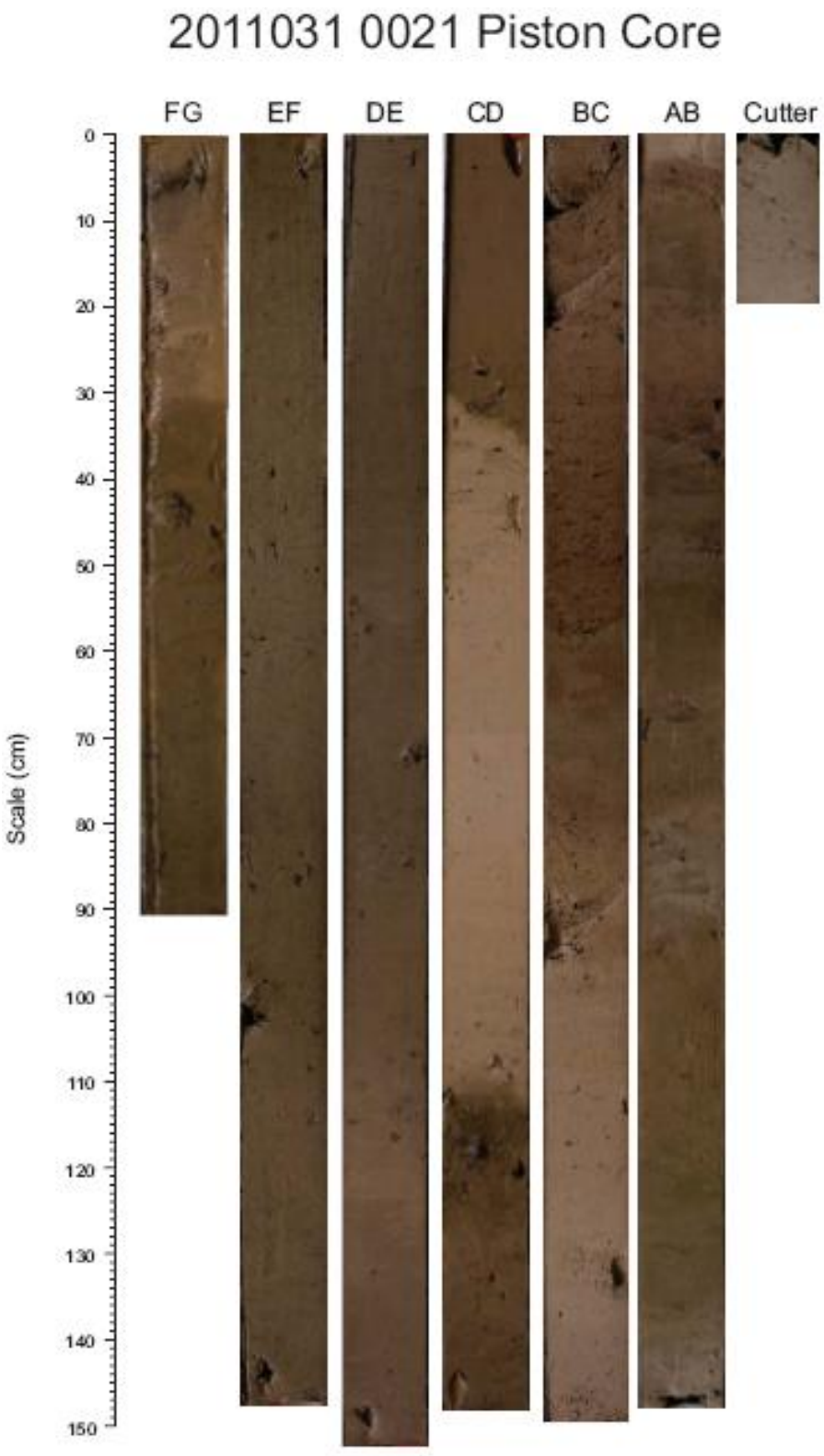

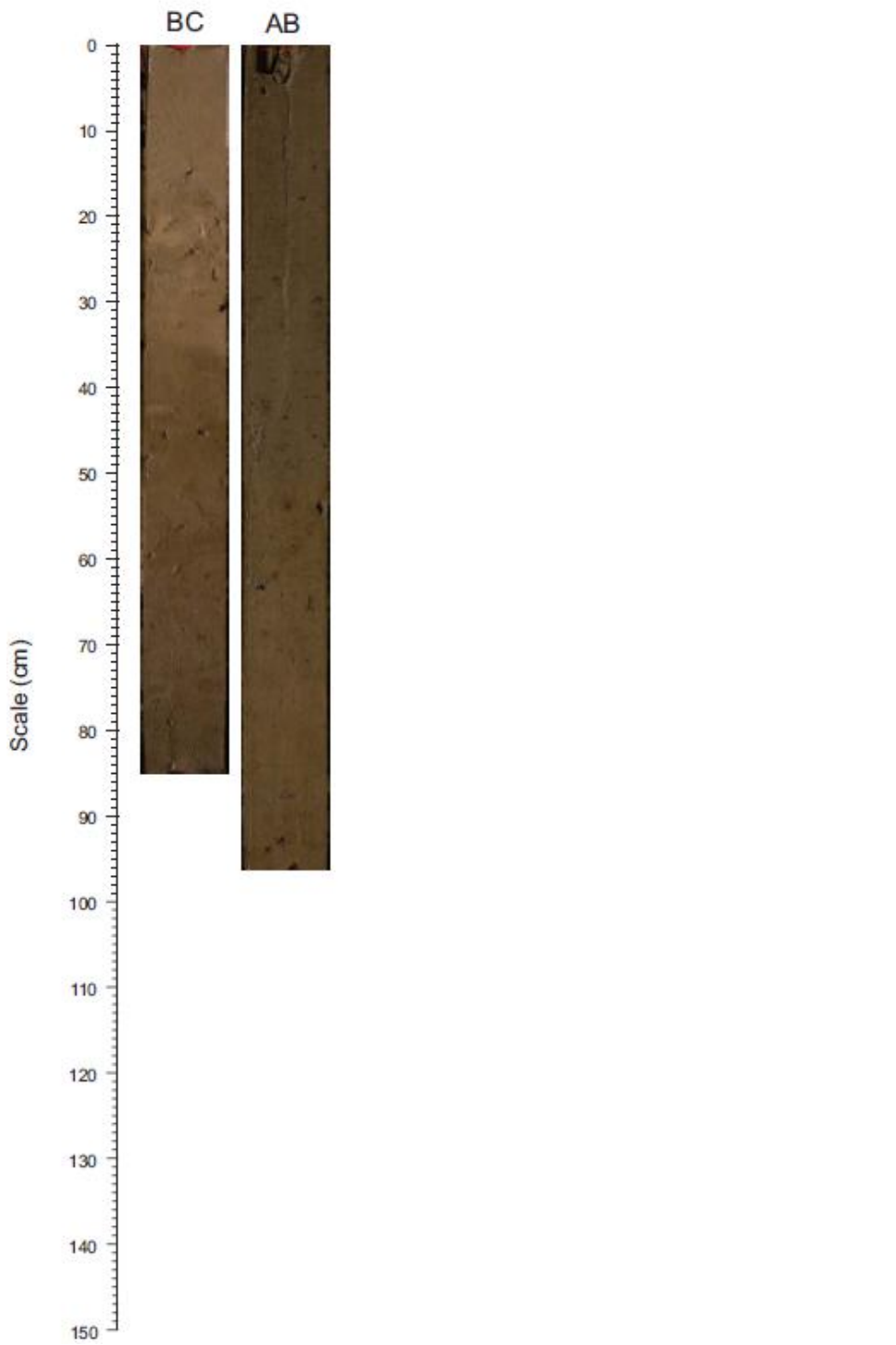
2011031 0021 Trigger Weight Core
BC
AB
Scale (cm)
0
10
20
30
40
50
60
70
80
90
100
110
120
130
140
150

2011031 0022 Piston Core

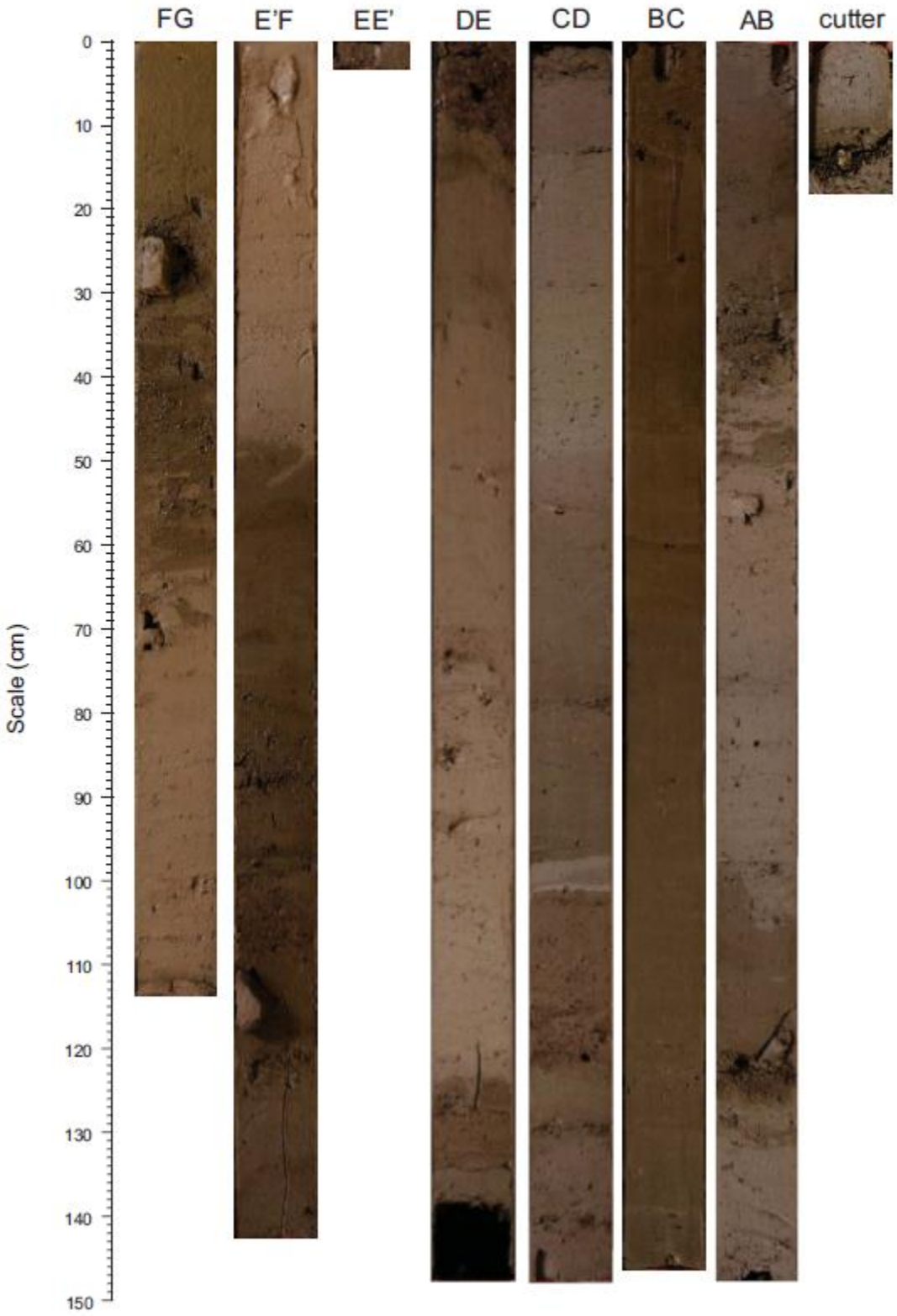

2011031 0022 Trigger Weight Core

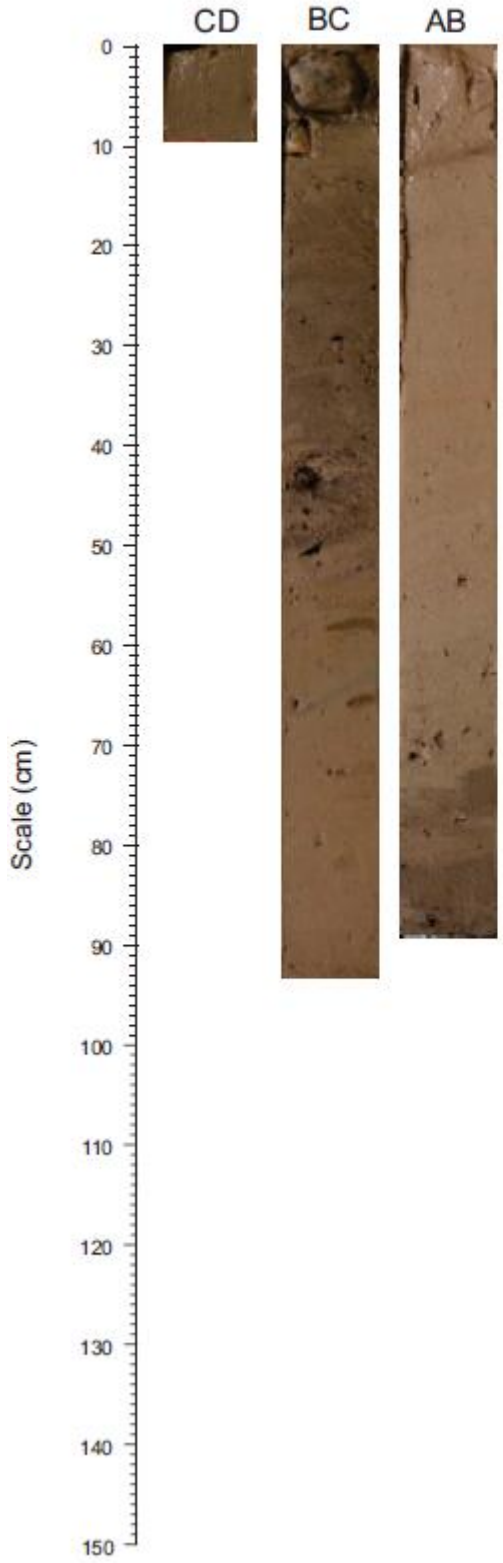

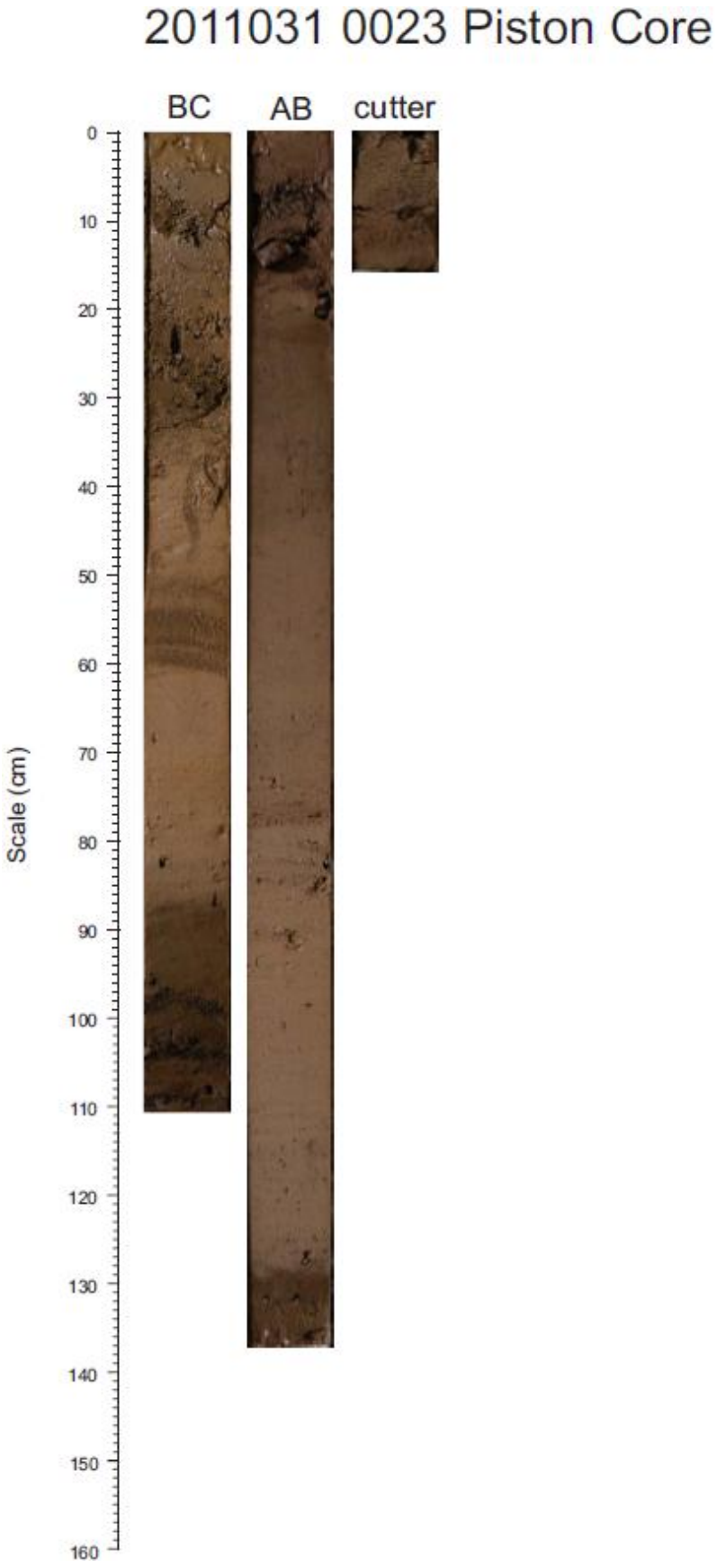
2011031 0023 Piston Core
BC
AB
cutter
Scale (cm)
0
10
20
30
40
50
60
70
80
90
100
110
120
130
140
150
160

2011031 0023 Trigger Weight Core

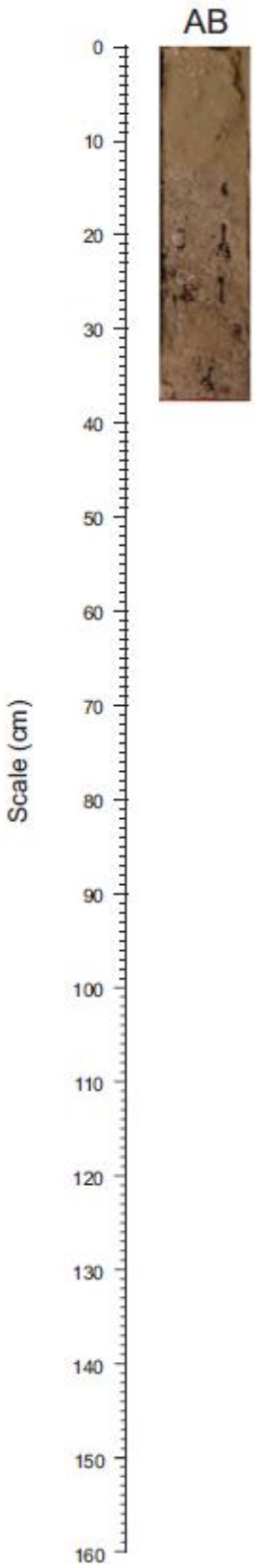

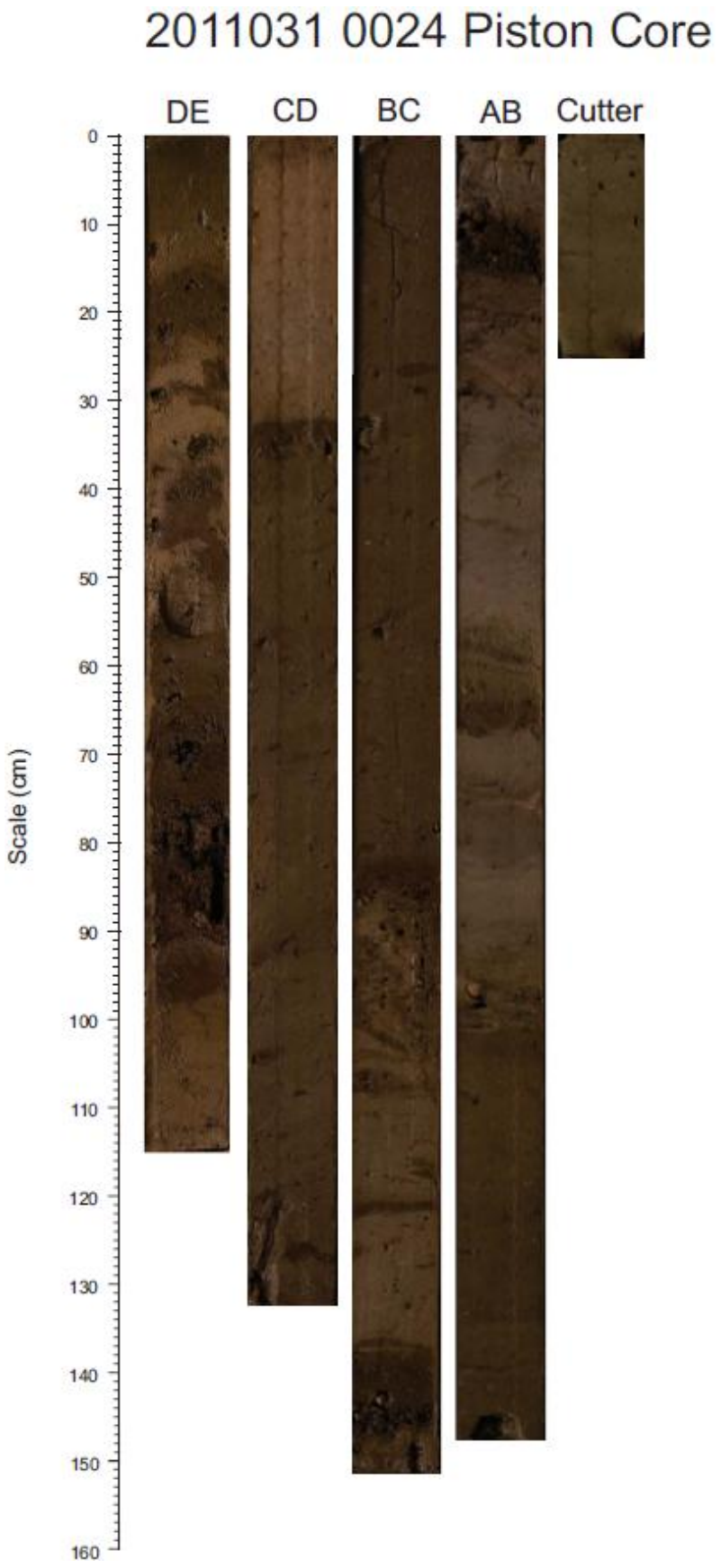
2011031 0024 Piston Core
DE
CD
BC
AB
Cutter
Scale (cm)
0
10
20
30
40
50
60
70
80
90
100
110
120
130
140
150
160

2011031 0024 Trigger Weight Core

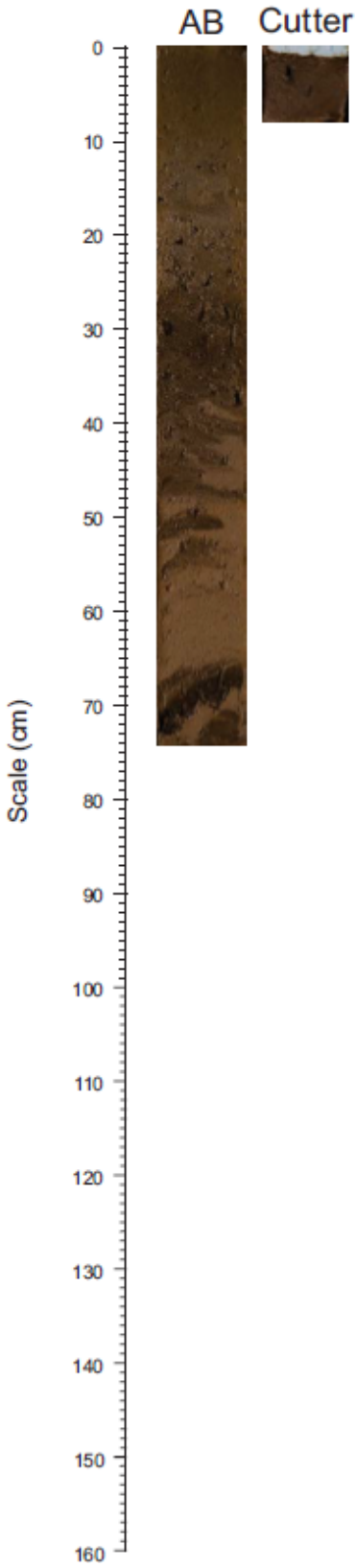

APPENDIX B: CORE X-RAY PHOTOGRAPHY

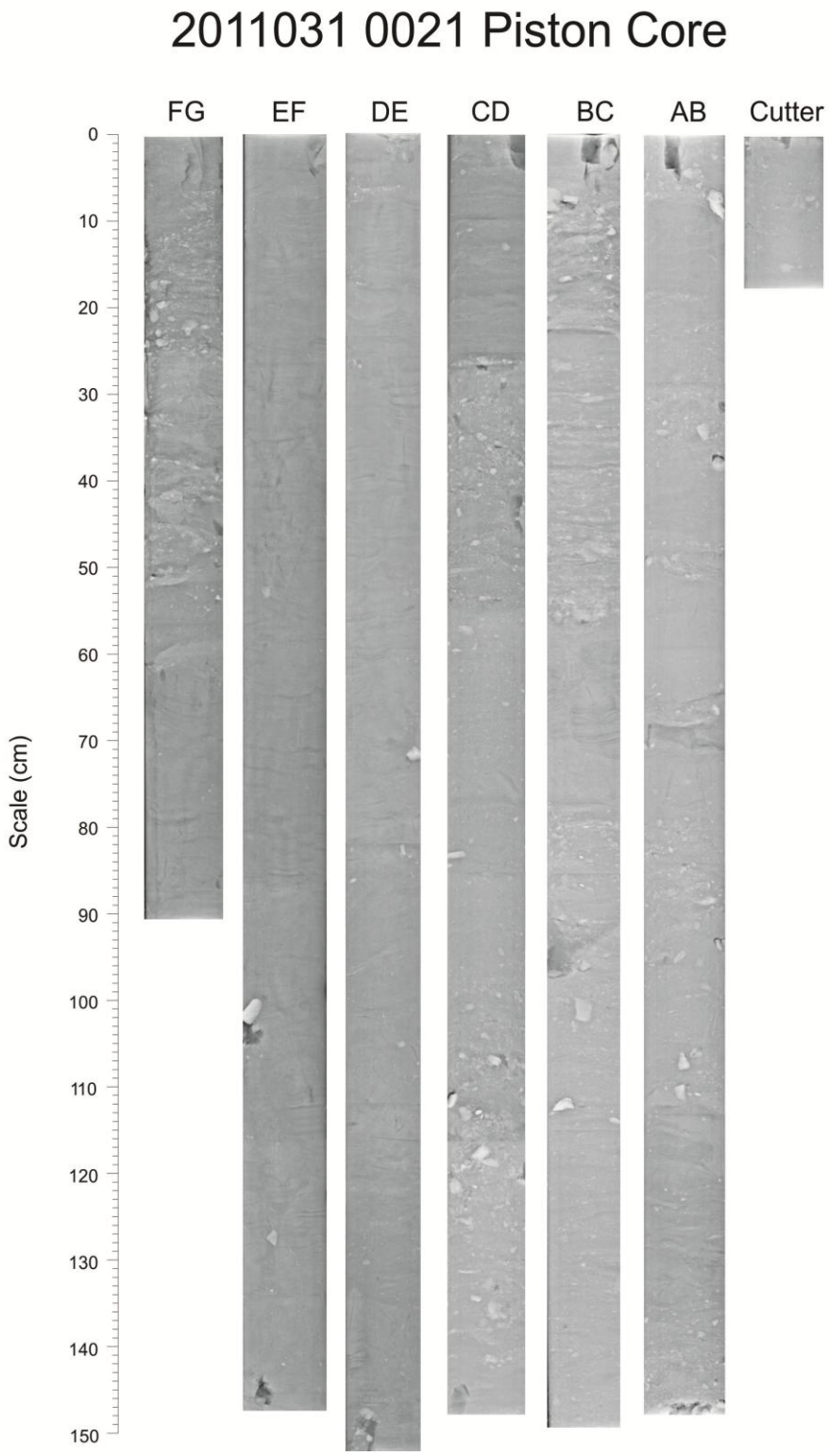

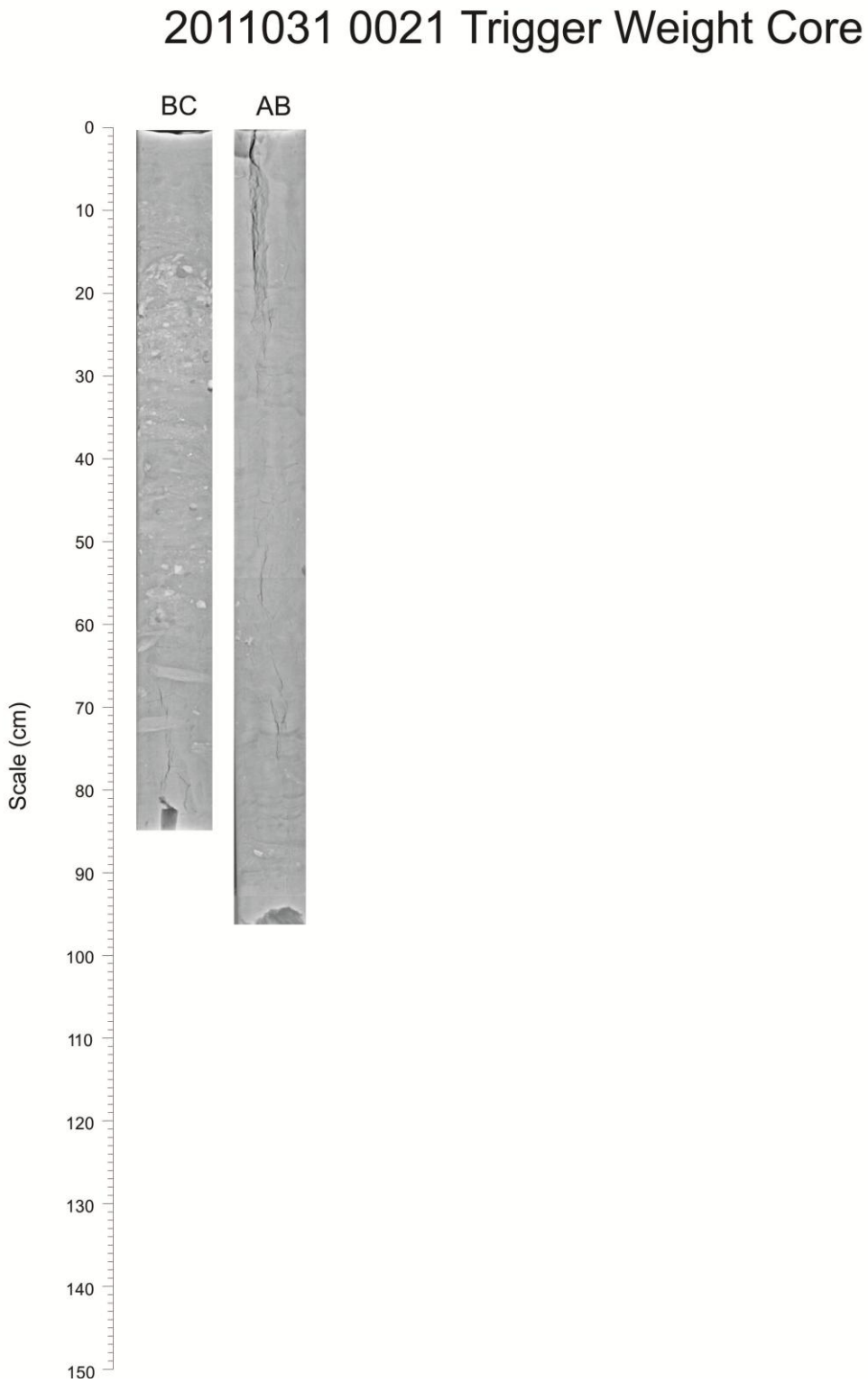
2011031 0021 Trigger Weight Core
BC
AB
Scale (cm)
0
10
20
30
40
50
60
70
80
90
100
110
120
130
140
150

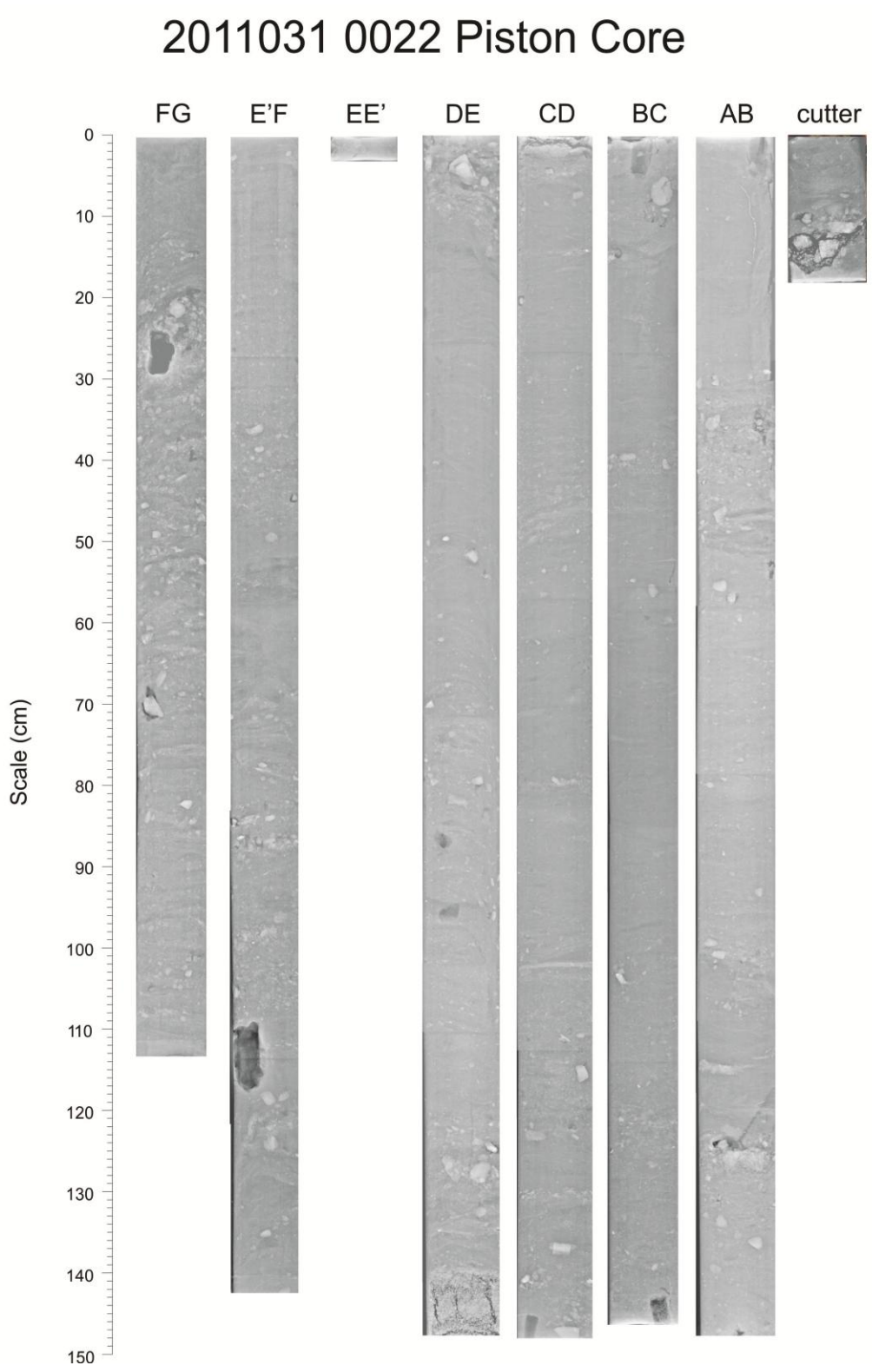
2011031 0022 Piston Core
FG
E'F
EE'
DE
CD
BC
AB
cutter
Scale (cm)
0
10
20
30
40
50
60
70
80
90
100
110
120
130
140
150

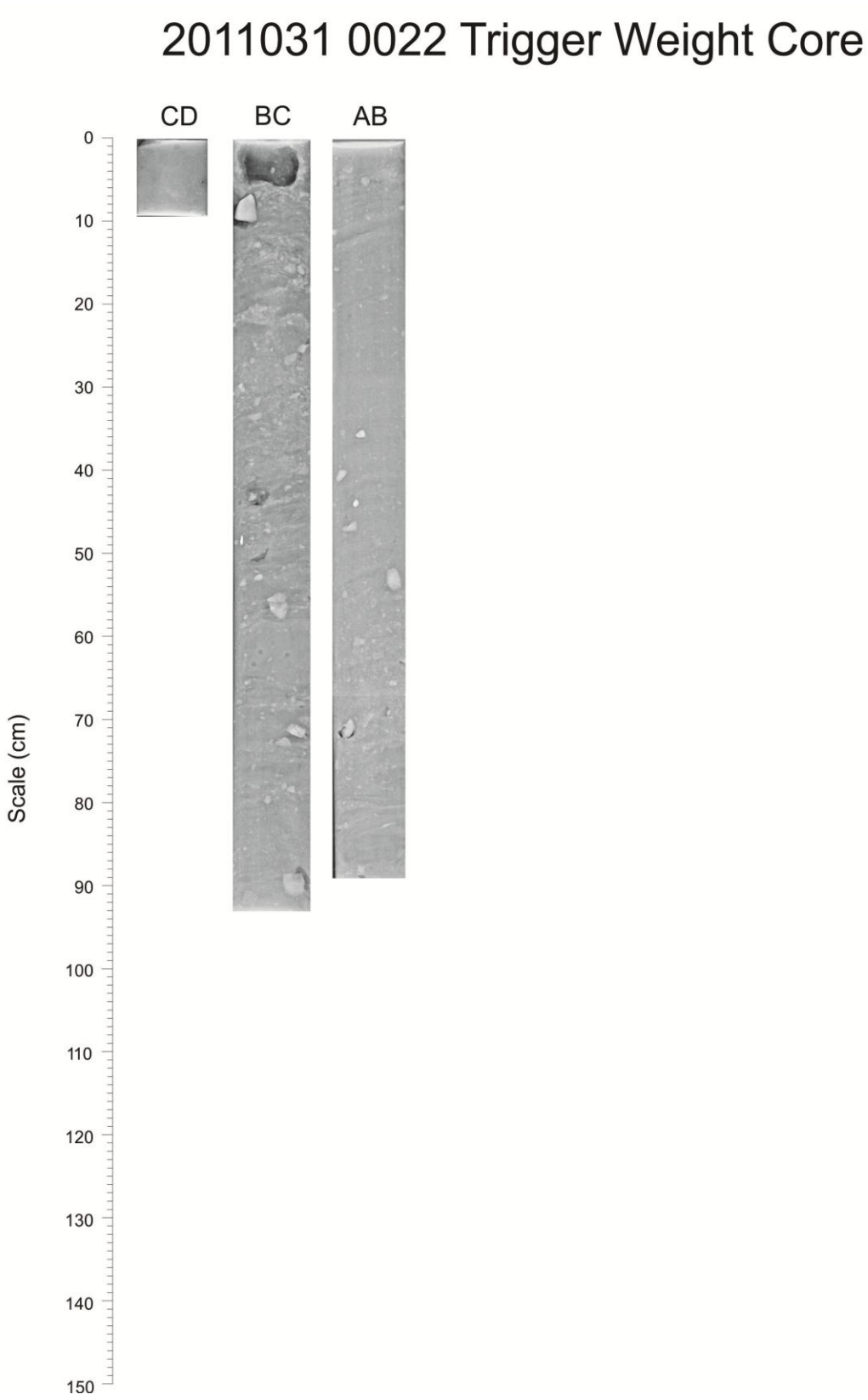
2011031 0022 Trigger Weight Core
CD
BC
AB
Scale (cm)
0
10
20
30
40
50
60
70
80
90
100
110
120
130
140
150

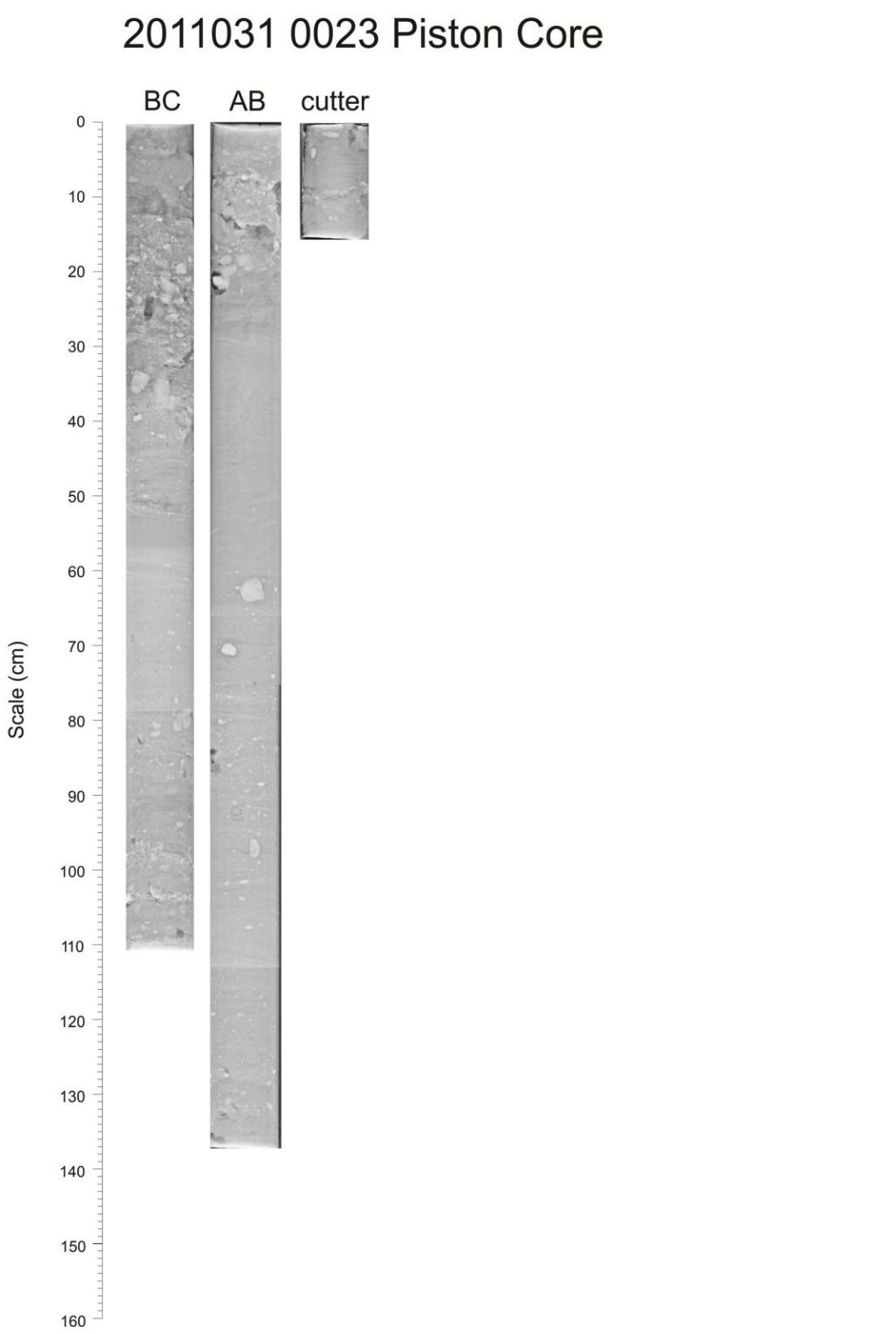
2011031 0023 Piston Core
BC
AB
cutter
Scale (cm)
0
10
20
30
40
50
60
70
80
90
100
110
120
130
140
150
160

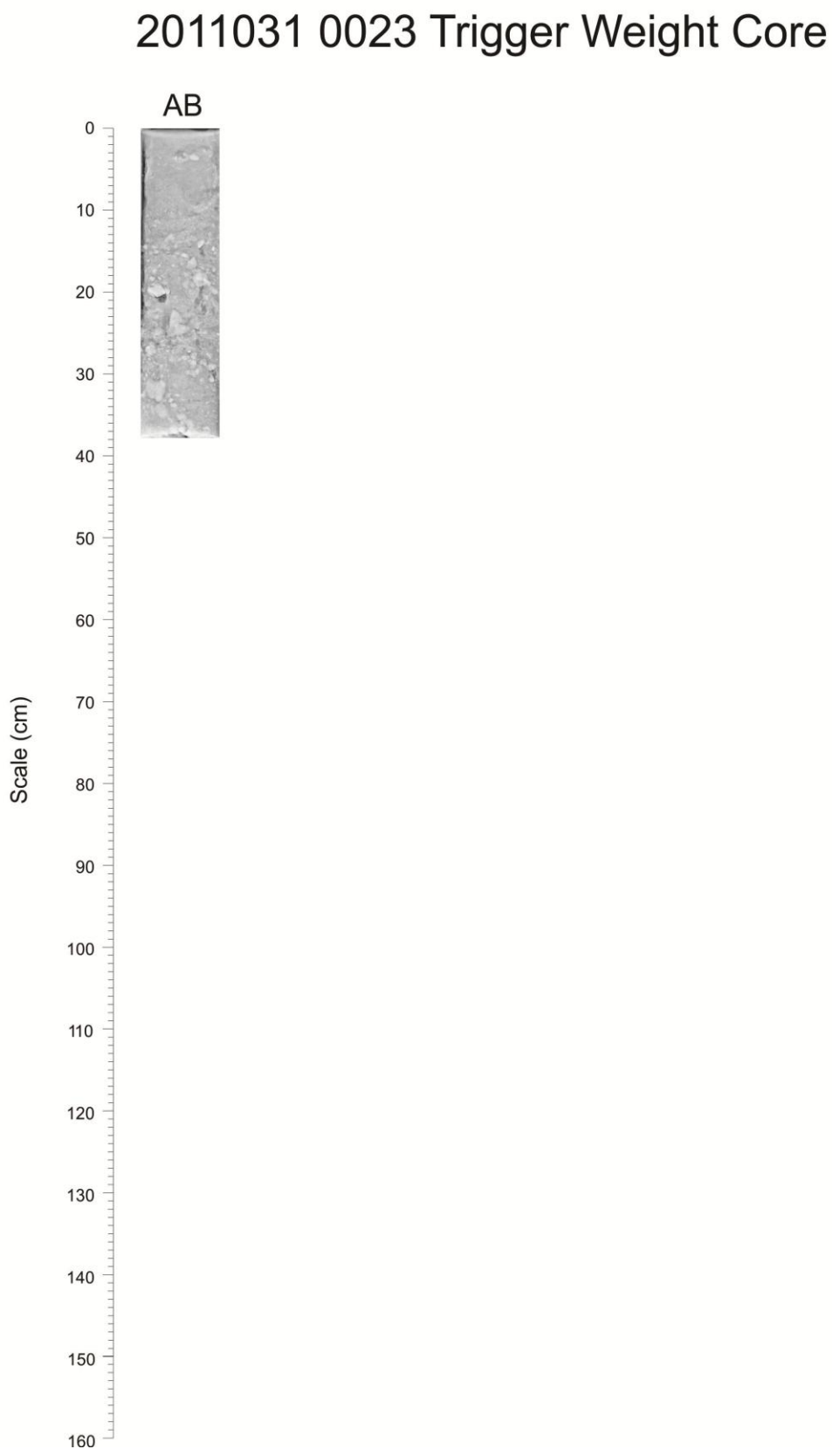
2011031 0023 Trigger Weight Core
AB
Scale (cm)
0
10
20
30
40
50
60
70
80
90
100
110
120
130
140
150
160

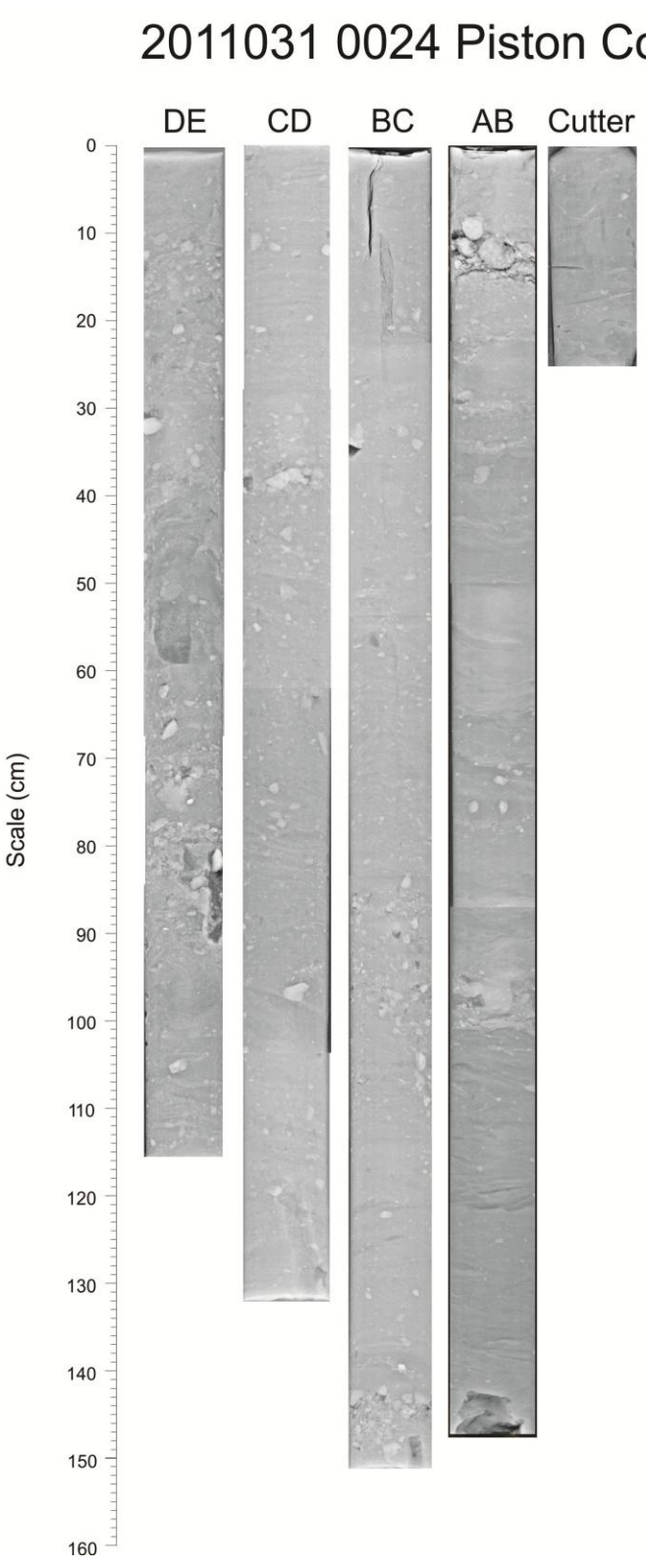
2011031 0024 Piston Core
DE
CD
BC
AB
Cutter
Scale (cm)
0
10
20
30
40
50
60
70
80
90
100
110
120
130
140
150
160

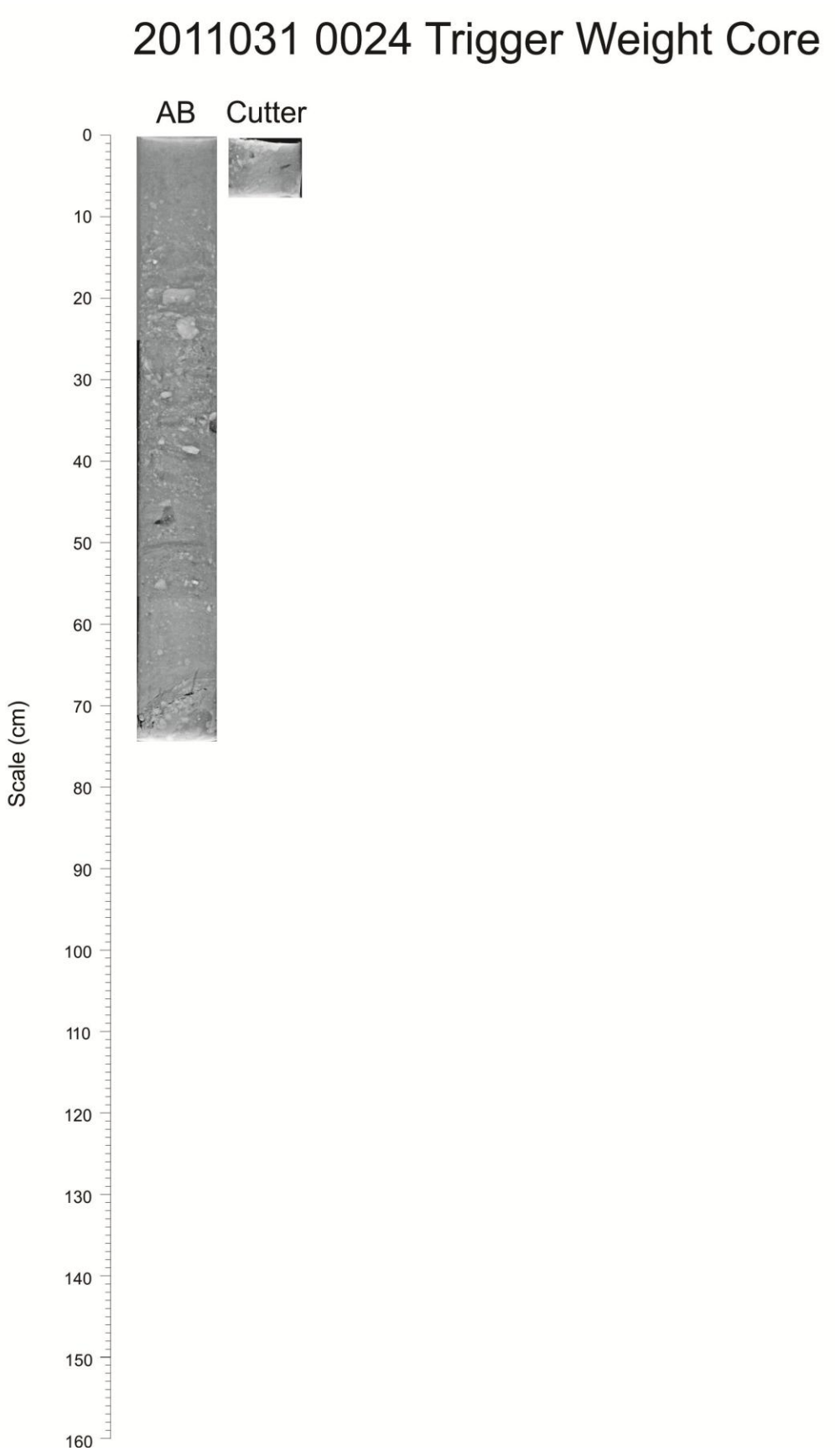
2011031 0024 Trigger Weight Core
AB
Cutter
Scale (cm)
0
10
20
30
40
50
60
70
80
90
100
110
120
130
140
150
160

APPENDIX C: PHYSICAL PROPERTIES AND SPECTROPHOTOMETRY

Note: Core lithology legend: dots represent sand/ silty sand/ sandy silt, and no symbol represents silt/silty clay.

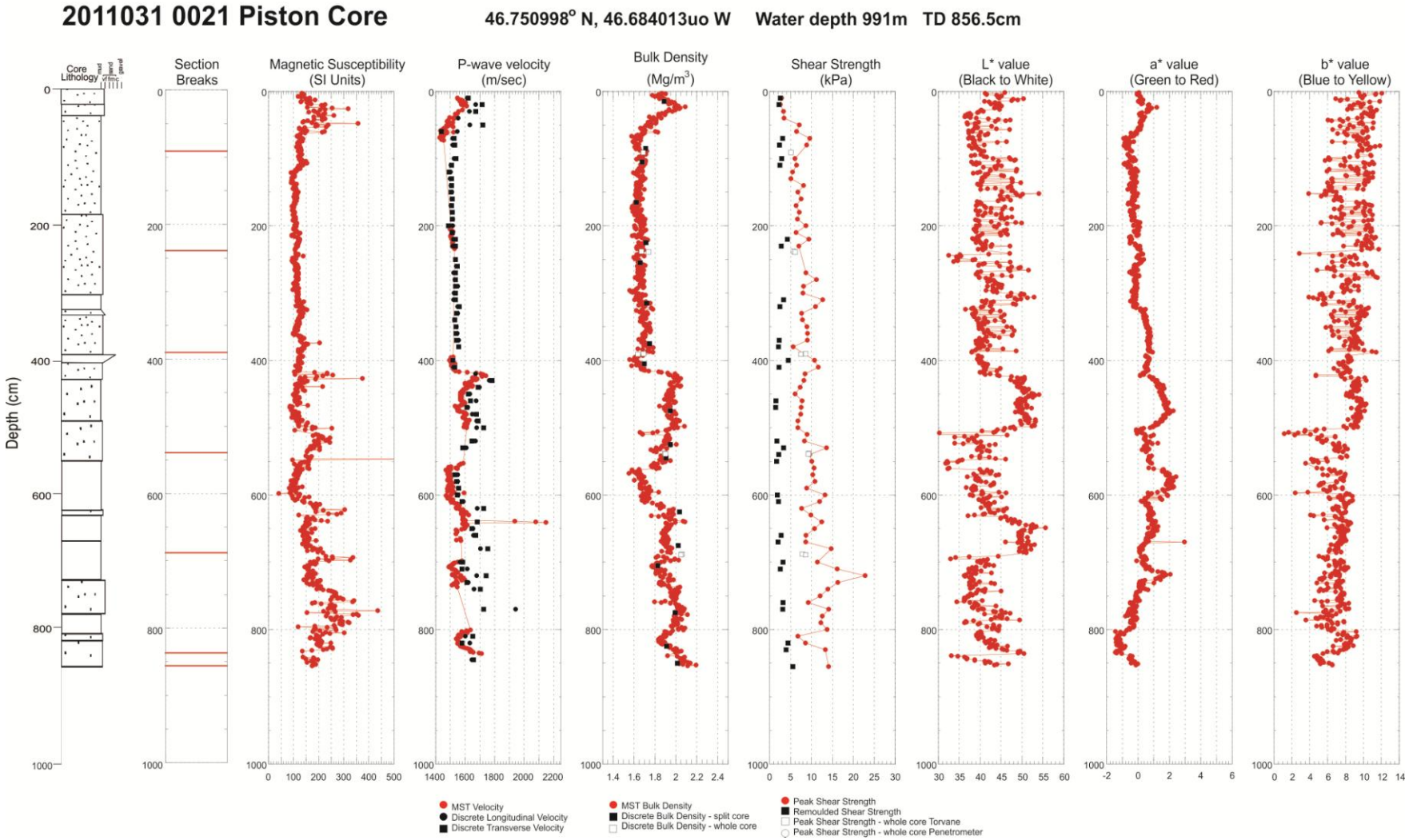

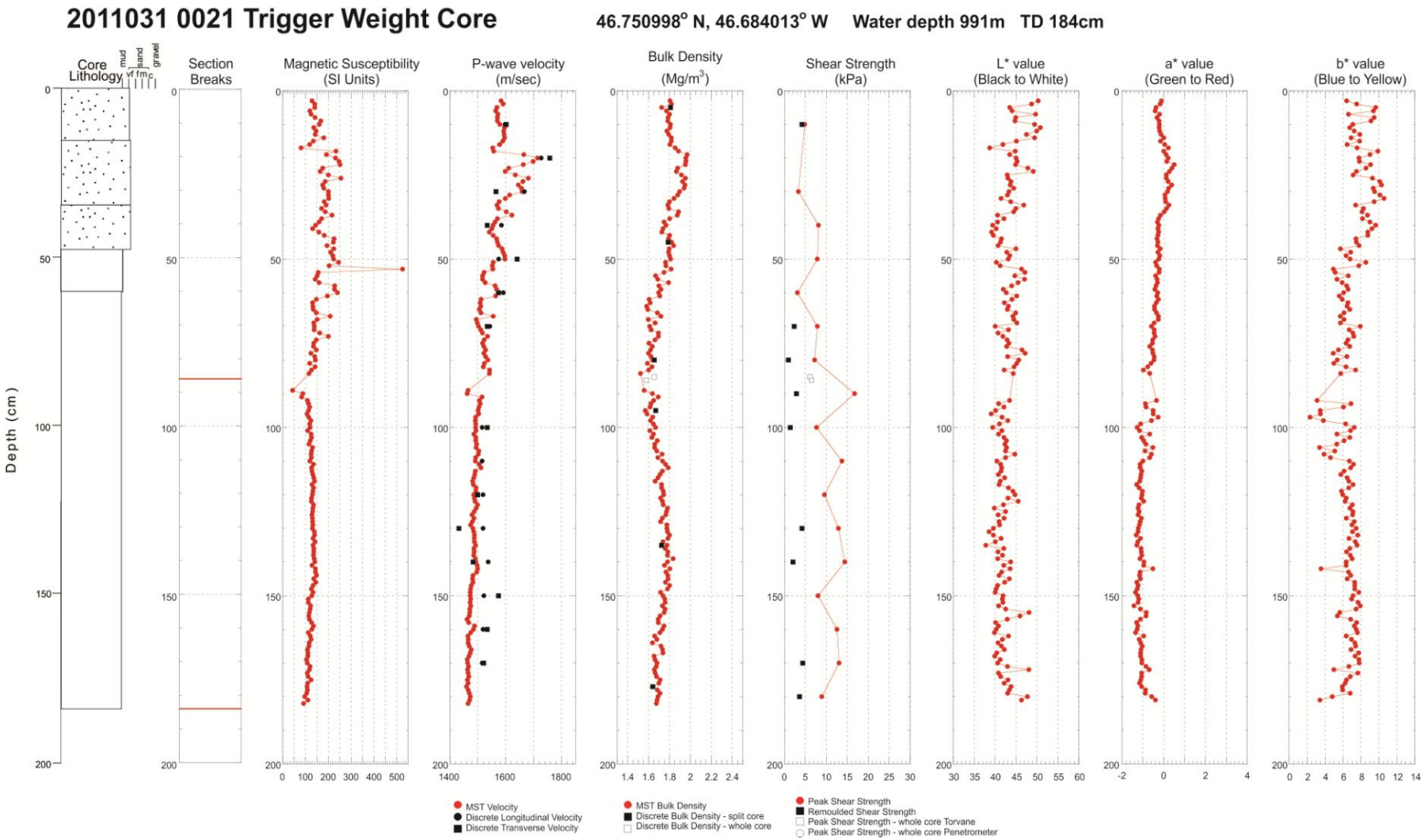
2011031 0021 Trigger Weight Core
46.750998° N, 46.684013° W Water depth 991m TD 184cm
Core Lithology
mud
sand
gravel
vf f m c
Section Breaks
Magnetic Susceptibility (SI Units)
P-wave velocity (m/sec)
Bulk Density (Mg/m3)
Shear Strength (kPa)
L* value (Black to White)
a* value (Green to Red)
b* value (Blue to Yellow)
Depth (cm)
MST Velocity
Discrete Longitudinal Velocity
Discrete Transverse Velocity
MST Bulk Density
Discrete Bulk Density - split core
Discrete Bulk Density - whole core
Peak Shear Strength
Remoulded Shear Strength
Peak Shear Strength - whole core Torvane
Peak Shear Strength - whole core Penetrometer

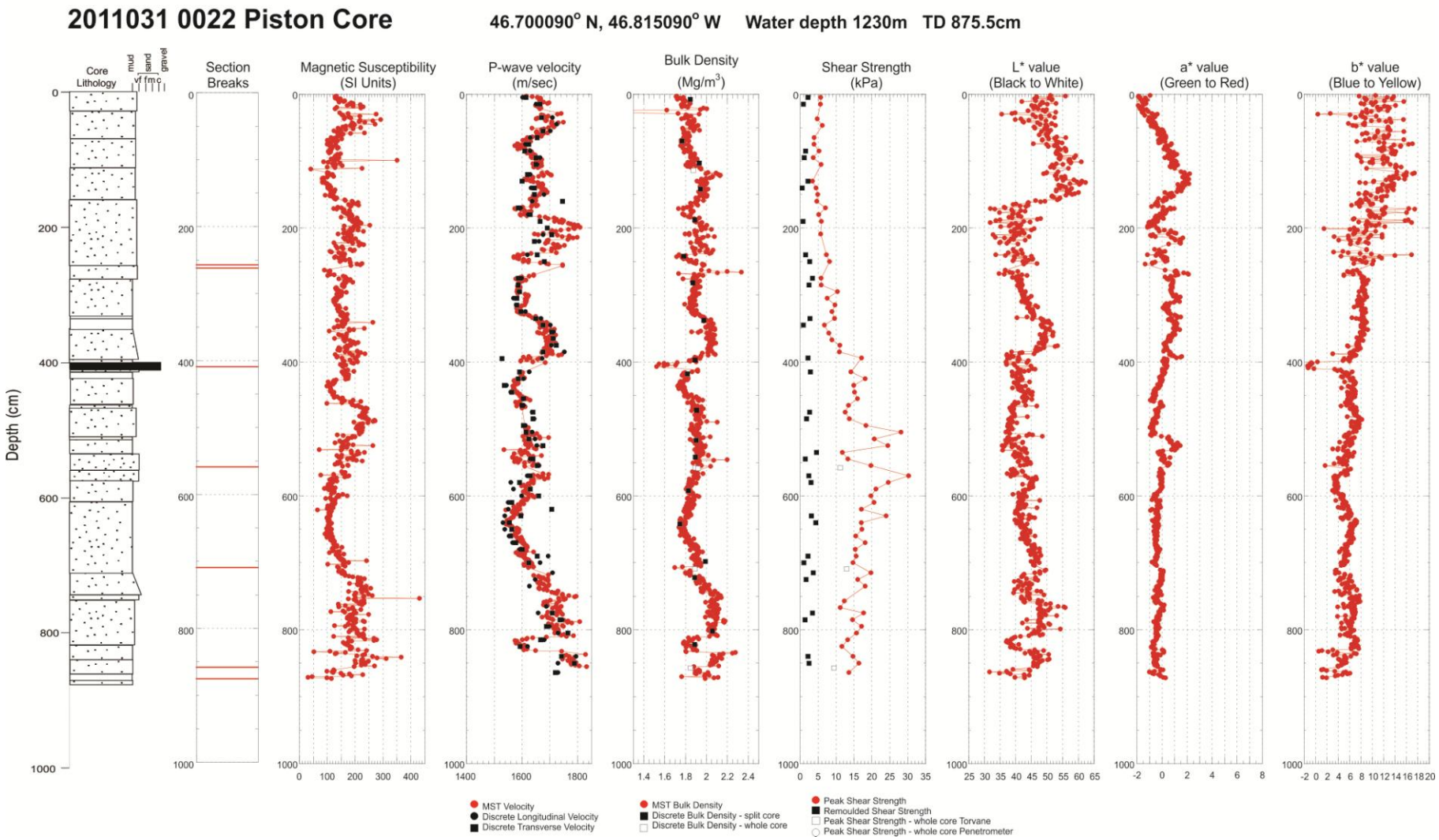
2011031 0022 Piston Core
46.700090° N, 46.815090° W Water depth 1230m TD 875.5cm
Core Lithology
mud
sand
gravel
vf f m c
Depth (cm)
Section Breaks
Magnetic Susceptibility (SI Units)
P-wave velocity (m/sec)
Bulk Density (Mg/m3)
Shear Strength (kPa)
L* value (Black to White)
a* value (Green to Red)
b* value (Blue to Yellow)
MST Velocity
Discrete Longitudinal Velocity
Discrete Transverse Velocity
MST Bulk Density
Discrete Bulk Density - split core
Discrete Bulk Density - whole core
Peak Shear Strength
Remoulded Shear Strength
Peak Shear Strength - whole core Torvane
Peak Shear Strength - whole core Penetrometer

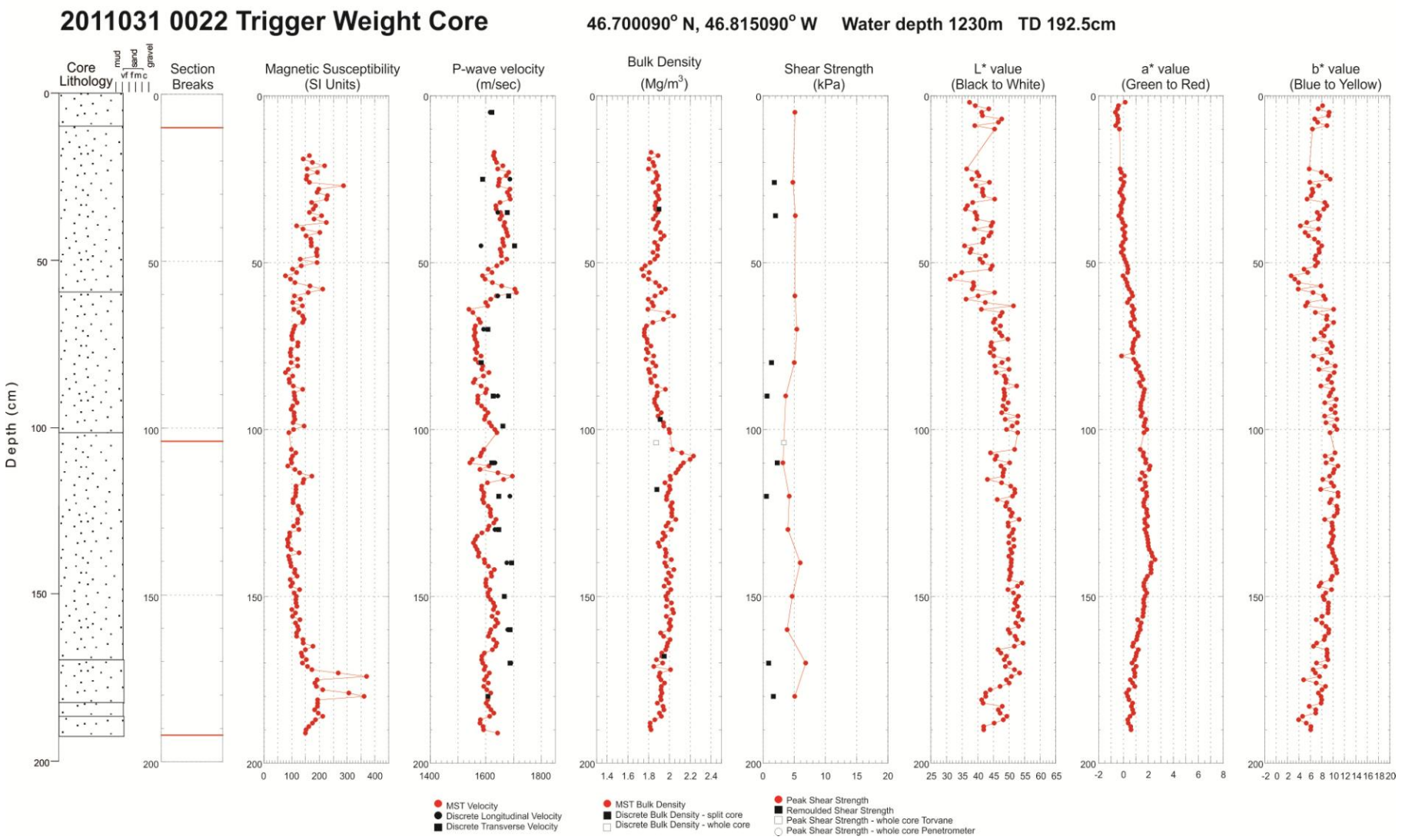
2011031 0022 Trigger Weight Core
46.700090° N, 46.815090° W Water depth 1230m TD 192.5cm
Core Lithology
mud
sand
gravel
vf f m c
Section Breaks
Magnetic Susceptibility (SI Units)
P-wave velocity (m/sec)
Bulk Density (Mg/m3)
Shear Strength (kPa)
L* value (Black to White)
a* value (Green to Red)
b* value (Blue to Yellow)
Depth (cm)
MST Velocity
Discrete Longitudinal Velocity
Discrete Transverse Velocity
MST Bulk Density
Discrete Bulk Density - split core
Discrete Bulk Density - whole core
Peak Shear Strength
Remoulded Shear Strength
Peak Shear Strength - whole core Torvane
Peak Shear Strength - whole core Penetrometer

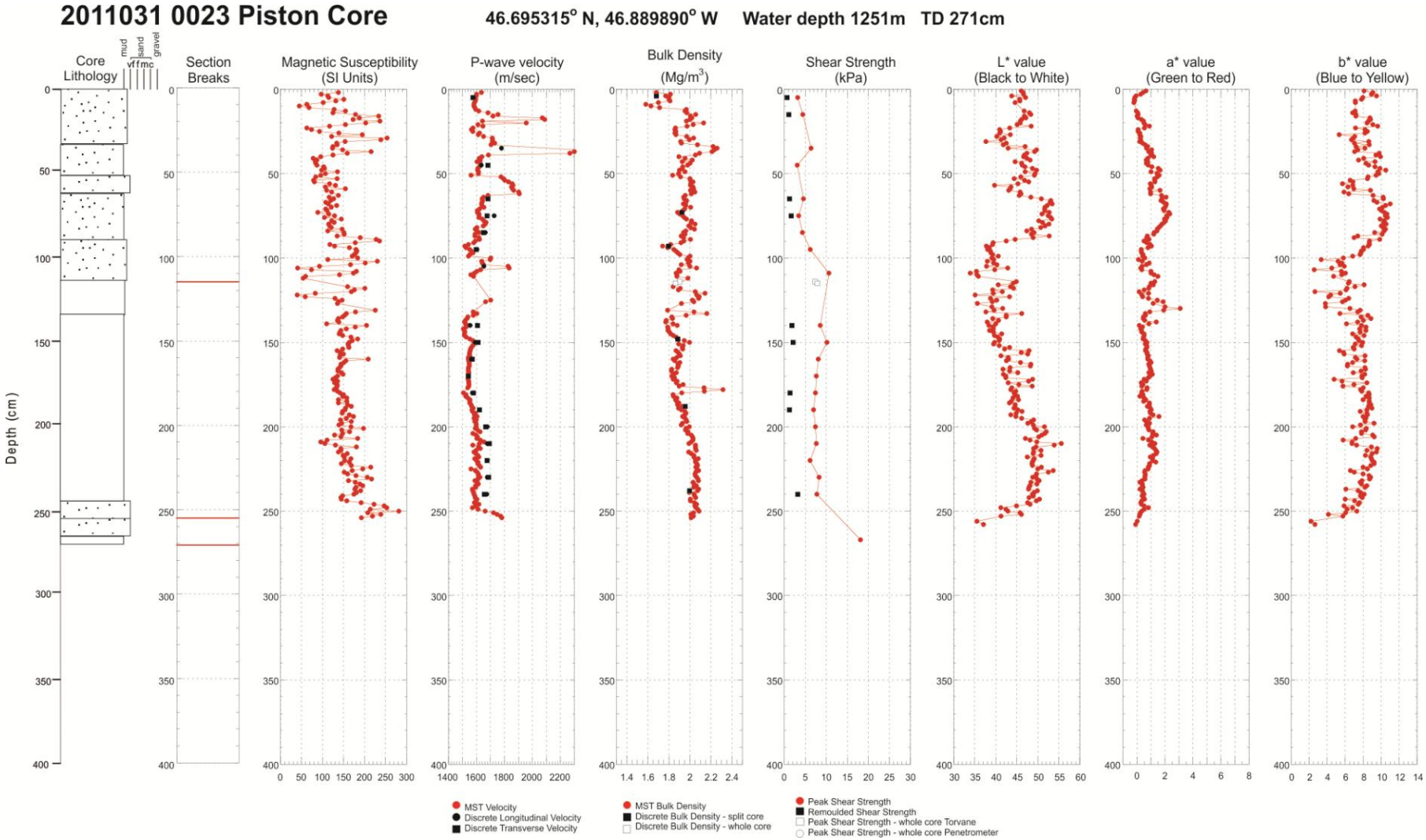
2011031 0023 Piston Core
46.695315° N, 46.889890° W
Water depth 1251m
TD 271cm
Core Lithology
mud
sand
gravel
vf f mc
Section Breaks
Magnetic Susceptibility (SI Units)
P-wave velocity (m/sec)
Bulk Density (Mg/m3)
Shear Strength (kPa)
L* value (Black to White)
a* value (Green to Red)
b* value (Blue to Yellow)
Depth (cm)
MST Velocity
Discrete Longitudinal Velocity
Discrete Transverse Velocity
MST Bulk Density
Discrete Bulk Density - split core
Discrete Bulk Density - whole core
Peak Shear Strength
Remoulded Shear Strength
Peak Shear Strength - whole core Torvane
Peak Shear Strength - whole core Penetrometer

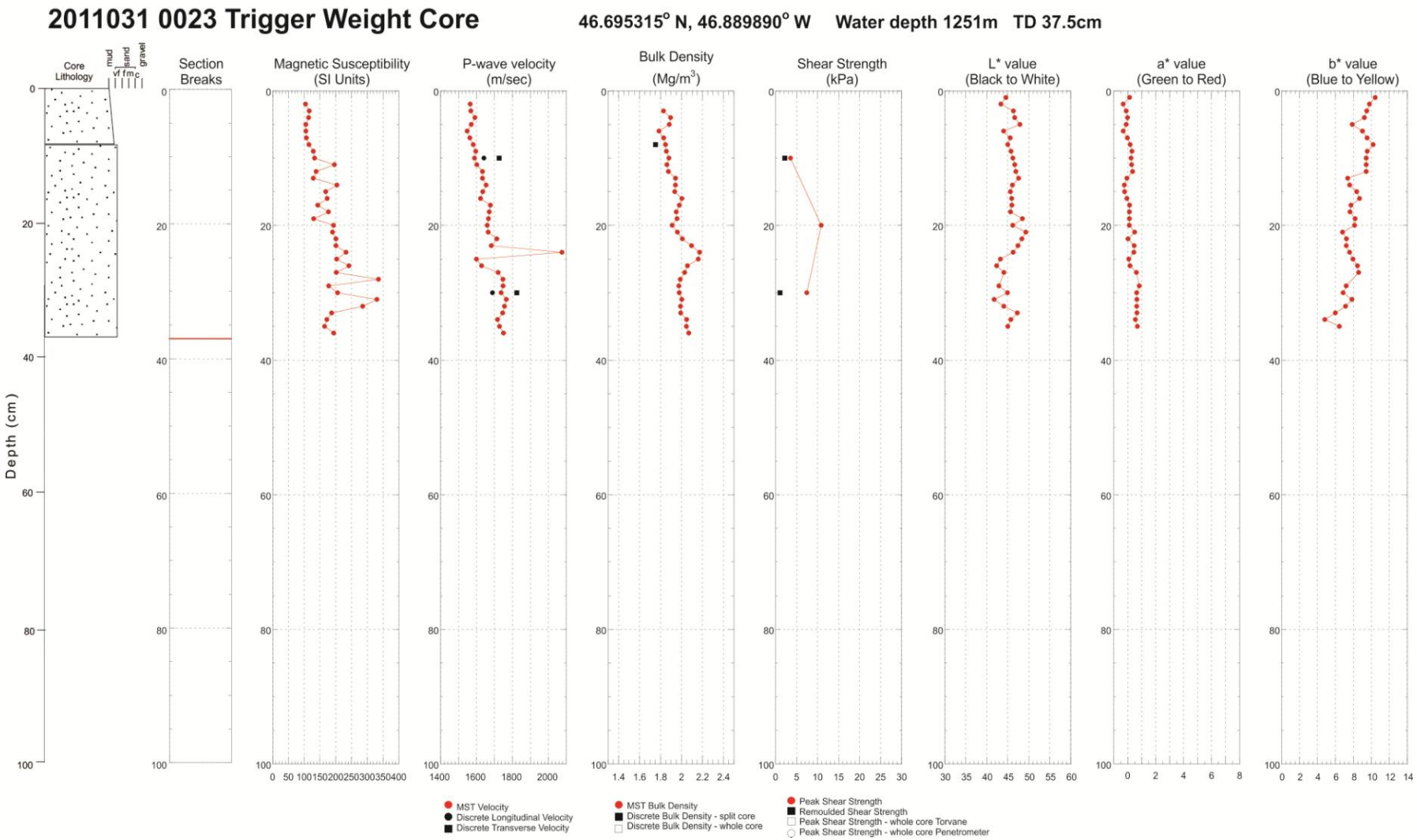
2011031 0023 Trigger Weight Core
46.695315° N, 46.889890° W Water depth 1251m TD 37.5cm
Core Lithology
mud
sand
gravel
vf f m c
Section Breaks
Magnetic Susceptibility (SI Units)
P-wave velocity (m/sec)
Bulk Density (Mg/m3)
Shear Strength (kPa)
L* value (Black to White)
a* value (Green to Red)
b* value (Blue to Yellow)
Depth (cm)
MST Velocity
Discrete Longitudinal Velocity
Discrete Transverse Velocity
MST Bulk Density
Discrete Bulk Density - split core
Discrete Bulk Density - whole core
Peak Shear Strength
Remoulded Shear Strength
Peak Shear Strength - whole core Torvane
Peak Shear Strength - whole core Penetrometer

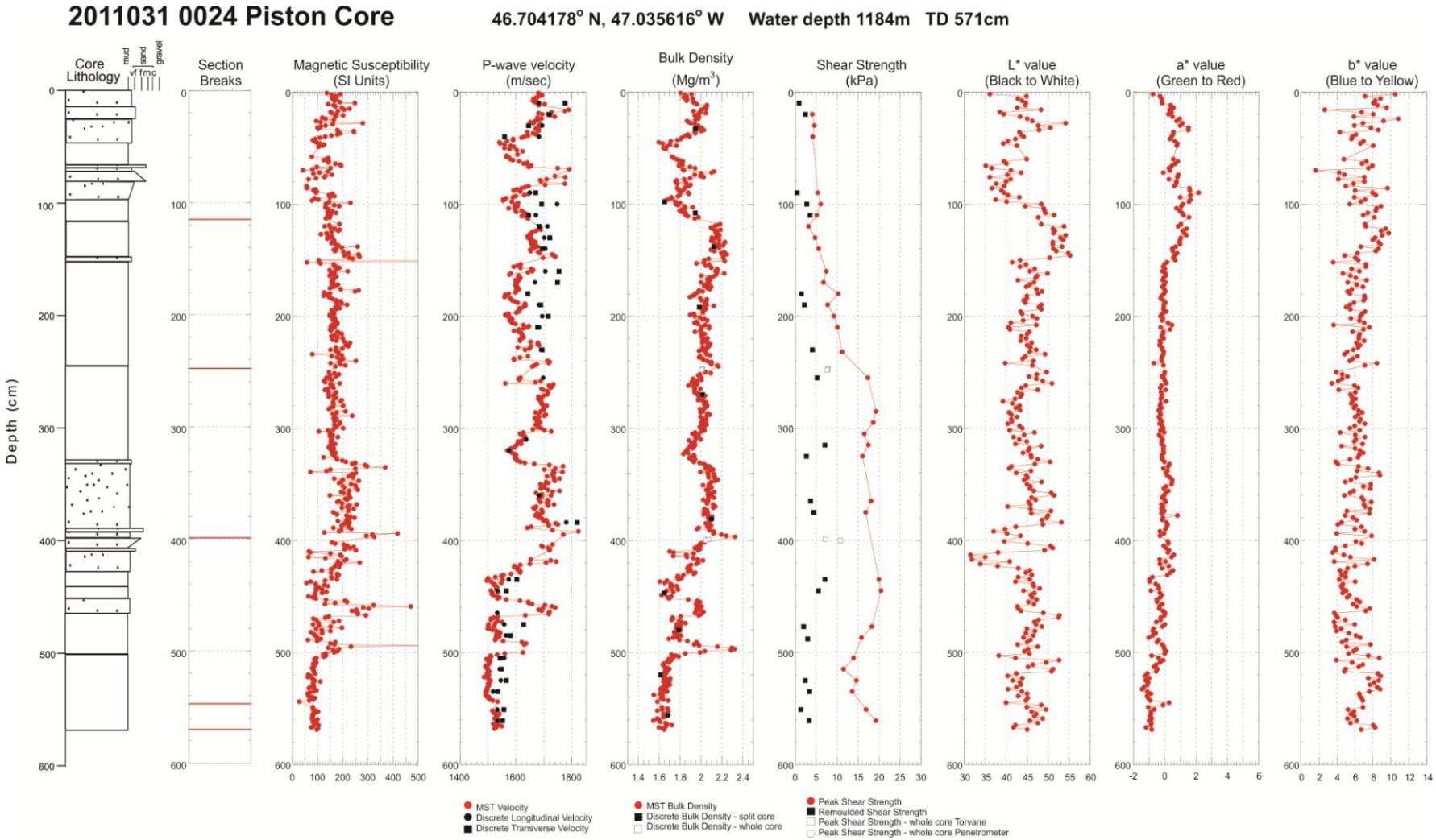
2011031 0024 Piston Core
46.704178° N, 47.035616° W Water depth 1184m TD 571cm
Core Lithology
mud
sand
gravel
vf f m c
Section Breaks
Magnetic Susceptibility (SI Units)
P-wave velocity (m/sec)
Bulk Density (Mg/m3)
Shear Strength (kPa)
L* value (Black to White)
a* value (Green to Red)
b* value (Blue to Yellow)
Depth (cm)
MST Velocity
Discrete Longitudinal Velocity
Discrete Transverse Velocity
MST Bulk Density
Discrete Bulk Density - split core
Discrete Bulk Density - whole core
Peak Shear Strength
Remoulded Shear Strength
Peak Shear Strength - whole core Torvane
Peak Shear Strength - whole core Penetrometer

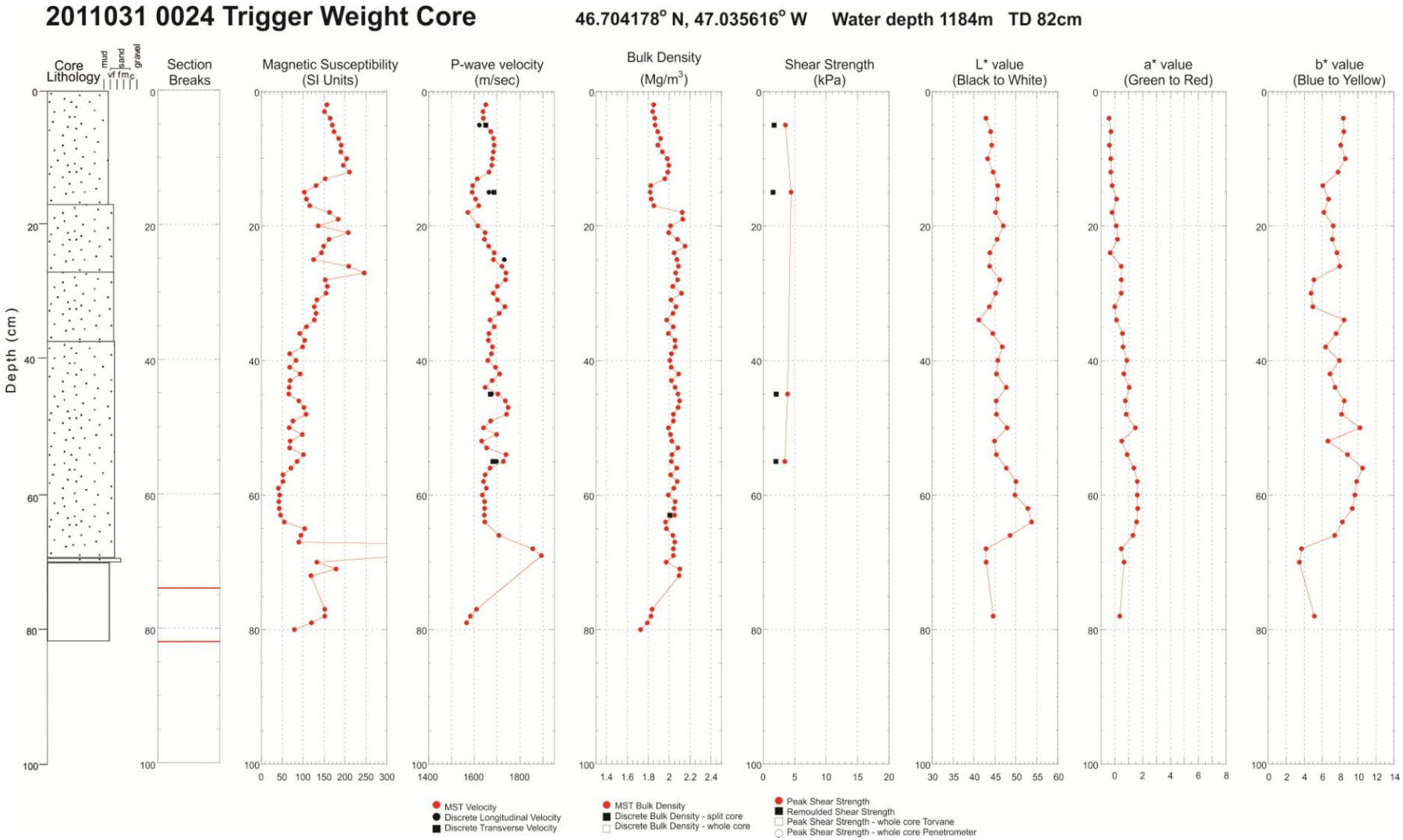
2011031 0024 Trigger Weight Core
46.704178° N, 47.035616° W Water depth 1184m TD 82cm
Core Lithology
mud
sand
gravel
vf f m c
Section Breaks
Magnetic Susceptibility (SI Units)
P-wave velocity (m/sec)
Bulk Density (Mg/m3)
Shear Strength (kPa)
L* value (Black to White)
a* value (Green to Red)
b* value (Blue to Yellow)
Depth (cm)
MST Velocity
Discrete Longitudinal Velocity
Discrete Transverse Velocity
MST Bulk Density
Discrete Bulk Density - split core
Discrete Bulk Density - whole core
Peak Shear Strength
Remoulded Shear Strength
Peak Shear Strength - whole core Torvane
Peak Shear Strength - whole core Penetrometer

APPENDICES D-H

Appendices D-H are contained in the Data Repository on the attached CD-ROM.